EFFECT OF STRESS ON PROPAGATION PROPERTIES OF PCF WITH DIFFERENT DESIGN PARAMETERS

By

Mst. Rokeya Khatun

MASTER OF SCIENCE IN INFORMATION AND COMMUNICATION TECHNOLOGY

Institute of Information and Communication Technology

Bangladesh University of Engineering and Technology

Feb 2012

The thesis titled "**Effect of Stress on Propagation Properties of PCF with Different Design Parameters"** submitted by Mst. Rokeya Khatun, Student ID: M04083106P (Session April/2008) has been accepted as satisfactory in partial fulfillment for the degree of Master of Science in Information and Communication Technology on 11 February 2012.

BOARD OF EXAMINERS

1. Chairman (Supervisor)

Dr. Md. Saiful Islam
Professor
IICT, BUET
Dhaka-1000, Bangladesh.

2. Member (Ex-Officio)

Dr. S. M. Lutful Kabir
Professor and Director
IICT, BUET
Dhaka-1000, Bangladesh.

3. Member

Dr. Md. Liakot Ali
Professor
IICT, BUET
Dhaka-1000, Bangladesh.

4. Member (External)

Md. Afzal Hossain
Group Captain (Senior Instructor)
Head, Department of Computer Science and Engineering (CSE)
Military Institute of Science and Technology (MIST)
Mirpur Cantonment, Dhaka-1216, Bangladesh.

CANDIDATE’S DECLARATION

It is hereby declared that this thesis or any part of it has not been submitted elsewhere for the award of any degree or diploma.

_____

Mst. Rokeya Khatun

TABLE OF CONTENTS

LIST OF FIGURES

LIST OF TABLES

LIST OF ABREVIATIONS

PCF	Photonic crystal fiber
M-TIR	Modified Total Internal Reflection
TIR-PCF	Total Internal Reflection Photonic Crystal Fiber
PBG	Photonic bandgap
PMD	Polarization mode dispersion
PMF	Polarization-maintaining fiber
MFD	Mode field diameter
EA	Effective area
FEM	Finite element method
PML	Perfectly Matched Layer
AFF	Air filling fraction

LIST OF SYMBOLS

n	Refractive index
n_{eff}	Effective refractive index
n_1	Refractive index of core
n_2	Refractive index of cladding
c	Velocity of light
Λ	Air hole to air hole distance (pitch)
d	Air hole diameter
R	Cross sectional radius of fiber
N_r	Number of air hole rings
I_1	Incident ray light
I_2	Refracted ray light
θ_a	Incident angle
θ_2	Angle of refraction
θ_c	Critical angle
β	Propagation constant
β_x	Propagation constant along x axis
β_y	Propagation constant along y axis
k	Vacuum wave number
λ	Wavelength of light
λ_{01}	Wavelength of LP_{01} mode
D	Dispersion
A_{eff}	Effective area
L	Fiber length
v_p	Phase velocity
ω	Angular frequency
P_i	Optical input power

P_o	Optical output power
F	Force
P	Pressure
ε_x	Strain in the body along the x-direction
ε_y	Strain in the body along the y-direction
ε_z	Strain in the body along the z-direction
u	Displacements along the x-axis directions respectively
v	Displacements along the y-axis directions respectively
γ_{xy}	Shear strain in the x-y plane
σ_x	Principal stress along x-directions
σ_y	Principal stress along y-directions
σ_z	Principal stress along z-directions
τ_{xy}	Shear strain in the x-y plane
E	Young's modulus
v	Poisson's ratio
G	Shear modulus
α	Thermal expansion coefficient
ΔT	Temperature change
B_e	Strain matrix
d^e	Displacements matrix
U^e	Strain energy of eth element,
De	Element matrix
A_e	6X6 element stiffness matrix
$\{h^e\}$	6X1 thermal stress vector
P_t	Total potential energy
C_1, C_2	Elasto-optic coefficient of the fiber or waveguide material
σ	Stress vectors
ε	Strain vectors
μ	Permeability
μ_r	Relative permeability
μ_0	Vacuum permeability

ε	Permittivity
ε_r	Relative permittivity
ε_0	Vacuum permittivity
H	Magnetic field
E	Electric field
r_{in}	Internal radius of PML
e	Thickness of PML
$s_x, \quad s_y, \quad s_z$	Complex-valued coordinating scaling parameters
AFF	Air filling fraction
A_{hole}	Area of the air hole inside the unit triangle
A_{cell}	Area of the unit triangle
AFF_{Sqr}	Air filling fraction for square PCF
AFF_{Hexa}	Air filling fraction for hexagonal PCF
AFF_{Octa}	Air filling fraction for octagonal PCF
A_s	Total air-hole cross sectional area for square PCFs
A_h	Total air-hole cross sectional area for hexagonal PCFs
A_o	Total air-hole cross sectional area for octagonal PCFs
$A_1, A_2, A_3,$	Sellmeier coefficients
B_1, B_2, B_3	

ACKNOWLEDGEMENT

First and foremost I offer my sincerest gratitude to the Almighty Allah for guiding us to conceptualize, develop and complete the thesis. Also this research project would not have been possible without the support of many people. It is a pleasure to convey my gratitude and humble acknowledgement to all of them.

In the first place I want to express special thanks and deepest gratitude to Prof .Dr. Md. Saiful Islam of IICT, BUET for his all advice, guidance and suggestions. Above all and the most needed, he provided me high-spirited encouragement and support in various ways to complete this research work.

I am pleased to thank Group Captain Md. Afzal Hossain, Senior Instructor and Head, Dept. of CSE, Military Institute of Science and Technology (MIST) for his help and advice, despite of his tight schedules.

I would also like to thank my family members, specially my husband, Md. Rajibul Alam for supporting and encouraging me to pursue this degree.

ABSTRACT

Optical fiber based wavelength division multiplexing (WDM) is widely used to satisfy the high bandwidth demand using optical network. But dispersion, non-linearity and attenuation restrict the wavelength region and transmission bit rate for conventional fiber. Photonic crystal fibers (PCFs) are micro-structured optical fiber which are constructed by single material with multiple air holes periodically arranged around the core. PCFs have ability to be single mode over a broad range of wavelengths. Large number of available design parameters of solid core PCF makes the dispersion, nonlinearity and confinement loss highly configurable. PCFs are of great interest for optical communication in new wavelength regions and for new optical devices. As the stress and thermal effect on PCFs can alter the propagation properties significantly, it is very important to know and study the properties of PCF to fully understand the feasibility of using it as sensor for stress civil structures or acoustic pressure in underwater and underground communication systems. In this research work the effect of external stress and design parameters on propagation properties for square, hexagonal and octagonal air-hole arranged PCFs have been analyzed and simulated. The fiber designs are carried out for all types of PCFs by varying number of air hole rings and air hole diameter and different amount of stress is applied on the PCFs boundary and the effective indices, birefringence are calculated as a function of stress. It is found that external stress on PCF causes stress distribution and fiber deformation in fiber cross section. This deformation is not same for all type of fibers and in all direction (x and y), which causes different effective index and birefringence for all types of PCFs. Results show that external stress affects more on propagation properties of hexagonal PCF than square or octagonal and this effect is lower for larger number of air hole rings and air hole diameter. Our findings will help to find the appropriate designing of PCF for some of particular application.

Chapter 1

INTRODUCTION

Optical fiber communication system is a subject of growing interest due to its extremely attractive features. Moreover, the rapid pace of advances in technology has surpassed the most optimistic predictions, creating additional advantages [1]. This has led researchers to put more effort on improving the various characteristics of different optical fibers by continuous study and research.

1.1 PHOTONIC CRYSTAL FIBER

Photonic crystal fibers (PCFs) are a new class of optical fibers. PCFs also known as microstructured fiber has arrays of holes running along its length [1]. Microstructured fibers guide light due to modified total internal reflection. Unlike conventional fibers, PCFs can be made entirely from a single material, typically undoped silica. The holes act to lower the effective refractive index in the cladding region and so that light is confined to the solid core, which has a relatively higher index. In a PCF, the number of holes and their sizes, shapes, orientations and placements can provide degrees of freedom and hence unique properties, which are not available in conventional optical fibers. The strong wavelength dependency of the effective refractive index and the inherently large design flexibility of the PCFs allow for a whole new range of novel properties [2-3]. Such properties include endlessly single-mode fibers, extremely nonlinear fibers and fibers with anomalous dispersion in the visible wavelength region. They could serve as a fiber host for developing a wide range of fiber devices for high power fiber laser, second harmonic generation, super continuum generation, radiation detection, etc. PCFs may be divided into two categories [4]:

i) **High index guiding fibers:** Similar to conventional fibers, high index guiding fibers are guiding light in a solid core by the modified total internal reflection (M-TIR) principle. The total internal reflection is caused by the lower effective index in the microstructured air-filled region.

ii) **Low index guiding fibers:** Low index guiding fibers guide light by the photonic bandgap (PBG) effect. The light is confined to the low index core as the PBG effect makes propagation in the microstructured cladding region impossible.

1.2 HIGH INDEX GUIDING FIBERS

PCFs with a ***solid core*** can operate on the same index guiding principle as conventional optical fiber. It relies on a high index core region, typically pure silica, surrounded by a lower effective index provided by the microstructured region that is shown in Fig.1.1. The refractive index of the microstructured cladding in PCFs exhibits a wavelength dependency very different from pure silica, which allows PCFs to be designed with a complete new set of properties. As an example, the strong wavelength dependence of the refractive index allows design of endlessly single-moded fibers, where only a single mode is supported regardless of optical wavelength. Furthermore, it is possible to alter the dispersion properties of the fibers, thereby making it possible to design fibers with an anomalous dispersion at visible wavelengths.

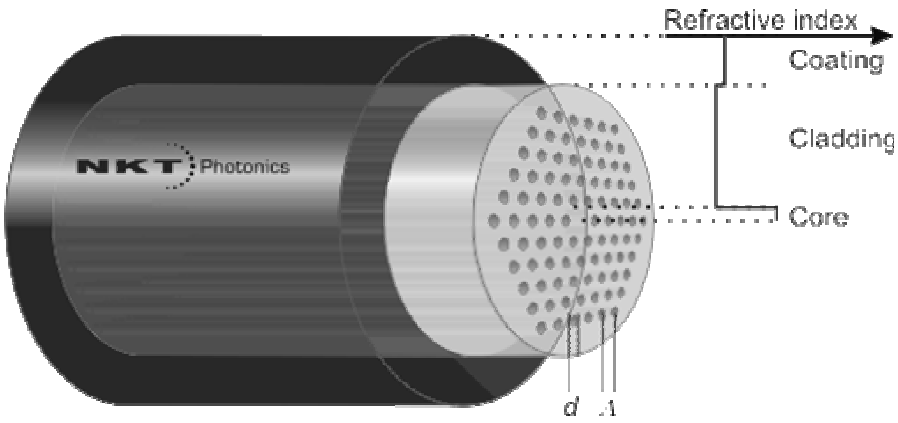

Fig.1.1 Hexagonal air hole arranged solid core PCF.

Index-guiding PCFs offer a lot of new opportunities. These opportunities stem from just a few special properties of the photonic crystal cladding, which are caused by the large refractive index contrast and the two-dimensional nature of the microstructure. These special properties allow achieving anomalous dispersion, the smallest attainable core size and the number of guided modes, the numerical aperture and the birefringence. Such structures are leading to novel sensors, high-power fiber lasers and to developments in other research fields. Due to precise control of the refractive index profile, fibers with extremely large mode field diameters are made possible, supporting high beam quality fiber guidance and amplification.

1.3 LOW INDEX GUIDING FIBERS

Photonic bandgap fibers are based on physical mechanisms fundamentally different from the M-TIR guiding fibers. The periodic microstructure in the PBG fiber cladding results in a so called photonic bandgab, where light in certain wavelength regions cannot propagate. In a PBG fiber, the core is created by introducing a defect in the PBG structure (e.g. an extra air hole), thereby creating an area where the light can propagate. As the light can only propagate at the defect region, a low index guiding core has been created. This is not possible in standard fibers and the low index guiding of PBG fibers therefore opens a whole new set of possibilities. In this way, it is possible to guide light in air, vacuum or any gas compatible with the fiber material.

1.3.1 Hollow Core PBG Fibers

A special class of PBG guiding fibers is the hollow core fibers, where the field is confined to an air-filled core. The basic structure of a hollow core PBG fiber is shown in Fig.1.2. Like other PBG fibers, air-core fibers only guide light in a limited spectral region. Outside this region, the fiber core is anti-guiding.

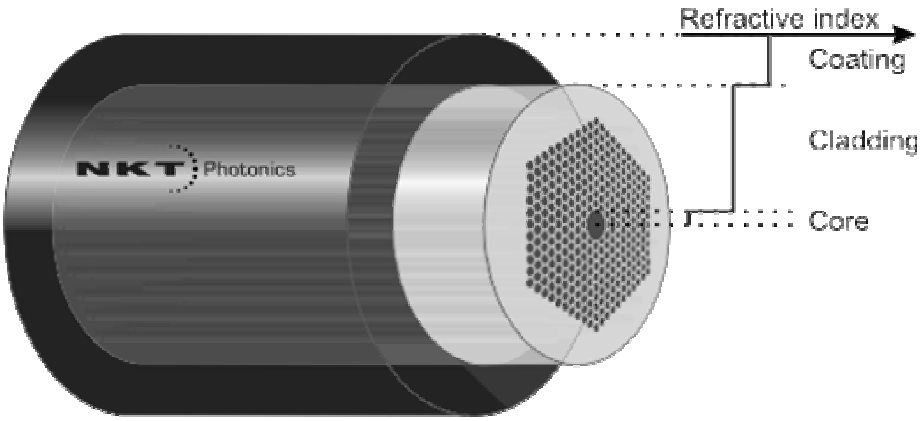

Fig.1.2 Hexagonal air hole arranged hollow core PCF.

Guiding light in a hollow core holds many promising applications like high power delivery without the risk of fiber damage, gas sensors or extreme low loss guidance in vacuum. Furthermore, this class of fiber has other spectacular properties not found in any other fiber type. They are almost

insensitive to bending (even at very small bending radii) and they have dramatically reduced sensitivity to Kerr effect (greater than 50), temperature transients (~6.5) and Faraday effect (smaller than 10). Extreme dispersion properties such as anomalous dispersion values in the thousands of ps/nm/km regime are easily obtained. Due to a negligible contribution from the core material (air), the total dispersion of PBG fibers is to a high degree dominated by waveguide dispersion.

1.3.2 Solid Core PBG Fibers

Another special class of PBG guiding fibers is the solid core PBG fibers. Here, the field is confined to a solid core and the cladding region typically consists of an array of high index regions embedded in silica material. Like other PBG fibers, solid core PBG fibers only guide light in a limited spectral region. This filtering effect in combination with a rare earth doped core such as Yb makes lasing and amplification possible at new wavelengths with weak fiber gain. Also, the combination of a doped solid core PBG fiber and special dispersion properties provides a new route for the laser community.

1.4 FABRICATION OF PHOTONIC CRYSTAL FIBER

Fabrication of PCF, like conventional fiber fabrication, starts with a fiber preform [5]. The Fig.1.3 depicts the fabrication process of microstructured optical fiber. PCF preforms are formed by stacking a number of capillary silica tubes and rods to form the desired air/silica structure. This way of creating the preform allows a high level of design flexibility as the core size and shape as well as the index profile throughout the cladding region can be controlled.

When the desired preform has been constructed, it is drawn to a fiber in a conventional high-temperature drawing tower and hair-thin photonic crystal fibers are readily produced in kilometer lengths. Through careful process control, the air holes retain their arrangement all through the drawing process and even fibers with very complex designs and high air filling fraction can be produced.

Finally, the fibers are coated to provide a protective standard jacket that allows robust handling of the fibers. The final fibers are comparable to standard fiber in both robustness and physical dimensions and can be both striped and cleaved using standard tools.

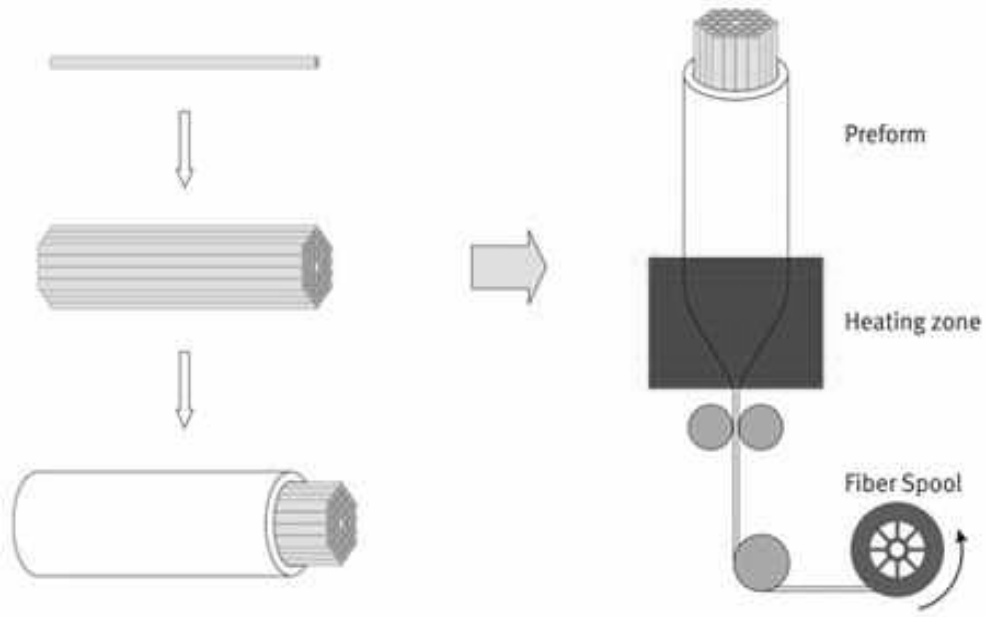

Fig.1.3 Fabrication process of microstructured optical fiber.

1.5 APPLICATIONS

The special properties of PCFs make them very attractive for a very wide range of applications. Some examples are [6]:

- Fiber lasers and amplifiers, including high-power devices, mode-locked fiber lasers, etc.
- Nonlinear devices *e.g.* for supercontinuum generation, Raman conversion, parametric amplification, or pulse compression
- Telecom components, *e.g.* for dispersion control, filtering or switching
- Fiber-optic sensors of various kinds
- Quantum optics, *e.g.* generation of correlated photon pairs, electromagnetically induced transparency, or guidance of cold atoms.

Even though PCFs have been around for several years, the huge range of possible applications is far from being fully explored. It is to be expected that this field will stay very lively for many years and many opportunities for further creative work, concerning both fiber designs and applications.

1.6 HISTORICAL DEVELOPMENT

The idea of a photonic crystal fiber was presented for the first time by Yeh et al. in 1978. They proposed to clad a fiber core with Bragg grating, which is similar to 1D photonic crystal. A photonic crystal fiber made of 2D photonic crystal with an air core was invented by P. Russell in 1992 and the first PCF was reported at the Optical Fiber Conference (OFC) in 1996. A short overview of PCF development is presented in the table [7].

Table 1.1 Overview of photonic crystal fibers development.

1978	Idea of the Bragg fiber
1992	Idea of the photonic crystal fiber with air core
1996	Fabrication of a single-mode fiber with photonic coating
1997	Endlessly singe mode PCF
1999	PCF with photonic bandgap and air core
2000	Highly birefringent PCF
2000	Supercontinuum generation with PCF
2001	Fabrication of a Bragg fiber
2001	PCF laser with double cladding
2002	PCF with ultra-flattened dispersion
2003	Bragg fiber with silica and air core
2004	Four-wave mixing effect control
2005	High energy with low-loss transitions between different PCFs
2006 to 2010	Analysis with different mechanism to improve performance in single mode region Application in communication fields, sensor, coupler, amplifier, medical science etc. Stress analysis to find out the stress effects on PCFs propagation properties

1.7 REVIEW OF PREVIOUS WORKS AND MOTIVATION

Propagation properties of PCFs have been investigated widely using different analysis techniques and tools [8-25]. Most of the investigation carried out without considering effect of stress. It is very important to know the properties of PCF to fully understand the feasibility of using it as sensor for stress civil structures or acoustic pressure in underwater and underground communication systems. From some recent research, it is found that the stress and thermal effect on fiber can alter the propagation properties of PCFs [26-32].

Okamoto *et al.* (1981) presented a theoretical and experimental investigation of the transverse load sensitivity of Bragg gratings in birefringent fibers to conforming contact. The transverse load sensitivity of commercially available birefringent fiber is experimentally measured for two cases of conforming contact. The theoretical and experimental results show that birefringent optical fiber can be used to make modulus-independent measurements of contact load [25].

Zhaoming Zhu *et al.* (2003) presented a numerical study of stress-induced birefringence in microstructured optical fibers (MOFs), using a finite-element method. They showed that birefringence varies with external stress and stress induced birefringence is reduced with increase of air hole diameter. Here the research carried out for hexagonal air hole arrangement with fixed pitch and different air hole diameters [27].

Marcin Szpulak *et al.* (2004) investigated external pressure induced birefringence of PCF for two specific hexagonal air hole arrangement. They calculated the sensitivity of phase group modal birefringence to hydrostatic pressure versus wavelength in two birefringent holey fibers of different construction. The results show that deformation of the holey structure and the stress-related contribution to the overall pressure sensitivities factors decrease the phase modal birefringence in both structures [28].

M. Shah Alam *et al.* (2004) discussed effects of external pressure on effective index and birefringence of PCFs. Here the research was carried out only for hexagonal air hole arrangement PCFs model with different air hole diameter [29].

The pressure sensitivity of two photonic crystal fibers (PCFs) was measured by Bock *et al.* (2006). They also successfully developed a PCF pressure sensor. Although its very small mode-field area does not match the mode-field areas of commercially available phase modulation (PM) optical fibers, successful operation of the sensor has been achieved [30].
Hongda Tian *et al.* (2008) investigated lateral stress induced characteristics of PCFs. The results of simulation show strong stress dependence of birefringence and confinement loss. Here hexagonal air hole arrangement with fixed pitch and air hole diameter was used [31].

M. A. Hossain *et al.* (2010) researched the effect of thermal and external stress on effective index, the birefringence and PMD. Here the research also carried on hexagonal air hole arrangement with fixed pitch and air hole diameter [32].

From previous works we have found that—

i) Most of the works are carried out to find the stress effect on birefringence property with hexagonal air hole arrangement in PCFs.

ii) A few works are done on confinement loss and PMD with limited design parameters.

iii) Still the effect of external stress on effective area, effective index and confinement loss for different structured PCFs is unexplored using different design parameters like- air hole arrangement (hexagonal, square and octagonal), pitch, air-hole diameter, number of air-hole rings and shapes.

It is also important to evaluate the effect of stress on propagation properties of PCFs with other possible air-hole arrangements and incorporating more design parameters. So in this work we have made an attempt to observe the effect of thermal and external stress on propagation properties of PCFs with hexagonal and octagonal air hole arranged PCF with different number of air hole rings and air hole diameter. In this paper it is shown that the effect of external stress is not same for different air hole arranged PCFs and hexagonal air hole arranged PCF is more sensitive than octagonal.

1.8 AIMS AND OBJECTIVES

PCFs recently attracted a great deal of interest because of their excellent propagation properties. Many research groups all over the world are making constant effort to establish the superiority of PCFs over conventional fibers because of its novel optical characteristics. Still PCF have some limitations like nonlinear effects, confinement loss and dispersion. Thermal and external stress can affect these propagation properties.

The main goal of this research is to determine the behavior of PCF under thermal and external stress using analytical and simulation method. To achieve the goal, the following tasks will be carried out:

i) To find the effect of different design parameters (air hole diameter, pitch, number of air hole rings, air hole arrangement) on propagation properties of PCF without considering external stress.

ii) To find the effect of external stress including thermal stress on propagation properties (effective index, effective area, confinement loss, dispersion) of square, hexagonal and octagonal air hole arranged PCF with different design parameters.

iii) To compare the results of propagation properties of PCF from step (i) and (ii).

1.9 LAYOUT OF THESIS

The thesis paper contains many sections and sub-sections, each of which explains a specific part of this thesis. Chapter 1 presents the basics conception of optical fiber which include different types of optical fibers, their applications, fabrication process and motivation. Chapter 2 discuss about the guiding mechanism and propagation properties that include effective index, birefringence, effective area, confinement loss, dispersion and others. Chapter 3 is the analysis method section where details of finite element method in stress analysis and optical analysis are discussed. Chapter 4 presents fiber design and materials properties. This chapter discuss about the PCFs structure and air filling fraction. Chapter 5 includes various results and corresponding graphical and physical explanation. The results are obtained under different stress conditions and variations of some structural parameters are also studied to optimize the design. Chapter 6 is the conclusion.

Chapter 2

LIGHT GUIDING MECHANISM OF PCF

Communication may be broadly defined as the transfer of information from one point to another. Fiber-optic communication is a method of transmitting information from one place to another by sending pulses of light through an optical fiber. Optical fiber is used by many telecommunications companies to transmit telephone signals, internet communication, and cable television signals. Due to much lower attenuation and interference, optical fiber has large advantages over existing copper wire in long-distance and high-demand applications [8-12].

In this chapter we have discussed the basic structure of optical fiber and PCF. Then, the light-guiding mechanisms are presented. In solid-core photonic crystal fibers, where light is confined in a higher refractive index region, modified total internal reflection is exploited, which is quite similar to the guiding mechanism of standard optical fibers.

2.1 STRUCTURE OF OPTICAL FIBER

An optical fiber is a dielectric waveguide that operates at optical frequencies. This fiber waveguide is normally cylindrical in form [3]. The basic structure of an optical fiber is shown in Fig.2.1. (a).

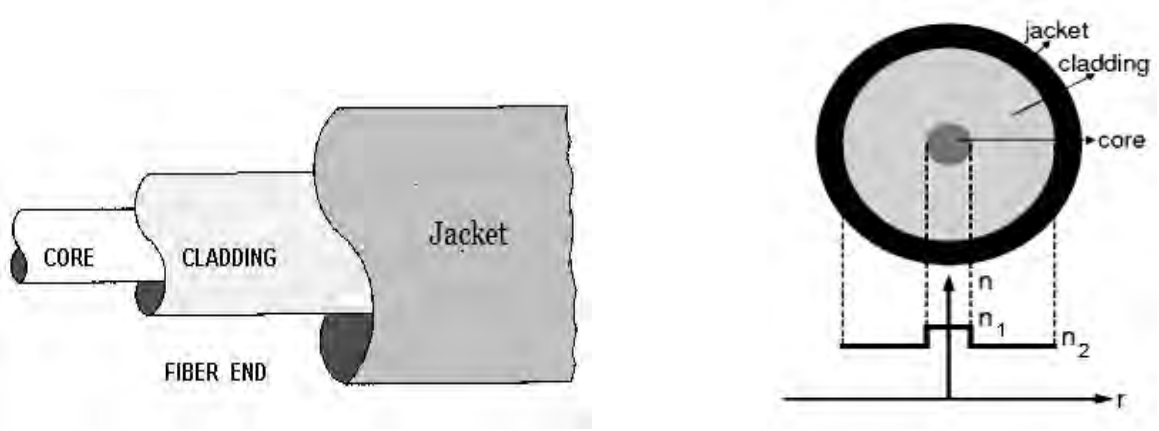

(a) (b)

Fig.2.1: (a) Basic structure of an optical fiber. (b) Cross section and refractive index profile of a conventional fiber.

The most widely accepted structure is the single solid dielectric cylinder with refractive index n_1 which is known as core. The core is surrounded by a solid dielectric cladding which has a refractive index n_2 and less than n_1. Refractive index profile of a conventional fiber is shown in Fig.2.1 (b). A conventional fiber with cylindrical symmetry consists of a central core surrounded by a cladding layer whose refractive index is slightly lower than that of the core. Such fibers are generally referred to as step-index fibers to distinguish them from graded-index fibers in which the refractive index of the core decreases gradually from centre to the core boundary.

2.2 PROPAGATION MECHANISM

The basic principle responsible for the guiding of light in conventional fibers is well known as (total internal reflection) TIR: A ray of light will be totally reflected at the interface between two dielectric media when it will incident from the medium with higher refractive index n_1 to lower n_2 and the incident angle is greater than the critical angle [1]. Where critical angle θ_c is the incident angle for which, angle of refraction θ_2 is 90º that is shown in Fig. 2.2.

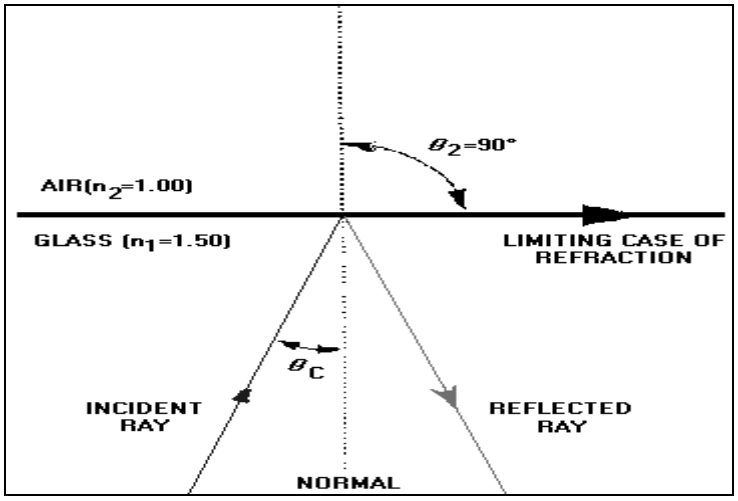

Fig.2.2 Critical angle and total internal reflection mechanism.

How a light ray is launched into a fiber is shown in Fig. 2.3. The incident ray I_1 enters the fiber at the angle θ_a. I_1 is refracted upon entering the fiber and is transmitted to the core-cladding interface. The ray then strikes the core-cladding interface at the critical angle (θ_c). I_1 is totally reflected back into the core and continues to propagate along the fiber. The incident ray I_1 enters the fiber at an angle

greater than θ_a. Again, I_2 is refracted upon entering the fiber and is transmitted to the core-cladding interface. I_2 strikes the core-cladding interface at an angle less than the critical angle (θ_c). I_2 is refracted into the cladding and is eventually lost. The light ray incident on the fiber core must be within the acceptance cone defined by the angle θ_a.

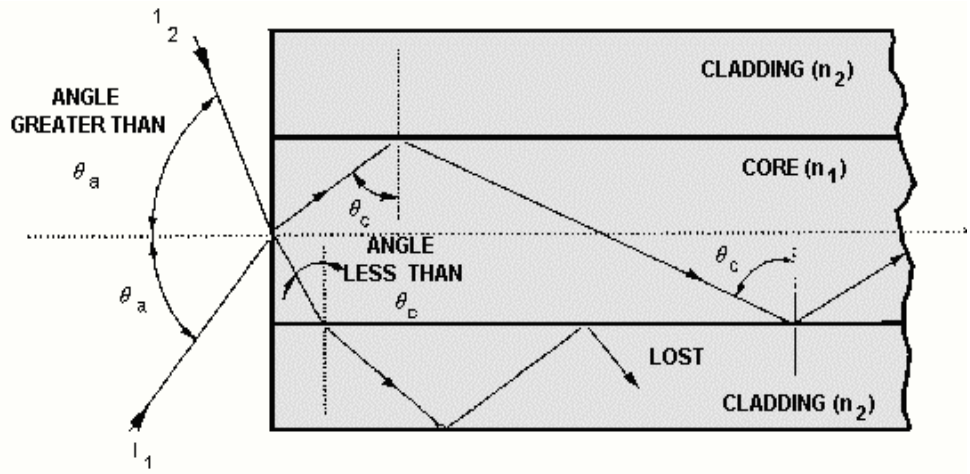

Fig.2.3 Guiding mechanism of light in optical fiber.

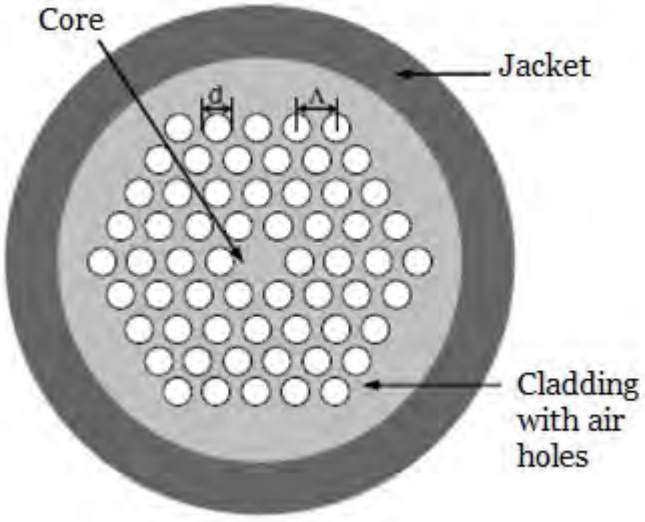

Fig.2.4 Schematic of a PCF cross section. The light grey areas are silica, the white areas are air holes and the dark grey areas are polymer coating. Λ is the hole-to-hole pitch and d is the hole diameter.

Like conventional fibers, PCFs contain the two-layer structure: a core and a cladding layer surrounding the core (Fig. 2.4). Total internal reflection photonic crystal fibers (TIR PCFs) are also

known as index-guiding PCFs. The most typical TIR PCFs have a solid core (often fabricated from pure silica) surrounded by a cladding with a regular periodic array of air holes. These air holes make the effective refractive index of the cladding region lower than pure silica, so light is confined to the solid core area, which has a relatively higher refractive index. A schematic cross section of such a PCF cross is given in Fig.2.4, where the two parameters which characterize the dimensions of PCFs are the hole-to-hole pitch Λ and the air hole diameter d [4].

From the guidance mechanism point of view, TIR PCFs guide light by TIR, as conventional fibers do. Thus it is convenient to establish an effective refractive index model to analyze the behaviors and characteristics of such PCFs since many concepts can be borrowed directly from conventional fibers.

However, this does not mean that TIR PCFs are just another kind of conventional fiber. There are three parameters known as hole-to-hole pitch Λ, air hole diameter d and core radius, ready to be controlled. The values of d/Λ and Λ, which are responsible for the air-filling ratio as well as the effective cladding index, can be adjusted over a large range. More degrees of design freedom enable TIR PCFs to exhibit some unique characteristics which are not obtainable in conventional fibers.

2.3 MODES OF PROPAGATION

Optical fiber is classified into two types on the basis of number of modes that propagate along the fiber [3].

(a) Single mode fiber: Single mode fibers allow only one mode to propagate, because the core size is small and approaches the operational wavelength. Single mode fibers currently exhibit the greatest transmission bandwidths and the lowest losses of the fiber transmission media [8-9].

(b) Multimode fiber: Multimode fibers allow the propagation of a finite number of guided modes along a channel. They have large core diameter and light can be launched to them easily. As the number of modes increases, the modal dispersion increases and this affects the system bandwidth.

2.3 GUIDING PROPERTIES OF OPTICAL FIBER

2.3.1 Effective Refractive Index

In homogeneous transparent media, the refractive index n can be used to quantify the increase in the wave number (phase change per unit length) caused by the medium: the wave number is n times higher than it would be in vacuum. The effective refractive index n_{eff} has the analogous meaning for light propagation in a waveguide; the propagation constant is the effective index times the vacuum wave number:

$$\beta = n_{eff} \frac{2\pi}{\lambda} \tag{2.1}$$

The effective refractive index depends not only on the wavelength but also (for multimode waveguides) on the mode in which the light propagates. For this reason, it is also called effective mode index [11-13].

Again effective refractive index is a number that quantify the phase delay per unit length in a waveguide, relative to the phase delay in vacuum. The rate of change of the fundamental LP_{01} mode propagating along a straight fiber is determined by the phase propagation constant β. It is directly related to the wavelength of LP_{01} mode λ_{01} by the factor of 2π. Hence:

$$\beta\lambda_{01} = 2\pi,$$

$$\text{or} \quad \lambda_{01} = \frac{2\pi}{\beta} \tag{2.2}$$

An effective refractive index for single mode fiber sometimes referred to as a phase index or normalized phase change coefficient, n_{eff} [13-14]. It is defined by the ratio of the propagation constant of the fundamental mode to that of the vacuum wave number, k:

$$n_{eff} = \frac{\beta}{k} \tag{2.3}$$

hence the wavelength of the fundamental mode λ_{01} is smaller than the vacuum wavelength λ by the factor $1/ n_{eff}$.

$$\lambda_{01} = \frac{\lambda}{n_{eff}} \tag{2.4}$$

2.3.2 Dispersion

Dispersion is the broadening or spreading of optical signal while it propagates inside the fiber. The phenomenon of spreading of optical pulse as it travels along the fiber and limits the information capacity of the fiber is known as dispersion. It cause the signal spread out and lose of original shape which makes difficult to detect by receivers at the end of fiber span [15-16]. The phenomenon is shown in Fig.2.6.

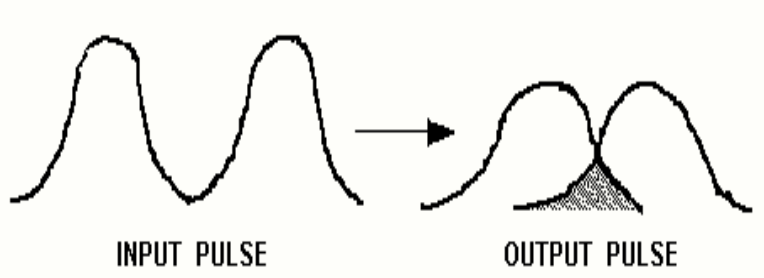

Fig.2.5 Effect of dispersion on optical signal.

Dispersion depends on the phase velocity or phase delay of light in some medium or device on some other parameter. The phase velocity of a wave is the rate at which the phase of the wave propagates in space. Phase velocity is given in terms of angular frequency ω and propagation constant β.

$$v_p = \frac{\omega}{\beta} \tag{2.5}$$

There are various different types of dispersion in optical fiber. These types are:

i) Chromatic dispersion
ii) Intermodal dispersion
iii) Polarization mode dispersion

2.3.2.1 Chromatic dispersion

The term “chromatic dispersion” covers all the phenomena associated with wavelength-dependent pulse spreading. Chromatic dispersion for single mode fiber can be divided into material and waveguide dispersion [16-17]. Material dispersion is caused by the wavelength dependence of the silica’s refractive index. Different colors light ray has different wavelength and light rays with different wavelengths travels with different speed. So at the fiber output the varying wavelength speed causes the light pulse spread in time.

$$D_{mat}(\lambda) = -\frac{\lambda}{c}\left|\frac{d^2 n_{eff}}{d\lambda^2}\right| \text{ ps/(nm.km)} \qquad (2.6)$$

Again waveguide dispersion is caused by the fact that light is guided by an optical fiber. After entering a singlemode fiber, an information carrying pulse is distributed between the core and the cladding. Its major portion travels within the core, the rest within the cladding. Both portions propagate at different velocities science the core and cladding has different refractive indexes. The pulse will spread simply because light is confined within a structure having different refractive indexes.

In a single mode fiber chromatic dispersion is sum of the material and waveguide dispersion.

$$D(\lambda) = D_{mat}(\lambda) + D_{wg}(\lambda) \text{ ps/(nm.km)} \qquad (2.7)$$

But waveguide dispersion in a single mode fiber is relatively small compared to material dispersion. So that, the chromatic dispersion parameter for unit length can be defined as:

$$D = -\frac{\lambda}{c}\left|\frac{d^2 n_{eff}}{d\lambda^2}\right| \text{ ps/(nm.km)} \qquad (2.8)$$

2.3.2.2 Intermodal dispersion

Intermodal dispersion results from different propagation characteristics of higher-order transverse modes in waveguides, such as multimode fibers. This effect can severely limit the possible data rate of a system for optical fiber communications based on multimode fibers. But single mode fiber does not show intermodal dispersion.

2.3.2.3 Polarization mode dispersion

The difference in refractive indexes along the x axis and the y axis, n_x and n_y respectively is called ***birefringence*** B [19-20].

$$B = n_x - n_y \qquad (2.9)$$

This formula implies that $n_x > n_y$; in other word, y is the fast axis, x the slow axis. Here "x" and "y" for these two axes have been chosen quite arbitrarily; usually the terms fast and slow are used to denote the appropriate axis.

In conventional single-mode fibers without birefringence design, *B* is small and changes randomly along the fiber because of variations in the core shape and the anisotropic stress acting on the core. Coupling between the two orthogonal polarization modes is easy and random. As a result, light launched into the fiber with linear polarization quickly reaches a state of arbitrary polarization. This effect results in the form of pulse spread called polarization-mode dispersion (PMD) that is shown in Fig.2.5. PMD is one of the limitations on high speed and high bit rate communication systems because it causes pulse spreading [18-19].

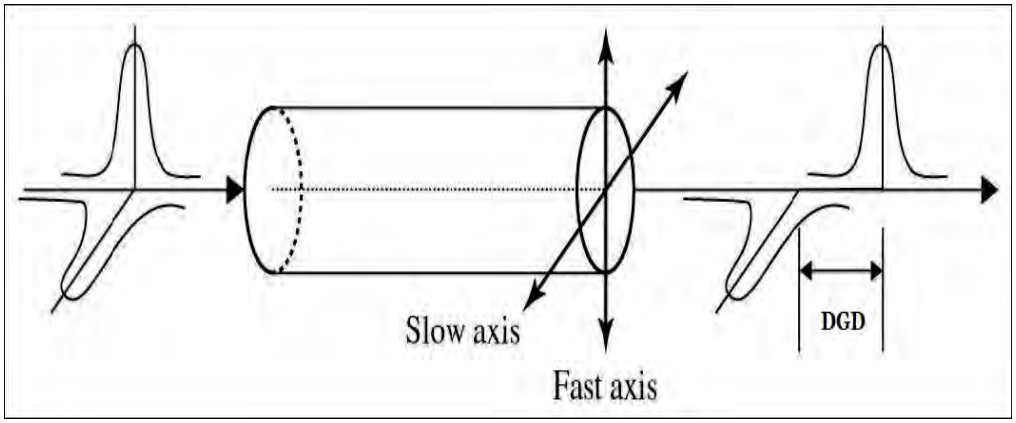

Fig.2.6 Schematic illustration of how birefringence induces a differential group delay (DGD) between the fast and slow polarization modes.

Again a large amount of birefringence can introduce intentionally in these fibers through design modifications so that small random birefringence fluctuations do not affect significantly the light polarization. In other words, coupling between the two orthogonal polarization modes can not occur because of the big difference between them. Such fibers are called polarization-maintaining (PM) fibers or highly birefringent fibers. Typically, B ~ 10^{-4} for PM fibers [20].

2.3.3 Mode field diameter

Although most light travels inside an optical fiber's core, the light actually spreads through a slightly larger volume including the inner edge of the fiber cladding. Mode field diameter is a measure of the spatial extent of the fundamental mode. It is generally taken as the distance between the opposite $1/e^2$ =0.135 points in relation to the corresponding value on the fiber axis.

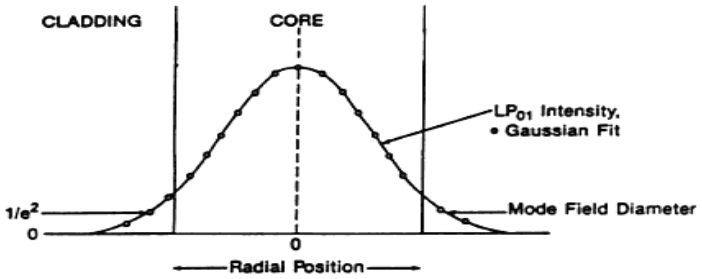

Fig.2.7 Mode field diameter of optical fiber.

Mode field diameter (MFD) is important for single mode fibers only. Its effect is so small in multimode fibers that it really doesn't matter any more. Mode field diameter plays an important role in estimating splice losses, source to fiber coupler losses, macro bending and micro bending losses, etc. For single mode fibers manufacturing, MFD is used as a rather more important parameter than fiber's core size.

2.3.4 Effective area

Effective area (EA) is a quantitative measure of the area which a waveguide or fiber mode effectively covers in the transverse dimensions [21]. Modes of fibers have smooth transverse profiles where the definition of a mode area is not straightforward, particularly for complicated mode shapes where e.g. some $1/e^2$ intensity criterion as for Gaussian beams is not sensible. A useful definition for the effective mode area is

$$A_{eff} = \frac{(\iint |E|^2 dxdy)^2}{\iint |E|^4 dxdy} \qquad (2.10)$$

where E is the electric field amplitude.

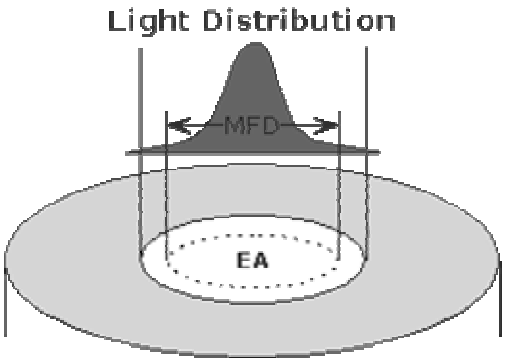

Fig.2.8 Effective area of optical fiber.

An important consequence of a small mode area is that the optical intensities for a given power level are high, so that nonlinearities become important. Also, small mode area is usually the consequence of strong guiding, where bend losses and other effects of external disturbances are weak.

2.3.5 Attenuation

Attenuation is the loss of optical power as light travels along the fiber [4]. Signal attenuation is defined as the ratio of optical input power (P_i) to the optical output power (P_o). Optical input power is the power injected into the fiber from an optical source. Optical output power is the power received at the fiber end or optical detector. The following equation defines signal attenuation as a unit of length:

$$\alpha_{db} L = 10\log_{10} \frac{P_i}{P_o} \qquad (2.11)$$

Signal attenuation is a log relationship. Length (L) is expressed in kilometers. Therefore, the unit of attenuation is decibels/kilometer (dB/km). Mainly, attenuation is caused by absorption, scattering, and bending losses. Each mechanism of loss is influenced by fiber-material properties and fiber structure. However, loss is also present at fiber connections and leakage.

2.3.5.1 Confinement loss

In both solid-core and hollow-core PCFs it is necessary to consider another contribution to the losses, that is the leakage or confinement losses [22]. These are due to the finite number of air-holes

which can be made in the fiber cross section. As a consequence, all the PCF guided modes are leaky. For example, in solid-core PCFs light is confined within a core region by the air-holes. Light will move away from the core if the confinement provided by the air-holes is inadequate [23]. Because of the finite transverse extent of the confining structure, the effective index is a complex value; its imaginary part $Im(n_{eff})$ is related to losses L (in decibels per meter) through the relation

$$L = \frac{40\pi.\mathrm{Im}(n_{eff}) \times 10^6}{\lambda \ln(10)} \quad . \tag{2.12}$$

This means that it is important to design such aspects of the PCF structure as air-hole diameter and hole-to-hole spacing, or pitch, in order to realize low-loss PCFs. In particular, the ratio between the air-hole diameter and the pitch must be designed to be large enough to confine light into the core. On the other hand, a large value of the ratio makes the PCF multi-mode. However, by properly designing the structure, the confinement loss of single-mode PCFs can be reduced to a negligible level.

Recently, several analyses have been performed in order to find the guidelines to design PCFs with negligible leakage losses [1.32–1.37dB]. It has been demonstrated a strong dependence of the confinement losses on the number of air-hole rings, especially for fibers with high air-filling fraction.

Chapter 3

STRESS ANALYSIS IN PCF

PCFs have many uses as underwater and underground communication systems, sensor for stress, polarization maintaining fiber etc [19-20], [30]. Depending on fiber uses the propagation properties also varies. In practical hydrostatic pressure, axial force, twisting, and elongation may cause fiber deformation and change of these propagation properties. The Optical fiber fabrication requires high temperature. Again, the fiber is drawn from a cylindrical structure at high temperature. When the fiber is cooled to room temperature, different portions of the fiber show different amount of expansion due to differences in the thermal expansion coefficient. This induces a stress which is termed as thermal stress. This effect results in the change of refractive indices as well as birefringence and other associated properties. So it is essential to perform stress analysis before calculating propagation modes, to observe the changes of propagation properties by both external and thermal stress [26-27]. At first we explain the stress analysis and then optical analysis.

3.1 STRESS ANALYSIS

Let us consider a body that is long along its z-axis direction compared to its cross sectional area, such as optical fibers and waveguides. In this case, strain in the body along the z-direction ε_z is considered to be zero, except at both ends. Then we can assume, $\varepsilon_z = 0$. Stress analysis based on this assumption is called a “plane strain problem” [28].

The relationship between displacement and strain is given by

$$\varepsilon_x = \frac{\partial u}{\partial x}, \tag{3.1a}$$

$$\varepsilon_y = \frac{\partial v}{\partial y}, \tag{3.1b}$$

$$\gamma_{xy} = \frac{\partial v}{\partial x} + \frac{\partial u}{\partial y}. \tag{3.1c}$$

Next, the relationship between stress and strain is generally expressed as

$$\varepsilon_x = \frac{1}{E}[\sigma_x - \nu(\sigma_y + \sigma_z)] + \alpha\Delta T; \tag{3.2a}$$

$$\varepsilon_y = \frac{1}{\mathrm{E}}[\sigma_y - \nu(\sigma_z + \sigma_x)] + \alpha\Delta T\,; \tag{3.2b}$$

$$\varepsilon_z = \frac{1}{\mathrm{E}}[\sigma_z - \nu(\sigma_x + \sigma_y)] + \alpha\Delta T; \tag{3.2c}$$

$$\gamma_{xy} = \frac{\tau_{xy}}{G} = \frac{2(1+\nu)}{E}\tau_{xy}\,; \tag{3.3}$$

Where, u and v be the displacements along the x- and y-axis directions respectively; ε_x, ε_y and ε_z are principal strains along x-,y- and z-directions respectively; γ_{xy} is shear strain in the x-y plane; σ_x, σ_y, σ_z are principal stress along x-,y- and z-directions respectively; τ_{xy} is shear strain in the x-y plane; E and ν are the Young's modulus and Poisson's ratio; G, α and ΔT are shear modulus, thermal expansion coefficient, and temperature change.

By putting ε_z =0 in (3.3), the relationship between stress and strain in the plane strain is given by

$$\sigma_x = \frac{E}{(1+\nu)(1-2\nu)}[(1-\nu)\varepsilon_y + \nu\varepsilon_x] - \frac{\alpha\mathrm{E}\Delta\mathrm{T}}{1-2\nu}\,, \tag{3.4a}$$

$$\sigma_y = \frac{E}{(1+\nu)(1-2\nu)}[(1-\nu)\varepsilon_y + \nu\varepsilon_x] - \frac{\alpha\mathrm{E}\Delta\mathrm{T}}{1-2\nu}\,, \tag{3.4b}$$

$$\sigma_z = \nu(\sigma_x + \sigma_y) - \alpha E\Delta T \tag{3.4c}$$

By putting σ_z =0 in (3.3), the relationship between stress and strain in the plane stress is given by

$$\sigma_x = \frac{\mathrm{E}}{1-\nu^2}[\varepsilon_x + \nu\varepsilon_y] - \frac{\alpha\mathrm{E}\Delta\mathrm{T}}{1-\nu}\,, \tag{3.5a}$$

$$\sigma_y = \frac{\mathrm{E}}{1-\nu^2}[\varepsilon_y + \nu\varepsilon_x] - \frac{\alpha\mathrm{E}\Delta\mathrm{T}}{1-\nu}\,. \tag{3.5b}$$

The components of stress, strain and initial strain due to thermal strain are expressed as

$$\{\sigma\} = \begin{pmatrix} \sigma_x \\ \sigma_y \\ \tau_{xy} \end{pmatrix} \tag{3.6}$$

$$\{\varepsilon\} = \begin{pmatrix} \varepsilon_x \\ \varepsilon_y \\ \gamma_{xy} \end{pmatrix} \tag{3.7}$$

$$\{\varepsilon_0\} = (1+\nu\alpha\Delta T)\begin{pmatrix} 1 \\ 1 \\ 0 \end{pmatrix} \tag{3.8}$$

Now the relation between stress and strain can be expressed by (3.7-3.9):

$$\{\sigma\} = D[\{\varepsilon\} - \{\varepsilon_0\}], \tag{3.9}$$

Where elasticity matrix $D = \frac{E}{(1+v)(1-2v)} \begin{bmatrix} (1-v) & v & 0 \\ v & (1-v) & 0 \\ 0 & 0 & (1-2v)/2 \end{bmatrix}$ (3.10)

So strain energy per unit length is obtained by

$$\text{Strain energy} = \frac{1}{2}\int\int \text{stress.(strain}-\text{initial strain)}\, dxdy = \frac{1}{2}\iint \{\sigma\}^t[\{\varepsilon\} - \{\varepsilon_0\}]dxdy \tag{3.11}$$

Where, $\{\sigma\}^t$ is a row vector of $\{\sigma\}$. The entire fiber structure is divided into small elements and the integral of (3.12) is carried out in each element.

If triangular elements are applied, the strain component in the eth (e=1-N) element are obtained as

$$\begin{pmatrix} \varepsilon_x \\ \varepsilon_y \\ \gamma_{xy} \end{pmatrix} = \frac{1}{2s_e} \begin{bmatrix} (y_j - y_k) & 0 & (y_k - y_i) & 0 & (y_i - y_j) & 0 \\ 0 & (x_k - x_j) & 0 & (x_i - x_k) & 0 & (x_j - x_i) \\ (x_k - x_j) & (y_j - y_k) & (x_i - x_k) & (y_k - y_i) & (x_j - x_i) & (y_i - y_j) \end{bmatrix} \begin{pmatrix} u_i \\ v_i \\ u_j \\ v_j \\ u_k \\ v_k \end{pmatrix} \tag{3.12}$$

where x_i, x_j, x_k and y_i, y_j, y_k are the x and y coordinates of the three vertices of the triangular element and s_e is the cross sectional area of eth element.

This is rewritten in matrix form as $\{\varepsilon^e\} = B_e\{d^e\}$, (3.13)

Where, B_e is strain matrix and d^e matrix represent displacements.

So the strain energy of eth element, $U^e = 0.5\iint \{\sigma^e\}^t[\{\varepsilon^e - \{\varepsilon_0^e\}\}]dxdy$ (3.14)

Where $\{\sigma^e\}^t = [\{\varepsilon^e\}^t - \{\varepsilon_0^e\}^t]D_e = [B_e^t\{d^e\}^t - \{\varepsilon_0^e\}^t]D_e$. (3.15)

In this equation, element matrix D_e may be different in each element since Young's modulus and Poisson's ratio are different in core and substrate region.

The strain energy of eth element can be expressed as

$$U_e = \frac{1}{2}\{d^e\}^t A_e\{d^e\} - \{d^e\}^t\{h^e\} \tag{3.16}$$

Where A_e is a 6X6 element stiffness matrix and $\{h^e\}$ is a 6X1 thermal stress vector, which are given by

$$A_e = s_e B_e^t D_e B_e \tag{3.17a}$$

$$\{h^e\} = s_e B_e^t D_e \{\varepsilon_0^e\}. \tag{3.17b}$$

The total strain energy is obtained by summing element strain energy:

$$U = \frac{1}{2}\{d\}^t A\{d\} - \{d\}^t \{H\} \tag{3.18}$$

Where $\{d\}$,A and $\{H\}$ are the 2n×1 global strain vector, the 2n×2n global stiffness matrix and the 2n×1 global thermal stress vector respectively.

An external force applied to the body is approximated by the force concentrated at the node on the surface of the body. The total work done by the external force is then given by

$$V = \{d\}^t \{f_L\}. \tag{3.19}$$

where $\{f_L\}$ is 2n×1 global load vector.

So the total potential energy, $P_t = [\frac{1}{2}\{d\}^t A\{d\} - \{d\}^t [\{H\} + \{f_L\}]]l$. (3.20)

Potential energy should be minimal by energy principle. So the partial derivative of P_t with respect to the displacement of each nodal point should be zero. We then have the 2nth order linear simultaneous equations:

$$A\{d\} = \{H\} + \{f_L\}. \tag{3.21}$$

The solution of the displacement vector is:

$\{d\} = A^{-1}[\{H\} + \{f_L\}]$

The solution gives the displacements at all nodal points of the fiber or waveguide under thermal stress and external forces.

In optical fibers or waveguides under stress, the original refractive index of the material changes due to photoelastic effect. The new refractive index for x and y polarized light can be calculated from the following equation:

$$\begin{bmatrix} n_x(x,y) \\ n_y(x,y) \\ n_z(x,y) \end{bmatrix} = \begin{bmatrix} n_{x0}(x,y) \\ n_{y0}(x,y) \\ n_{z0}(x,y) \end{bmatrix} - \begin{bmatrix} C_1 & C_2 & C_2 \\ C_2 & C_1 & C_2 \\ C_2 & C_2 & C_1 \end{bmatrix} \begin{bmatrix} \sigma_x(x,y) \\ \sigma_y(x,y) \\ \sigma_z(x,y) \end{bmatrix} \tag{3.22}$$

Here, C_1, C_2 are the elasto-optic coefficient of the fiber or waveguide material, n_{x0} , n_{y0} and n_{z0} are the unstressed refractive indices of the material and n_x, n_y and n_z are the main diagonal element of the anisotropic refractive index tensor.

3.2 FINITE ELEMENT METHOD

To study the distribution of stresses in an optical fiber, the finite element method (FEM) is a highly suitable method to be applied due to its flexibility and power [13-14]. For this purpose, the equilibrium equations need to be established through minimizing the total energy (P_t) of the fiber system,

$$P_t = \text{internal work} - \text{external work} = \frac{1}{2} l \int_s \sigma^t \varepsilon ds - l \int_L [d]^t F dl \quad (3.23)$$

Where l is the length of the optical fiber, σ and ε are the stress and strain vectors respectively, d the displacement vector at any point, and F is the external forces applied. The first integration takes place over the cross section of the fiber and the second integration along the boundary of the fiber section. The first integration represents the internal strain energy, while the second indicates the work contribution of the applied loads.

3.3 OPTICAL ANALYSIS

Optical analysis is performed for calculating the effective mode indices for different modes propagating within the fiber [8-12]. It involves dealing with perpendicular hybrid mode waves. The mode analysis is made on a cross-section in the x-y plane of the fiber.

3.3.1 Perfectly Matched Layers

Perfectly Matched Layer (PML) is an absorbing layer specially studied to absorb without reflection the electromagnetic waves [22-23]. Using this layer, we can estimate the confinement loss of any optical fibre. The PML formulation can be deduced from Maxwell's equations by introducing a complex-valued coordinate transformation under the additional requirement that the wave impedance should remain unaffected. From the implementation viewpoint, it is more practical to describe the PML as an anisotropic material with losses.

To define a PML, add an additional modeling domain (subdomain) outside the boundaries that you would like to be absorbing. The PML can have arbitrary thickness and is specified to be made of an artificial absorbing material. The material has anisotropic permittivity and permeability that match the permittivity and permeability of the physical medium outside the PML in such a way that there are no reflections. Introduce a new sub domain representing an absorbing layer with anisotropic material parameters

permeability, $\mu = \mu_0 \mu_r L$ and

permittivity, $\varepsilon = \varepsilon_0 \varepsilon_r L$.

An eigenvalue equation for the magnetic field ***H*** is derived from Helmholtz equation

$$\nabla \times (\vec{\varepsilon}^{-1} \nabla \times \quad) - k_0^2 \vec{\mu} \quad = 0 \tag{3.24}$$

In 2-dimensional case, a circular PML is an absorbing region surrounding the fiber structure [34]. The thickness is noted e and the internal radius r_{in}, (ρ-r_{in}) is the distance inside the PML measured from the interface between the PML and the edge of the computational window. The PML is schematically shown in Fig.3.2:

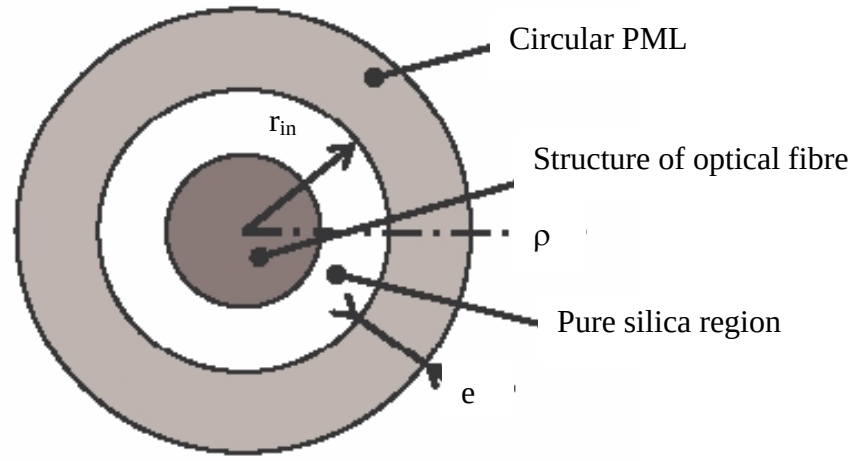

Fig.3. 1 Cross section of optical fiber surrounded by circular PML.

For the cylindrical PML, assuming cylindrical coordinates (ρ,φ,z), we get

$$L = \begin{bmatrix} L_{xx} & L_{xy} & 0 \\ L_{yx} & L_{yy} & 0 \\ 0 & 0 & L_{zz} \end{bmatrix} \tag{3.25}$$

where

$$L_{xx} = s_z \left(\frac{s_\varphi}{s_\rho} \cos^2 \varphi + \frac{s_\rho}{s_\varphi} \sin^2 \varphi \right)$$

$$L_{xy} = s_z \cos\varphi \sin\varphi \left(\frac{s_\varphi}{s_\rho} - \frac{s_\rho}{s_\varphi} \right)$$

$$L_{yx} = s_z \cos\varphi \sin\varphi \left(\frac{s_\varphi}{s_\rho} - \frac{s_\rho}{s_\varphi} \right)$$

$$L_{yy} = s_z \left(\frac{s_\varphi}{s_\rho} \sin^2\varphi + \frac{s_\rho}{s_\varphi} \cos^2\varphi \right)$$

$$L_{zz} = \frac{s_\rho s_\varphi}{s_z}$$

The parameters s_ξ, s_ψ and s_ζ are the complex-valued coordinating scaling parameters. The interpretation of the parameters s_ρ, s_φ and s_z is the same as for s_ξ, s_ψ and s_ζ. The s_φ and s_z to be 1 in all regions, and let s_ρ take the following form

$$s_\rho = \begin{cases} 1 - j.\frac{3\lambda}{4\pi ne}.\left(\frac{\rho - r_{in}}{e} \right)^2 .\ln\left(\frac{1}{R} \right), & \text{In PML region} \\ 1 & \text{In other regions} \end{cases}$$

where R is a theoretical reflection coefficient at the interface between the PML and the edge of the computational window. The absorption of the PML will be optimal when reflection coefficient R at the interface between PML and pure silica region is small.

The wave propagates in the z direction and has the form

$$(x, y, z, t) = \quad (x, y) e^{j(\omega t - \beta z)} \tag{3.26}$$

where ω is the angular frequency and β the propagation constant. An eigenvalue equation for the magnetic field $\boldsymbol{H}$ is derived from Helmholtz equation in the fiber cross section reduces to:

$$\nabla \times ([n]^{-2} \nabla \times \quad) - k_0^2 \quad = 0 \tag{3.27}$$

which is solved for the eigenvalue $\lambda = -\beta^2$.

As boundary condition along the outside of the cladding the magnetic field is set to zero. Because the amplitude of the field decays rapidly as a function of the radius of the cladding this is a valid boundary condition.

This condition is expressed by the equation: $\times \quad = 0$

For a confined mode there is no energy flow in the radial direction, thus the wave must be evanescent in the radial direction in the cladding. This is true only if

$$n_{eff} > n_2$$

On the other hand, the wave cannot be radially evanescent in the core region. Thus

$$n_2 < n_{eff} < n_1$$

The waves are more confined when n_{eff} is close to the upper limit in this interval.

Effective mode index of a confined mode, $n_{eff} = \frac{\beta}{k_0}$

The effective index (n_{eff}) found here is a complex number and the real part is used to calculate dispersion and the imaginary part is used for confinement loss calculation.

Chapter 4

PCF DESIGN PRINCIPLES

High-index guiding PCFs have a solid core surrounded by a cladding with a regular periodic array of air holes. That show excellent propagation properties in contrast of conventional fibers. All of these properties are related to the fiber design, namely, pitch, air-hole diameter and number of air-hole rings around the core. In this chapter we shall discuss about the fiber design that we have considered for our experiment. We shall also find out the air filling ratios for different designed PCFs.

4.1 PCF DESIGNING PARAMETERS

We are considering three types of air hole arrangements for designing PCFs.

- Square PCF (the structures are designed by square air hole arrangement).
- Hexagonal PCF (the structures are designed by hexagonal air hole arrangement).
- Octagonal PCF (the structures are designed by octagonal air hole arrangement).

Here solid core index guiding PCFs are made by only single material (SiO2), where refractive index n_s=1.45 [6]. Operating wave length varies from 1μm to 2μm. External stress is considered here from 0Pa to 5GPa, d is the air-hole diameter, Λ is pitch (distance between two air holes) and Nr is the number of air hole rings [8-9].

The dimensions of the structures of square and hexagonal PCFs initially are-

Cross sectional radius, R = 12.0 μm

Pitch, Λ =2.5 μm

Number of air hole rings, Nr = 1, 2, 3 and 4

PML width, e = 1 μm

Air hole diameter, d = 1.4 μm.

To compare the propagation properties of both square and hexagonal PCFs the designs are varied by changing number of air hole rings assuming that other parameters are same.

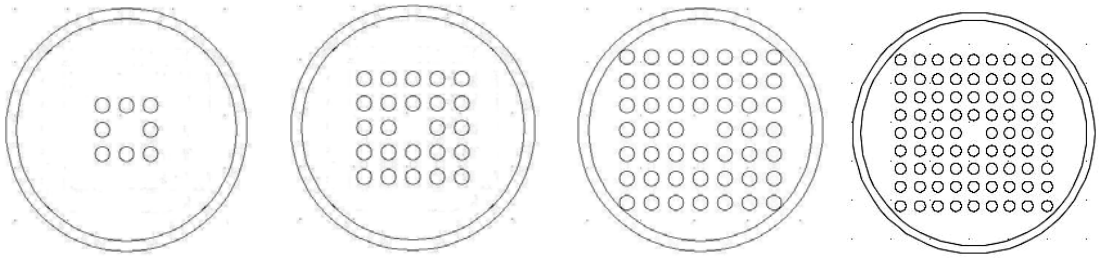

(a) (b) (c) (d)

Fig.4.1 shows the cross-section of square PCF, where (a) Nr=1, (b) Nr=2, (c) Nr=3 and (d) Nr=4.

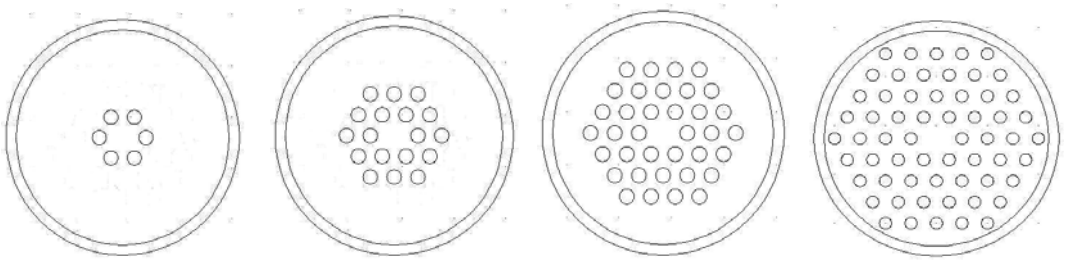

(a) (b) (c) (d)

Fig.4.2 shows the cross-section of hexagonal PCF, where (a) Nr=1, (b) Nr=2, (c) Nr=3, (d) Nr=4.

For hexagonal and octagonal structures initially the dimensions of the structure are-

Cross sectional radius, R = 12.0 μm

Pitch, Λ =2.5 μm

Number of air hole rings, Nr = 4

PML width, e = 1 μm

Air hole diameter, d = 0.8 μm, 1.0 μm, 1.2 μm, 1.4 μm 1.6 μm

Designs are varied by changing air hole diameter.

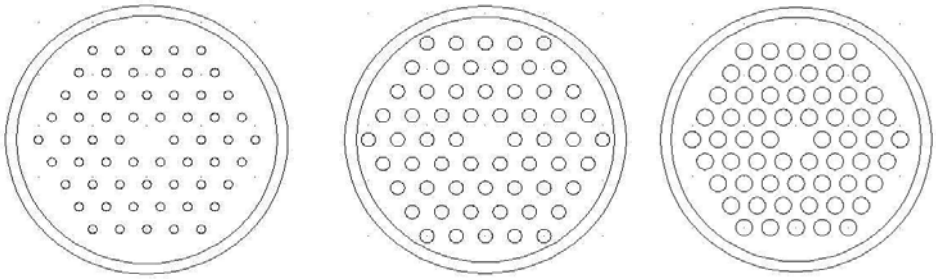

(a) (b) (c)

Fig.4.3 shows the cross-section of hexagonal PCF, where (a) d=0.8μm, (c) d=1.2μm, (c) d=1.6μm.

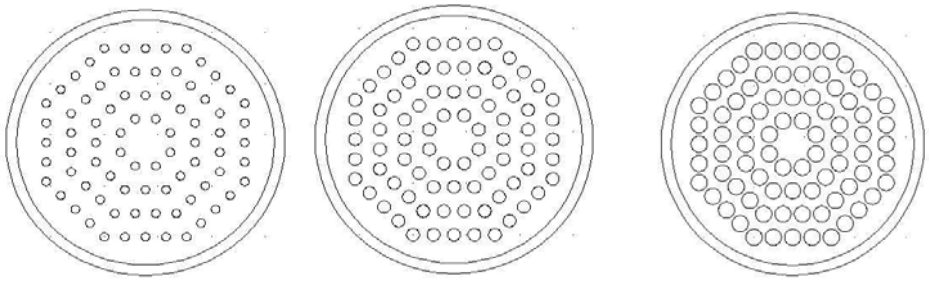

(a) (b) (c)

Fig.4.4 shows the cross-section of octagonal PCF, where (a) d=0.8μm, (b) d=1.2μm, (c) d=1.6μm.

4.2 AIR FILLING FRACTION

Air filling fraction (AFF) of PCF is the ratio of total area of air in fiber cross section to total cross sectional area of the fiber [10-11]. It presents the amount of air in the fiber cross section.

$$AFF = \frac{A_{hole}}{A_{cell}} \tag{4.1}$$

where,

A_{hole}= area of the air hole inside the unit triangle,

A_{cell}= area of the unit triangle.

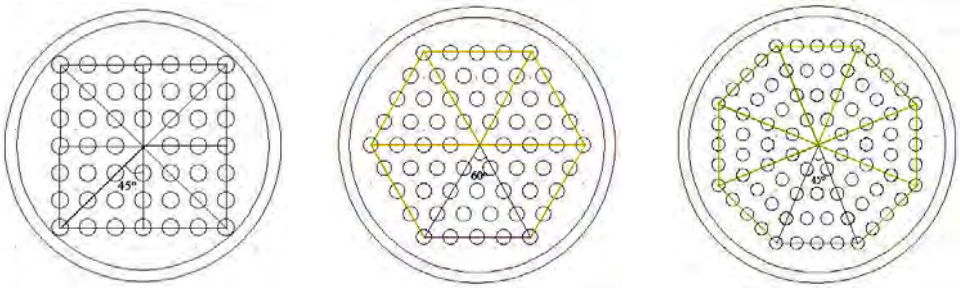

(a) (b) (c)

Fig.4.5 Fiber cross section (a) square, (b) hexagonal, (c) octagonal PCF.

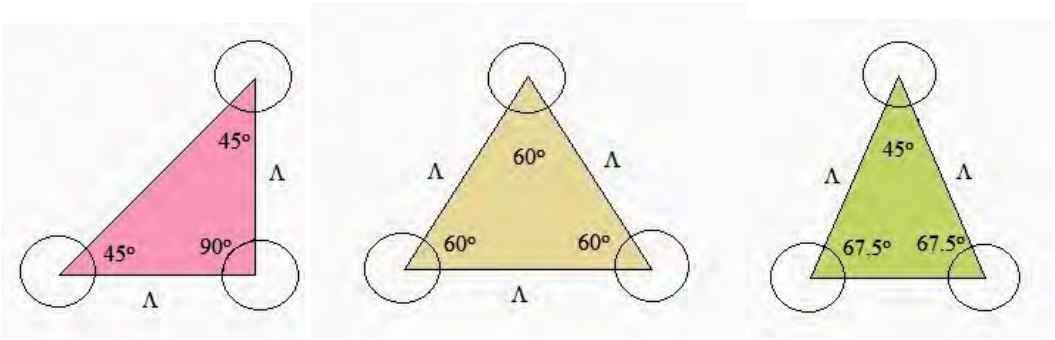

(a) (b) (c)

Fig.4.6 The unit triangle (a) square, (b) hexagonal, (c) octagonal PCF.

Area of a circular air hole, $a_{hole} = \pi r^2$

where, $r = \frac{d}{2}$

$$\therefore a_{hole} = \pi \frac{d^2}{4} \tag{4.2}$$

The unit triangle has ½ area of an air hole. Because, it covers 180^o area of a circular air hole.
So area of air hole in a triangle,

$$A_{hole} = \frac{a_{hole}}{2} = \pi \frac{d^2}{2 \times 4} = \pi \frac{d^2}{8} \tag{4.3}$$

From the figure we can see that the unit triangle for square PCF is a right triangle.
We know that the area of a right triangle is

$$Area = \frac{1}{2} \times base \times height \ .$$

We get the area of unit triangle for square PCF according to the rules of right angle,

$$A_{cell(Sqr)} = \tfrac{1}{2} \Lambda^2 .$$

$\therefore$ Air filling fraction for square PCF is

$$AFF_{Sqr} = \frac{A_{hole}}{A_{cell(Sqr)}} = \frac{\frac{\pi d^2}{8}}{\frac{1}{2}\Lambda^2} = \frac{\pi}{4} \times \left(\frac{d}{\Lambda}\right)^2 = 0.7854 \times \left(\frac{d}{\Lambda}\right)^2 \tag{4.4}$$

Again we know that the area of a triangle also can be calculated by the following equation

$$Area = \frac{1}{2} \times a \times b \times Sin(C)$$

where, a and b are the lengths of two sides and C is the angle between them.

We get the area of unit triangle for hexagonal PCF by following equation (4.1),

$$A_{cell(Hexa)} = \frac{1}{2}\Lambda^2 \times Sin(60^o) = \frac{1}{2}\Lambda^2 \times \frac{\sqrt{3}}{2} = \frac{\sqrt{3}}{4}\Lambda^2 \tag{4.5}$$

$\therefore$ Air filling fraction for hexagonal PCF is

$$AFF_{Hexa} = \frac{A_{hole}}{A_{cell(Hexa)}} = \frac{\frac{\pi d^2}{8}}{\frac{\sqrt{3}}{4}\Lambda^2} = \frac{\pi}{2\sqrt{3}} \times \left(\frac{d}{\Lambda}\right)^2 = 0.969 \times \left(\frac{d}{\Lambda}\right)^2 \tag{4.6}$$

Similarly we get the area of unit triangle for octagonal PCF by following equation (4.1),

$$A_{cell(Octa)} = \frac{1}{2}\Lambda^2 \times Sin(45^o) = \frac{1}{2}\Lambda^2 \times \frac{1}{\sqrt{2}} = \frac{1}{2\sqrt{2}}\Lambda^2 \tag{4.7}$$

$\therefore$ Air filling fraction for octagonal PCF is

$$AFF_{Octa} = \frac{A_{hole}}{A_{cell(Octa)}} = \frac{\frac{\pi d^2}{8}}{\frac{1}{2\sqrt{2}}\Lambda^2} = \frac{\pi}{2\sqrt{2}} \times \left(\frac{d}{\Lambda}\right)^2 = 1.11 \times \left(\frac{d}{\Lambda}\right)^2 \tag{4.8}$$

From the above equations (4.4), (4.6) and (4.8) we find that

$$AFF_{Sqr} \angle AFF_{Hexa} \angle AFF_{Octa}$$

Total number of air holes in square PCFs is

$$N_s = \sum_{i=0}^{Nr} i \times 8 = \frac{1}{2} N_r \times (N_r + 1) \times 8 . \tag{4.9}$$

Total number of air holes in hexagonal PCFs is

$$N_h = \sum_{i=0}^{Nr} i \times 6 = \frac{1}{2} N_r \times (N_r + 1) \times 6 . \tag{4.10}$$

Total number of air holes in octagonal PCFs is

$$N_o = \sum_{i=0}^{Nr} i \times 8 = \frac{1}{2} N_r \times (N_r + 1) \times 8 . \quad (4.11)$$

We considered here only circular shape air holes and area of each air hole is πr^2. Under same number of air hole rings and air hole diameter A_s, A_h and A_o are the total air-hole cross sectional area for square, hexagonal and octagonal PCFs respectively.

$$A_s = N_s \times \pi r^2 \quad (4.12)$$

$$A_h = N_h \times \pi r^2 \quad (4.13)$$

$$A_o = N_o \times \pi r^2 . \quad (4.14)$$

From (4.12), (4.13) and (4.14) it can be shown that $A_0 = 1.33 A_h$ and $As = 1.33 A_h$. That means total air-hole cross sectional area for square and octagonal PCFs is about 33% greater than hexagonal with same Nr and d.

4.2 SELLMEIER EQUATION AND COEFFICIENT

For the specification of a wavelength-dependent refractive index of a transparent optical material, it is common to use Sellmeier formula [33]. This formula is very useful, as it makes possible to describe accurately the refractive index of material in a wide wavelength range with only a few so-called Sellmeier coefficients, which are usually obtained from measured data with some least-square fitting algorithm. Sellmeier coefficients for many optical materials are available in databases.

In its most general form, the Sellmeier equation is given as:

$$n^2(\lambda) = 1 + \sum_i \frac{A_i \lambda^2}{\lambda^2 - B_i} \quad (4.15)$$

The usual form of the equation for glass is

$$n^2(\lambda) = 1 + \frac{A_1 \lambda^2}{\lambda^2 - B_1} + \frac{A_2 \lambda^2}{\lambda^2 - B_2} + \frac{A_3 \lambda^2}{\lambda^2 - B_3} \quad (4.16)$$

where n is the refractive index, λ is the vacuum wavelength, and A_1, A_2, A_3, B_1, B_2 *and* B_3 are experimentally determined Sellmeier coefficients. These coefficients are usually quoted for λ in micrometers. The value of the coefficients is given in Table 4.1.

Table 4.1: Sellmeier coefficients.

Material	A_1	B_1 (µm)	A_2	B_2 (µm)	A_3	B_3 (µm)
Silica (SiO_2)	0.6961663	0.0684043	0.4079426	0.1162414	0.8974794	9.896161

By calculation,

$n = 1.444$

where, operating wavelength, λ is taken to be 1.55 µm.

For analysis of the fiber, the geometrical and mechanical parameters are shown in Table 4.2.

Table 4.2: Core, cladding and hole parameters.

Parameter	Core (SiO_2)	Cladding(SiO_2)	Air hole
Young's modulus, E	7830 Kg/mm^2	7830 Kg/mm^2	1.42×10^5 pa
Poisson's ratio, ν	0.186	0.186	0.186
Elasto-optic coefficient	$C_1=0.757\times10^{-12}$ m^2/N $C_2=0.4185\times10^{-11}$ m^2/N	$C_1=0.757\times10^{-12}$ m^2/N $C_2=0.4185\times10^{-11}$ m^2/N	$C_1=0.757\times10^{-12}$ m^2/N $C_2=0.4185\times10^{-11}$ m^2/N
Thermal expansion coefficient, α	2×10^{-6} /°C	1×10^{-6} /°C	3.43×10^{-3} /°C

Chapter 5

RESULTS AND DISCUSSION

To carry out our experiment here we have considered three different types of air hole arrangements for fiber design (square, hexagonal and octagonal). We have used COMSOL Multiphysics as a modeling and simulation tool, where a combination of structural mechanics module and electromagnetic module has been used to carry out the stress analysis and optical mode analysis of the PCFs respectively [34]. The Finite Element Method (FEM) offers the ability to examine arbitrary fiber configurations, specifically through deformation where the fiber is no longer circularly symmetric [13-14]. Electromagnetic module has been used to carry out the stress analysis and optical mode analysis of the PCFs respectively. External stress causes change of refractive index of fiber and we have obtained this result from plain stress analysis then we have used these results as input information for optical analysis by FEM. We have got the modal effective index as the output of optical analysis. For all types of fibers we have observed the effect of stress on their propagation properties like– effective index, birefringence, confinement loss, effective area and polarization mode dispersion. Then we have compared the results for square, hexagonal and octagonal PCFs. Thus our research findings will help to identify the proper design scheme of PCF for particular application.

5.1 SQUARE PCFs

Depending on the air arrangement the PCFs are called square, hexagonal, octagonal etc. Square PCFs are designed by square air hole arrangement [9]. Here we have designed different square PCFs by varying number of air hole rings. At first we designed the PCFs using COMSOL metaphysics drawing environment. To observe stress effect on the PCFs we have to find out the propagation properties of unstressed and stressed PCFs. For unstressed PCFs optical analysis is performed for calculating the effective mode indices for different modes propagating within the fiber. Then we carried out stress analysis to investigate the diversity of propagation characteristics in PCFs under

lateral forces from different directions. Stress distribution in the fiber's cross section and deformation of the fiber's structure both factor induces different modal effective index in both axis (x and y). The stress-induced effective index of the fundamental guided mode, birefringence and confinement loss are analyzed here separately.

Fig. 5.1 shows the vector displacement over the cross section of the PCF under external stress with a maximum displacement and the minimum displacement, where the arrow direction shows pressure is applied uniformly from all directions. Fig.5.2 shows the surface total displacement for hexagonal air-hole arrangement, which occurred due to effect of external stress and causes deformation in fiber structure. This deformation causes change in material refractive index. The effect of stress on the refractive index also causes a change in the mode field distribution. For the fundamental *x* polarized mode, the surface power flow is shown in the Fig.5.3.

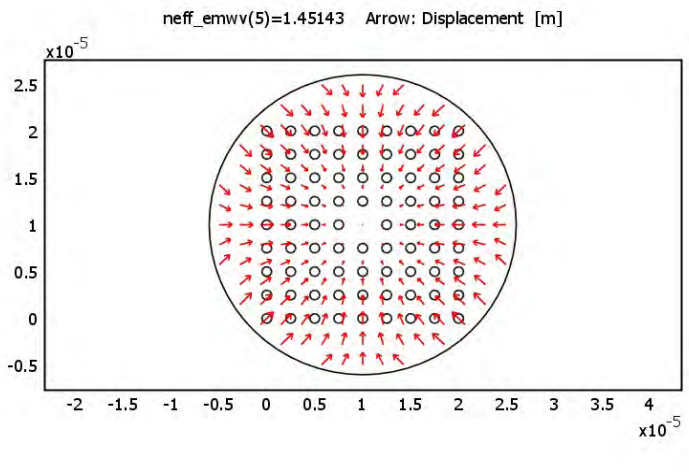

Fig. 5.1 Arrow displacement under external stress for square air hole arrangement PCF with external stress 5GPa, where d=1.2µm, Λ=2.5 µm and Nr=4.

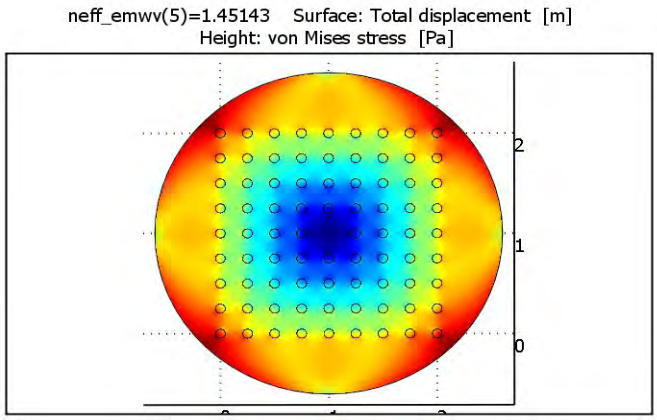

Fig. 5.2 Surface total displacement under external stress for square air hole arrangement PCF with external stress 5GPa, where d=1.2μm, Λ=2.5μm and Nr=4.

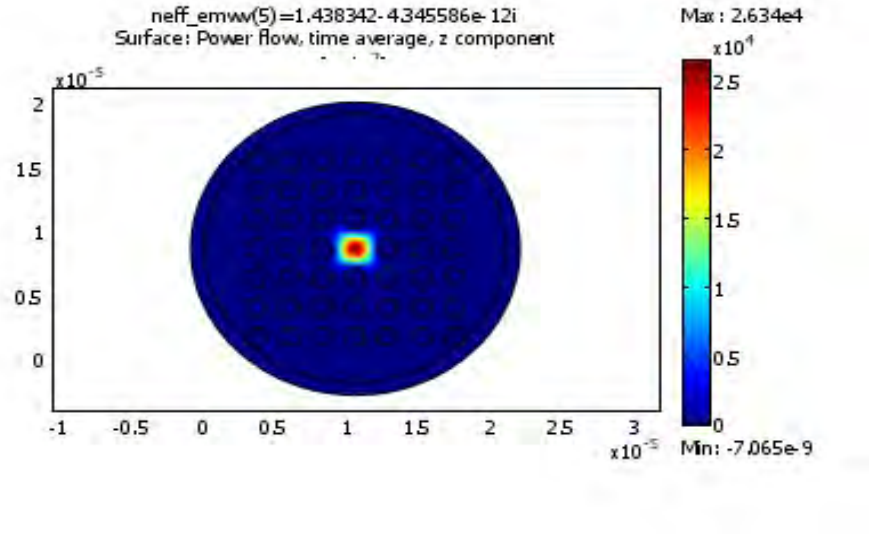

Fig. 5.3 Surface power flow, time average z component under external stress for square air hole arrangement with external stress 5GPa, where d=1.4μm, Λ=2.5μm and Nr=4.

5.1.1 Effective Index

At first we have considered unstressed PCF to observe the variation of effective index as a function of wavelength. Fig.5.4 shows that effective index decreases with the increase of wavelength, where we considered λ=1μm to 2 μm, d=1.6 μm, Λ=2.5μm and Nr=4. This result matches with the result found in [14].

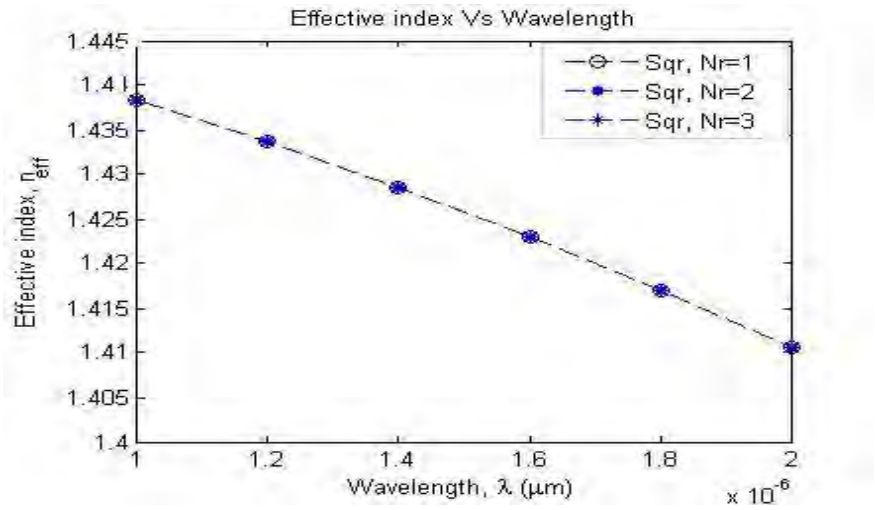

Fig. 5.4 Effective index as a function of wavelength for unstressed square air hole arrangement, where λ=1.55μm, d=1.4μm and Λ=2.5μm.

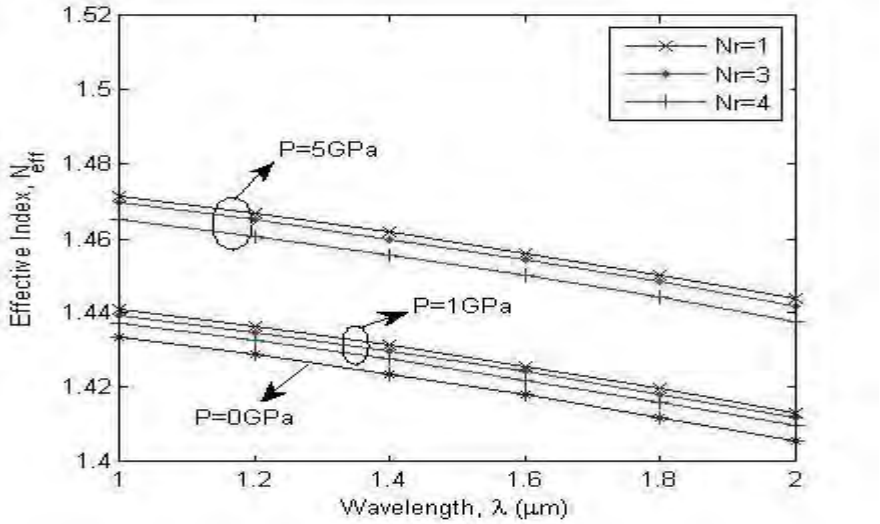

Fig. 5.5 Effective index as a function of wavelength and external stress for square air hole arrangement, where λ=1.55μm, d=1.4μm and Λ=2.5μm.

The stress-induced corrections of the refractive index are known from plain stress analysis; we utilized these data as input information for optical analysis by FEM. We have got the modal effective index as the output of optical analysis. The stress induced effective index is not same for different structured PCFs. To observe the stress effect on fibers propagation properties we applied 0, 1 and 5 GPa pressure on fiber boundary. This pressure has been applied uniformly from each side. We have changed the fiber structure by varying number of air hole rings 1, 3 and 4. To compare this changes for different number of air hole ring PCFs we considered all parameters same (λ=1.55μm,

d=1.55 µm, Λ=2.5µm) for all structures. Fig.5.5 shows that effective index decreases with the increase of wavelength for all square air hole arranged PCFs with Nr=1, 3 and 4. It also shows that external stress causes change of effective index. Without considering external stress (P=0GPa) effective indices remains almost same for PCFs with Nr=1, 3 and 4. Furthermore, with the increase of external stress effective index increases but this change is noticeable for P=5GPa than P=1GPa.

5.1.2 Birefringence

External stress on PCF causes stress distribution and fiber deformation in fiber cross section. This deformation is not same for all type of fiber and in all direction (x and y), which causes different birefringence for square PCFs. For unstressed (P=0GPa) square PCFs birefringence is very small and it is negligible. Considering external stress it increases with the increase of stress. But this changes is very small and it is order of 10^{-6} for square PCF with Nr=4. Fig.5.6 depicts the variation of birefringence as a function of wavelength and external stress for square PCFs with Nr=1, 2 and 3. Here 1GPa and 5GPa external stress have been applied on fiber boundary to observe the stress effect on birefringence properties. From the figure we can see that birefringence increases with the increase of wavelength and the change is more with larger operating wavelength. It is also found that external stress induced birefringence become higher for lower number of air hole rings with whole operating wavelengths (1µm to 2µm).

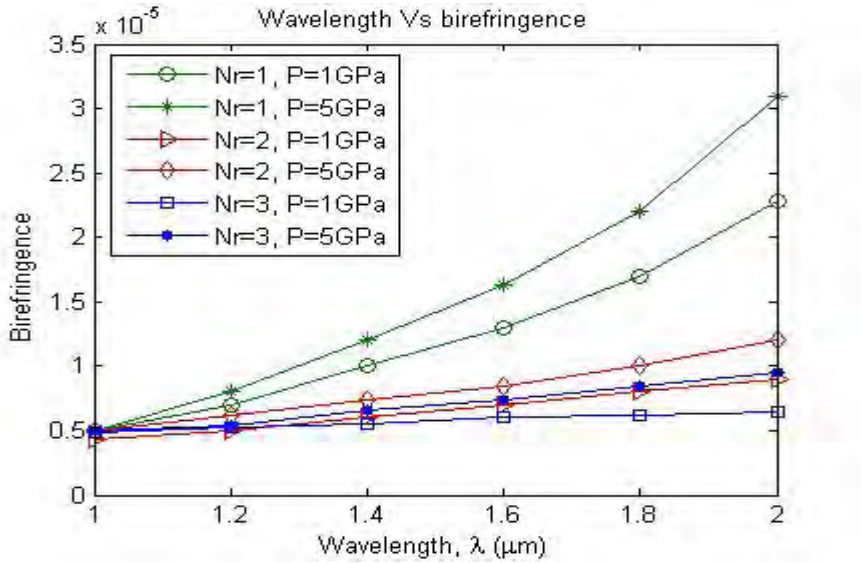

Fig. 5.6 Birefringence as a function of wavelength and external stress for square PCFs with different number of air hole rings, where d=1.4μm, Λ=2.5μm and R=12.0μm.

5.1.3 Confinement Loss

Without considering external stress confinement loss as a function of wavelength and number of air hole rings for square PCFs with Nr=1, 2, 3 and 4 are shown in Fig.5.7. The comparison between the confinement losses of square PCFs with Nr=1 and 2, Nr=2 and 3, Nr=3 and 4 are shown in Fig.5.7 (a), (b) and (c) respectively. The figures depict that confinement loss increases with the increases of wavelength. We also found that confinement loss reaches of order of 10^{-4} for the square PCF with Nr=1. But it significantly decreases with the increase of number of air hole rings. At 1.6^{-6} μm wavelength unstressed square PCF with Nr=1 shows confinement loss 6.5^{-4}, Nr=2 shows 2.934^{-6} and Nr=3 shows 3.751^{-9}. Fig.5.8 (a), (b), (c) and (d) shows confinement loss as a function of wavelength and external stress for square PCFs with Nr=1, Nr=2, Nr=3 and Nr=4 respectively. In each case it is found that confinement loss increases with the increase of external stress. Furthermore we have found that external stress induced confinement loss increases sharply for PCFs with lower number of air hole rings than higher number of air hole rings. External stress induced confinement loss for PCFs with Nr=1 changes from order of 10^{-4} (P=0GPa) to 10^{1} (P=5GPa). Confinement loss for square PCFs with lower number of air hole rings are more stress sensitive than higher number of air hole rings.

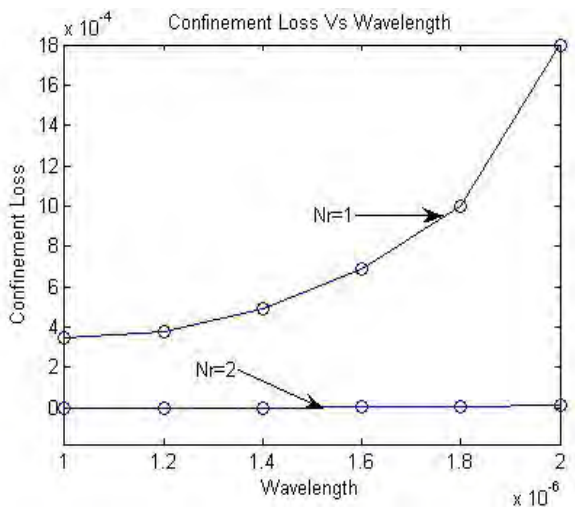

(a)

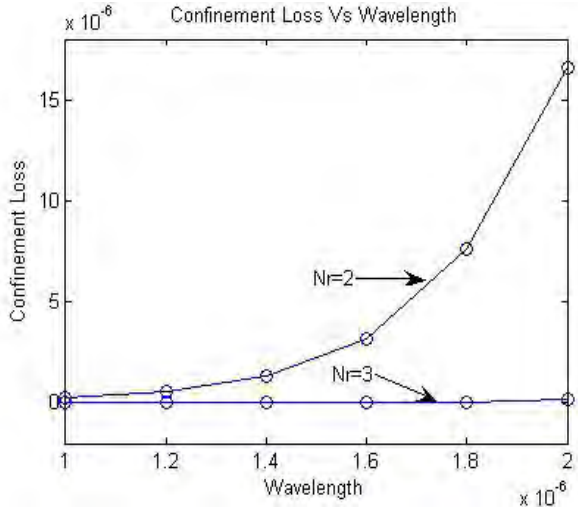

(b)

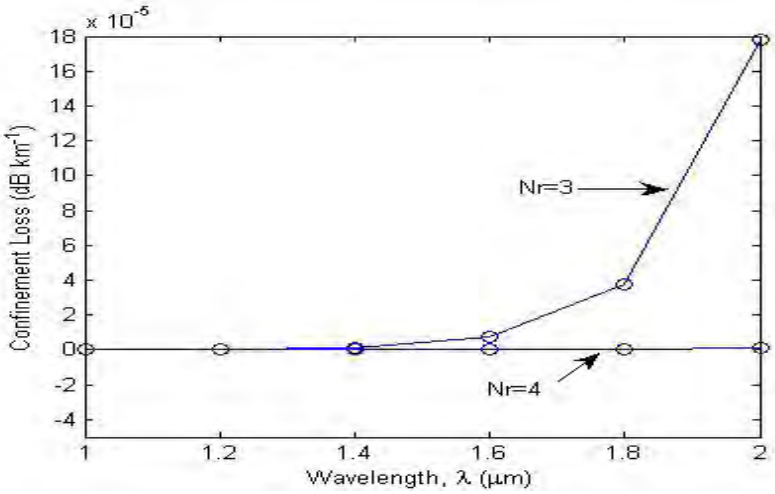

(c)

Fig.5.7 Confinement loss as a function of wavelength for square PCFs, where d=1.4μm, Λ=2.5μm, e=1μm, R=12.0μm and (a) Nr=1 and 2, (b) Nr=2 and 3, (c) Nr=3 and 4

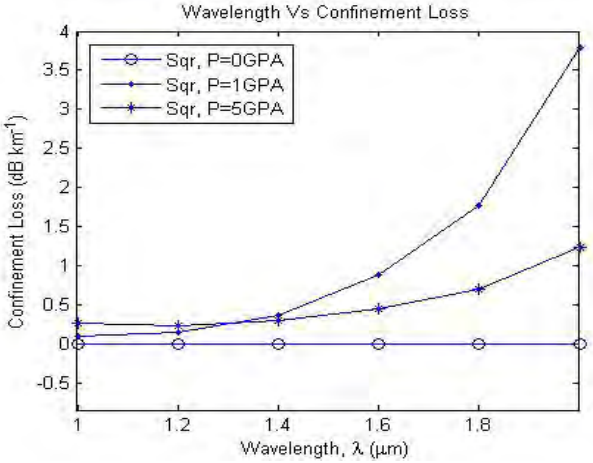

(a)

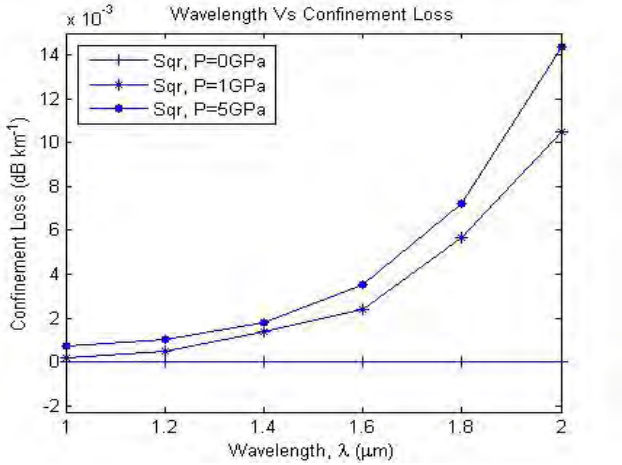

(b)

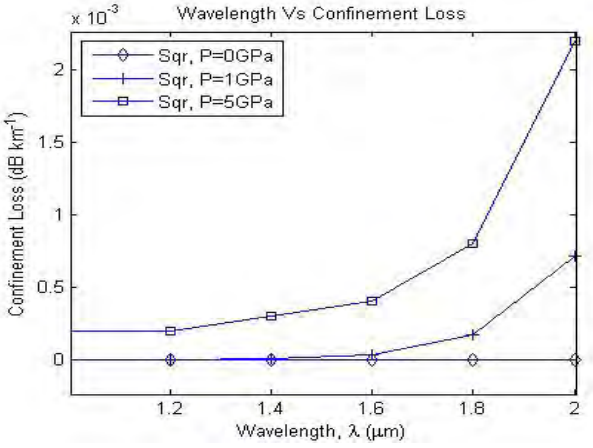

(c)

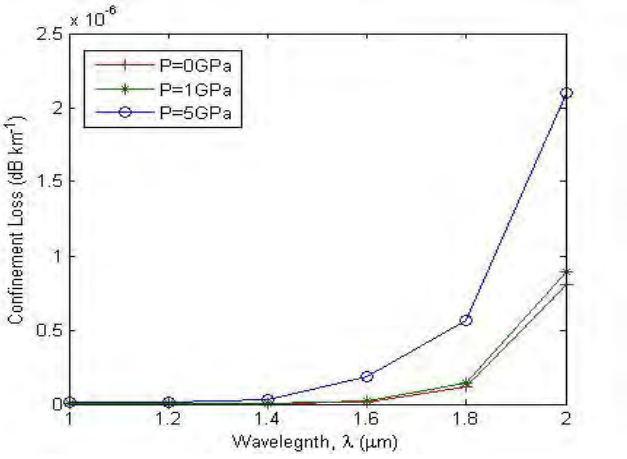

(d)

Fig.5.8 Confinement loss as a function of wavelength and external stress for square PCFs, where d=1.4μm, Λ=2.5μm, e=1μm, R=12.0μm and (a) Nr=1, (b) Nr=2, (c) Nr=3 and (d) Nr=4.

5.1.4 Effective area

Fig.5.9 shows without considering external stress effective area increases with the increase of wavelength for square PCFs with Nr=1, 2, 3 and 4, where d=1.4μm, Λ=2.5μm and R=12.0μm. It also shows that effective area of square shape PCFs always greater for lower number of air hole rings than higher number of air hole rings. But with the increase of number of air hole rings effective area decreases more sharply with longer wavelength. Fig.5.10 depicts effective area increases with the increase of external stress, where d=1.44μm, Λ=2.5μm, Nr=4, R=12.0μm and λ=1.55μm. But this change is very small. Again Fig.5.11 presents external stress induced effective area increases more sharply for smaller wavelength than larger.

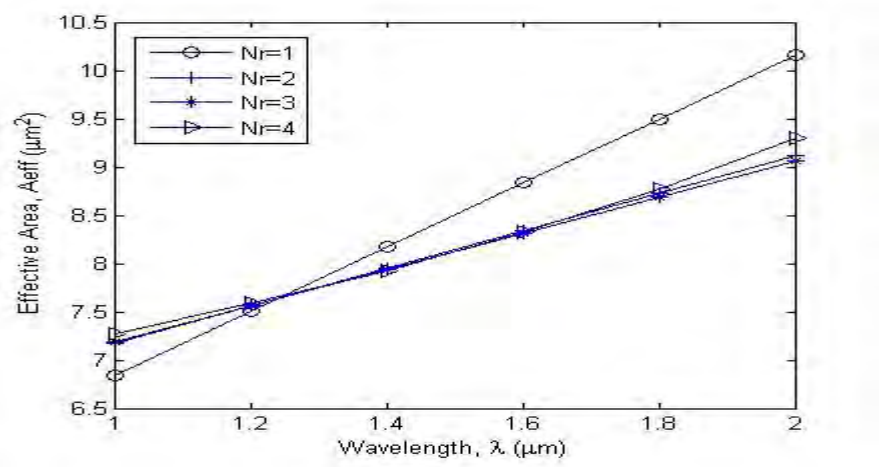

Fig.5.9 Without considering external stress effective area as a function of wave length for square PCFs, where d=1.4μm, Λ=2.5μm and R=12.0μm.

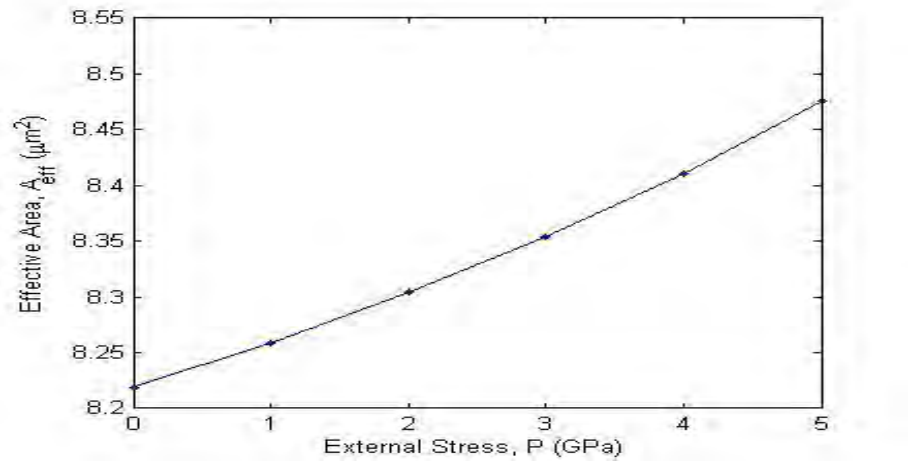

Fig.5.10 Effective area as a function of external stress for square PCFs, where d=1.44μm, Λ=2.5μm, Nr=4, R=12.0μm and λ=1.55μm.

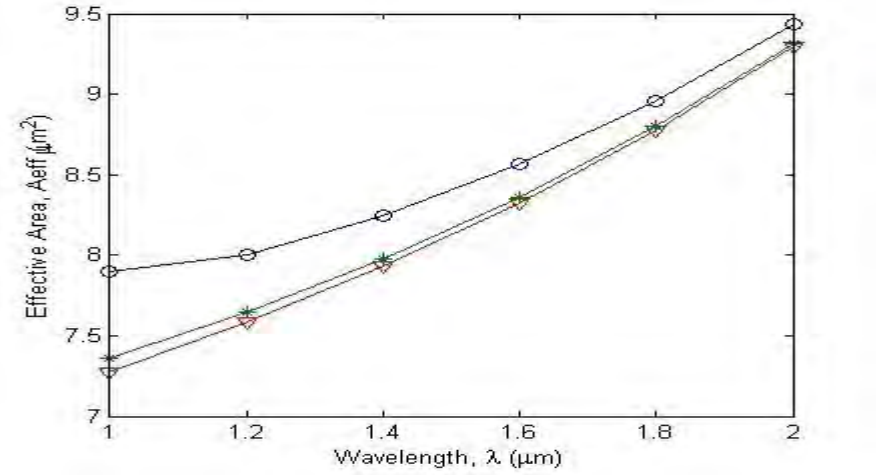

Fig.5.11 Effective area as a function of wavelength and external stress for square PCFs, where d=1.44μm, Λ=2.5μm, Nr=4 and R=12.0μm.

5.1.5 Dispersion

For square lattice PCFs without any external stress dispersion increases almost linearly with the increase of wavelength which is shown in Fig.5.12, where d=1.4μm, Λ=2.5μm P=0GPa and λ=1.55μm. It also shows dispersion increases with the increase of number of air hole rings but this change is very small. Furthermore Fig.5.13 shows the external stress effect on square PCF with Nr=4. From the figure it is clear that external stress induces dispersion and with higher external stress dispersion is also high.

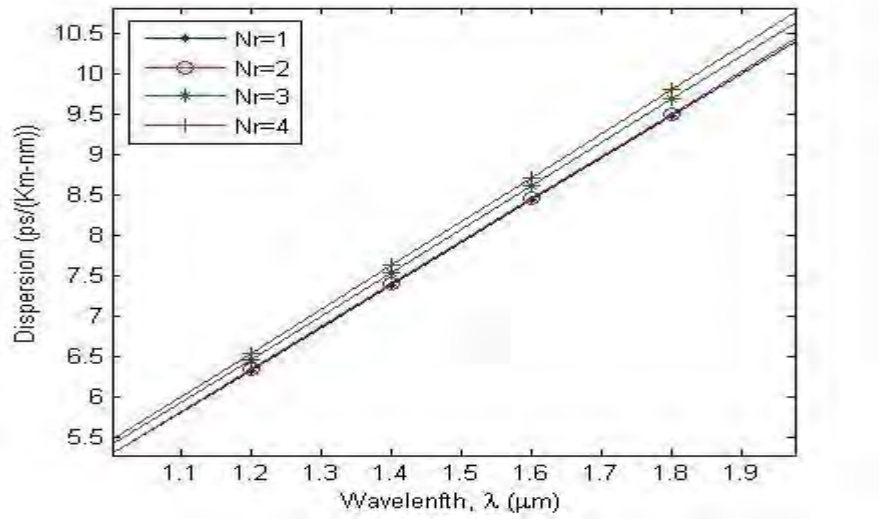

Fig. 5.12 Dispersion as a function of wavelength and number of air hole rings for square PCFs, where d=1.4μm, Λ=2.5μm, P=0GPa and λ=1.55μm.

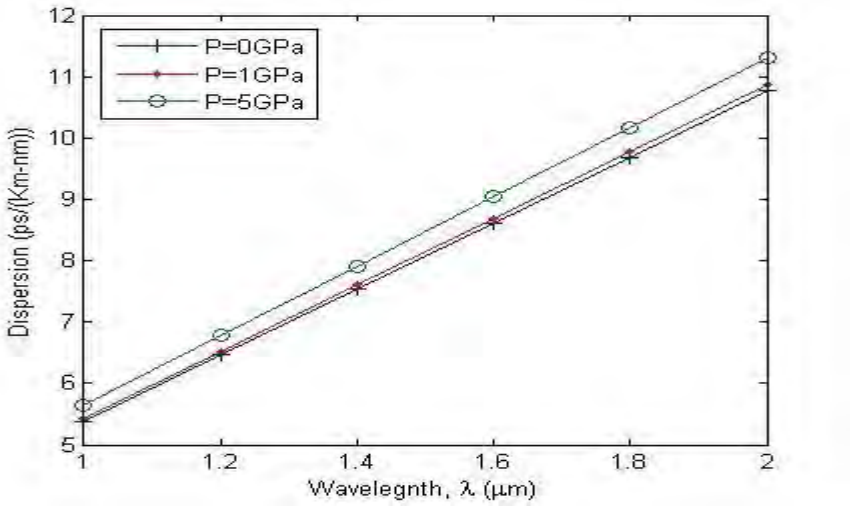

Fig. 5.13 External stress induced dispersion as a function of wavelength for square PCFs, where d=1.4μm, Λ=2.5μm and Nr=4.

5.2 HEXAGONAL PCFs

Here hexagonal PCFs are designed by hexagonal air hole arrangement in fiber cross section. Like square PCFs air holes for hexagonal PCFs are considered only circular shaped. From chapter 4 it is clear AFF is greater for hexagonal PCF than square. Again with same air hole diameter, pitch and number of air hole rings total area of air in fiber cross section is greater for square.

To observe the effect of design parameters on fiber propagation properties we have varied air hole diameters and number of air hole rings to design different fiber structures. Then we identified the changes of effective index, birefringence, confinement loss and effective area with the change of design parameters. Again to observe stress effect on different structured PCFs different external stress has been applied uniformly on fiber boundary from all direction.

The stress distribution over the hexagonal PCF cross section is shown in Fig5.14, where d=1.2μm, Λ=2.5 μm and Nr=4. It shows arrow displacement under external stress, where the arrow direction shows pressure is applied uniformly from all directions. Fig.5.15 shows the surface total displacement for hexagonal air-hole arrangement, which occurred for external stress effect and causes deformation in fiber structure. This deformation causes change in material refractive index. The effect of stress on the refractive index also causes a change in the mode field distribution. The Fig.5.16 shows the surface power flow for the fundamental *x* polarized single mode. It also shows the modal solution gives complex effective refractive index.

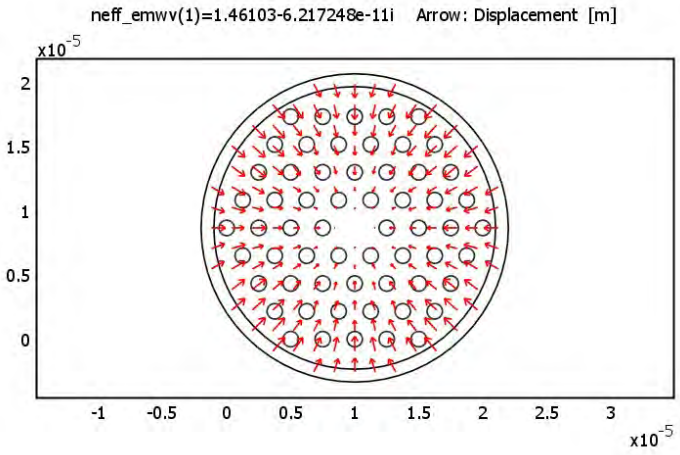

Fig. 5.14 Arrow displacement under external stress for hexagonal air hole arrangement PCF with external stress 5GPa, where d=1.2µm, Λ=2.5 µm and Nr=4.

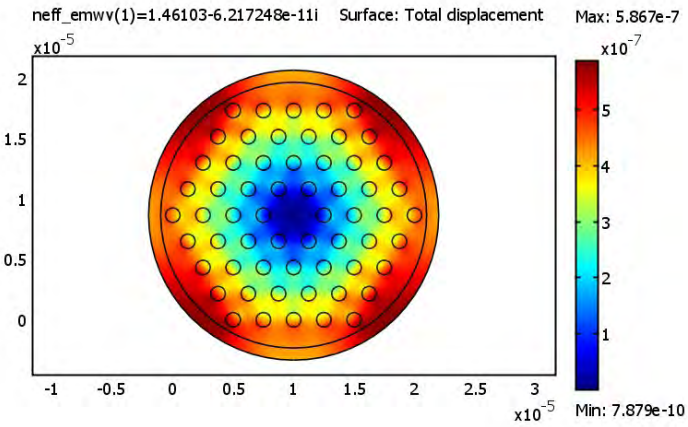

Fig. 5.15 Surface total displacement under external stress for hexagonal air hole arrangement PCF with external stress 5GPa, where d=1.2µm, Λ=2.5µm and Nr=4.

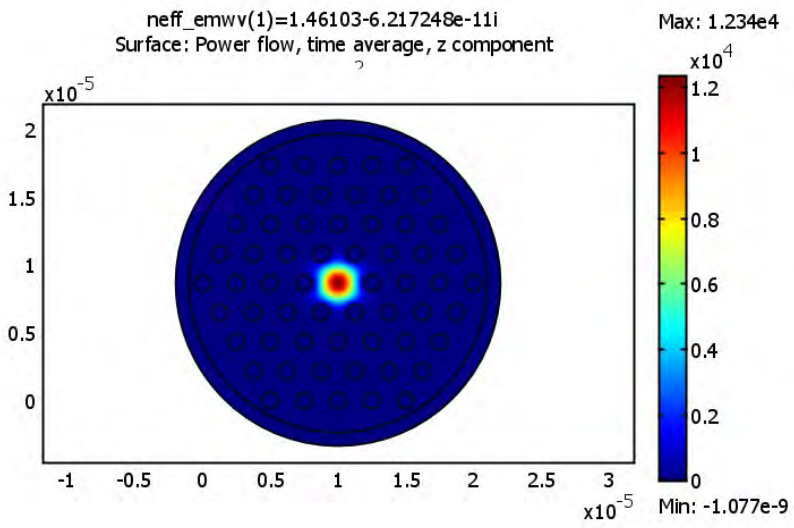

Fig. 5.16 Surface power flow, time average z component under external stress for hexagonal air hole arrangement with external stress 5GPa, where d=1.4µm, Λ=2.5µm and Nr=4.

5.2.1 Effective Index

Effective index of hexagonal PCFs with different structure have been observe here. At first we observed the change of effective index as a function of wavelength for hexagonal PCFs with different number of air hole rings (Nr=1, 2, 3 and 4) then we find out the change of effective index with different air hole diameter. Fig.5.17 shows effective index as a function of wavelength and external stress, where d=1.4µm and Λ=2.5µm. We can observe from this figure that effective index decreases with the increase of wavelength and hexagonal PCFs with larger number of air hole rings shows lower effective index. Again, unstressed hexagonal PCFs with different number of air hole ring show almost same effective index. Furthermore it also depicts that higher external stress induces higher effective index. The stress effect is comparatively higher for the PCFs with larger Nr.

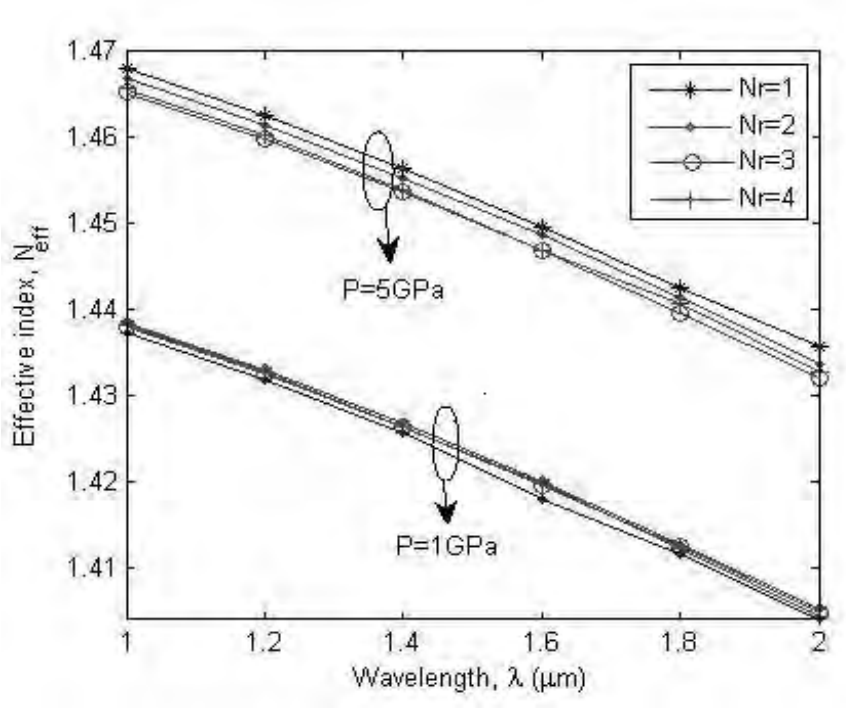

Fig.5.17 Effective index as a function of wavelength and external stress for hexagonal air hole arrangement, where d=1.4μm and Λ=2.5μm.

External stress causes fiber deformation and stress distribution in fiber cross section. These facts make change of effective index. Amount of deformation varies depending on fiber AFF and PCFs with different AFF have been designed here by varying air hole diameter (d=0.8μm to 1.6 μm). Fig.5.18 shows the changes of effective index as a function of external stress and air hole diameter, where λ=1.55μm, Λ=2.5μm and Nr=4. It depicts that effective index increases linearly with the increase of external stress. Again it shows that effective index is higher for PCFs with larger air hole diameter.

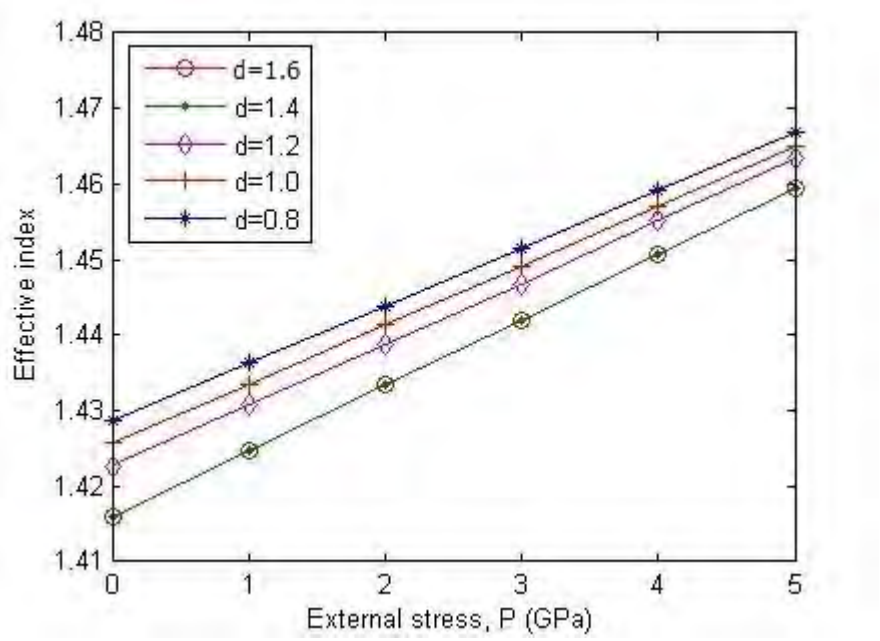

Fig.5.18 Effective index as a function of external stress and air hole diameter for hexagonal air hole arrangement, where λ=1.55μm, Λ=2.5μm and Nr=4.

5.2.2 Birefringence

Stress distribution in the fiber's cross section and deformation of the fiber's structure both factor induces different modal effective index in both axis (x and y), which causes modal birefringence. So stress induced birefringence is also different for hexagonal PCFs with different designed structure. Here external stress induced changes of birefringence property for different hexagonal PCFs have been observed by varying number of air hole rings and air hole diameter. Fig. 5.19 shows birefringence as a function of wavelength, number of air hole rings and external stress for hexagonal air hole arrangement, where d=1.4μm and Λ=2.5μm. From this figure we can see that birefringence increases with the increase of wavelength. Again it shows that birefringence is very high for Nr=1 (order of 10^{-4}) and it decreases very sharply for higher number of air hole rings. At Nr=4 birefringence is order of 10^{-6} and external stress induced changes is very negligible. It also depicts that with the increase of external stress birefringence also increases. Fig.5.20 shows birefringence as a function of external stress and air hole diameter for hexagonal air hole arrangement, where λ=1.55μm, d=1.4μm, Λ=2.5μm and Nr=4. This figure shows that birefringence increases with the increase of air hole diameter as well as external stress.

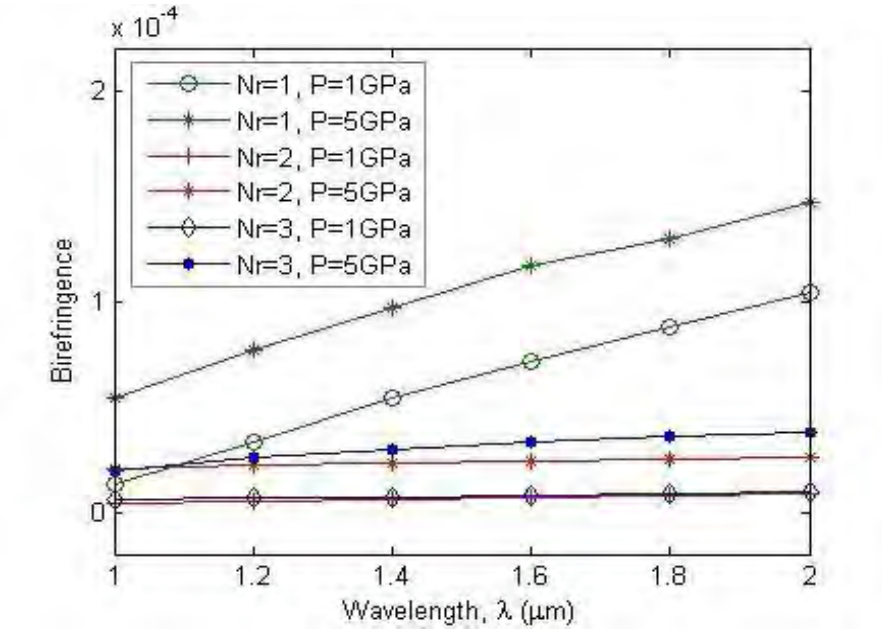

Fig.5.19 Birefringence as a function of wavelength, number of air hole rings and external stress for hexagonal air hole arrangement, where d=1.4μm and Λ=2.5μm.

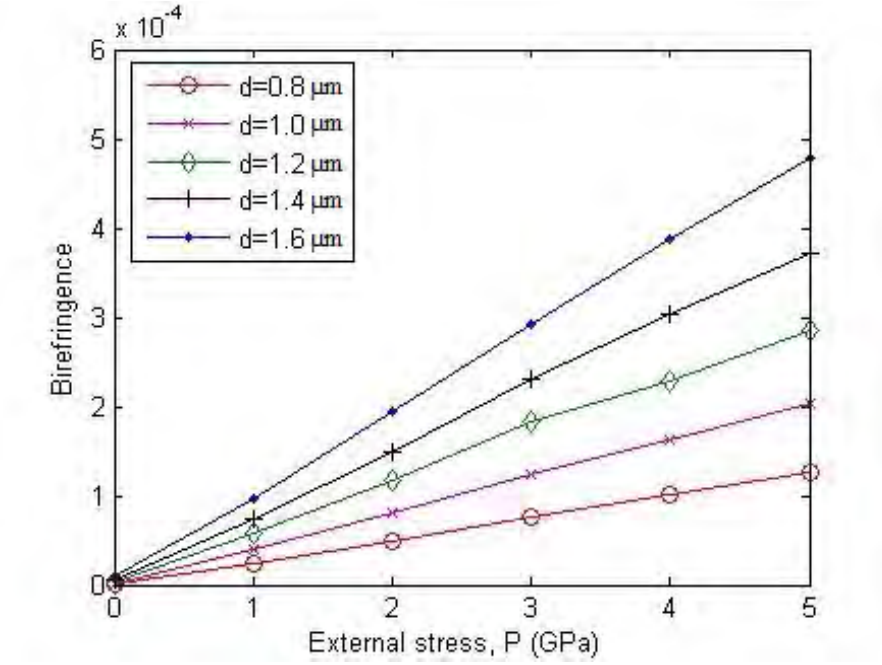

Fig.5.20 Birefringence as a function of external stress and air hole diameter for hexagonal air hole arrangement, where λ=1.55μm, d=1.4μm, Λ=2.5μm and Nr=4.

5.2.3 Confinement Loss

All the PCF guided modes are leaky. In solid-core PCFs light is confined within a core region by the air-holes. Light will move away from the core if the confinement provided by the air-holes is inadequate. Because of the finite transverse extent of the confining structure, the effective index is a complex value; its imaginary part is related to losses. Due to external stress deformation of the fiber's structure causes confinement loss.

External stress effect on confinement loss as a function of wavelength and number of air hole rings for unstressed hexagonal PCFs with Nr=1, 2, 3 and 4 are shown in Fig.5.21, where P=0GPa, d=1.4μm, Λ=2.5μm, e=1μm, R=12. The variation of confinement loss against external stress for hexagonal PCFs with Nr=1 and 2, Nr=2 and 3, Nr=3 and 4 are shown in Fig.5.21 (a), (b) and (c) respectively. The figures show that confinement loss increases with the increases of wavelength but it significantly decreases with the increase of number of air hole rings. We also found that confinement loss reaches of the order of 10^{-3} for the hexagonal PCF with Nr=1. At 1.6^{-6} μm wavelength hexagonal PCF with Nr=1 shows confinement loss 5^{-3}, Nr=2 shows 3.934^{-6} and Nr=3 shows 7.249^{-9}. Fig.5.22 shows confinement loss as a function of wavelength and external stress, where λ=1.55μm, d=1.4μm, Λ=2.5μm and Nr=4. It is clear from the figure that higher external stress induces higher confinement loss. Again from the Fig.5.23 it is clear that confinement loss gradually decreases with the increase of air hole diameter, where λ=1.55μm, d=1.4μm, Λ=2.5μm and Nr=4. It also shows that confinement loss increases with the increase of external stress and it is very high for larger external stress with smaller air hole diameter.

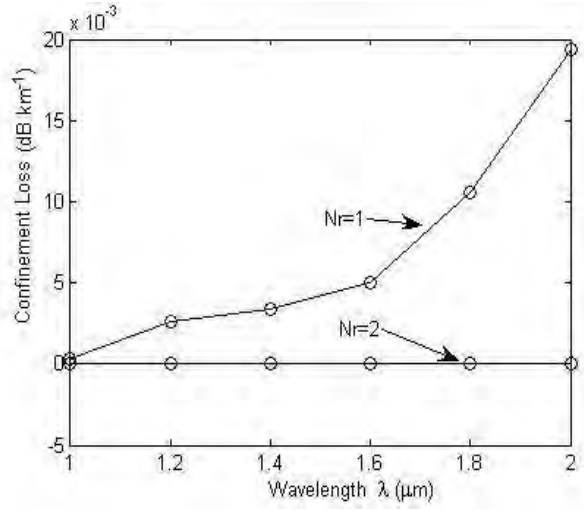

(a)

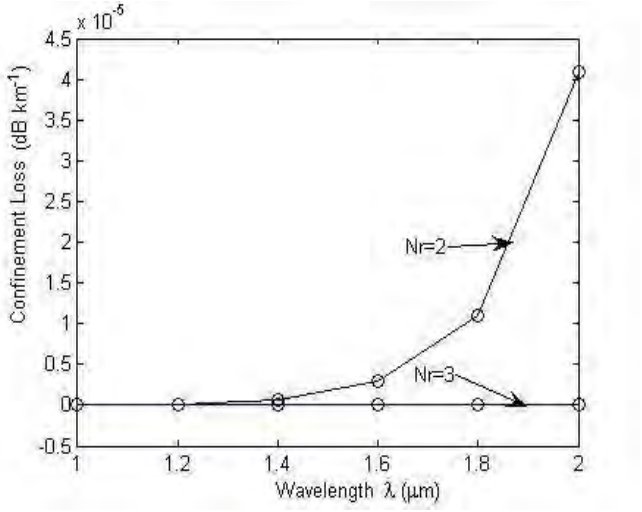

(b)

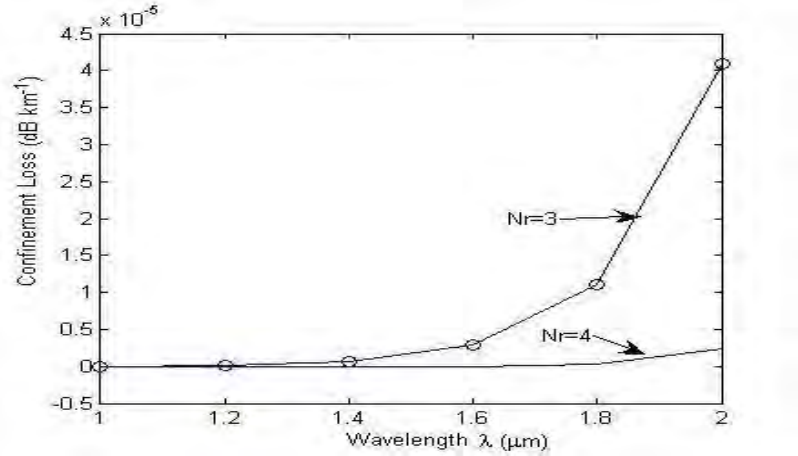

(c)

Fig.5.21 Confinement loss as a function of wavelength for hexagonal PCFs, where P=0GPa, d=1.4μm, Λ=2.5μm, e=1μm, R=12.0μm and (a) Nr=1 and 2, (b) Nr=2 and 3, (c) Nr=3 and 4.

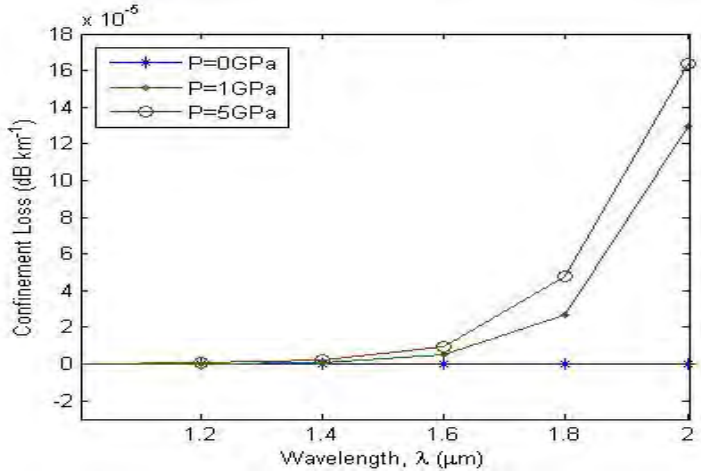

Fig.5.22 Confinement loss as a function of wavelength and external stress for hexagonal PCFs, where λ=1.55μm, d=1.4μm, Λ=2.5μm and Nr=4.

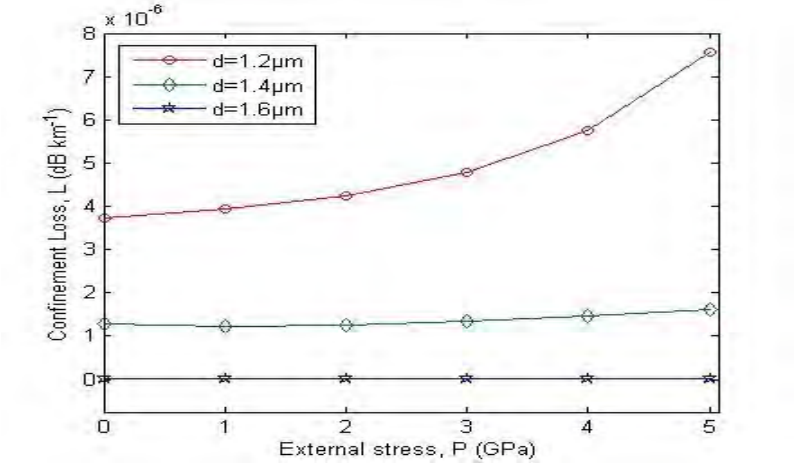

Fig.5.23 Confinement loss as a function of external stress and air hole diameter for hexagonal PCFs, where λ=1.55μm, Λ=2.5μm and Nr=4.

5.2.4 Effective area

Effective area increases with the increase of external stress for hexagonal PCFs. Fig.5.24 shows effective area as a function of wavelength and number of air hole rings, where P=0GPa, d=1.4μm and Λ=2.5μm. From the figure we can see that hexagonal PCF with Nr=1 shows comparatively higher effective area than Nr=2, 3 and 4. Again it also shows that effective area increases with the increase of wavelength and it is almost same for higher number of air hole rings.

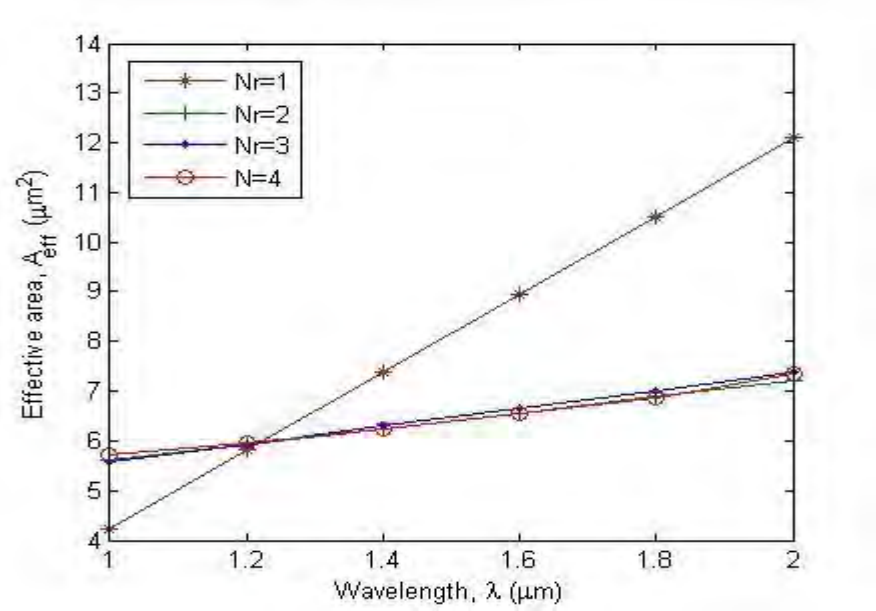

Fig.5.24 Effective area as function of wavelength and number of air hole rings for hexagonal PCFs, where P=0GPa, d=1.4μm and Λ=2.5μm.

Fig.5.25 depicts the change of effective area against air hole diameter, where λ=1.55μm, d=1.4μm, Λ=2.5μm, P=0GPa and Nr=4. We get from the results that effective area decreases with the increase of air hole diameter and this change is very sharp for smaller air hole diameter than larger. Fig.5.26 shows the comparison between 0GPa, 1GPa and 5GPa external stress induced effective areas as a function of wavelength, where d=1.4μm, Λ=2.5μm and Nr=4. The figure depicts that effective area increases as a function of wavelength in hexagonal air hole arranged PCF. It also shows that with the increase of external stress effective area also increases but the rate of change is higher for shorter wavelength than longer.

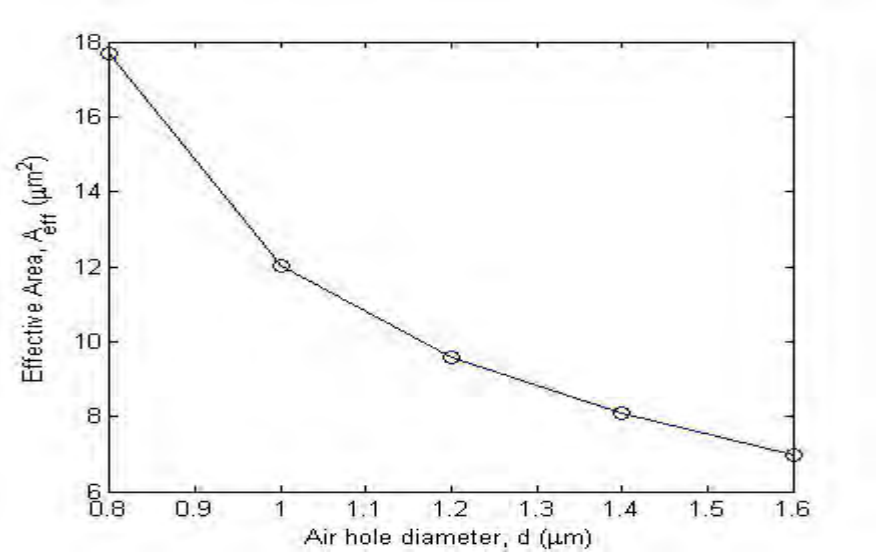

Fig.5.25 Effective area as a function of air hole diameter for hexagonal PCF, where λ=1.55μm, d=1.4μm, Λ=2.5μm, P=0GPa and Nr=4.

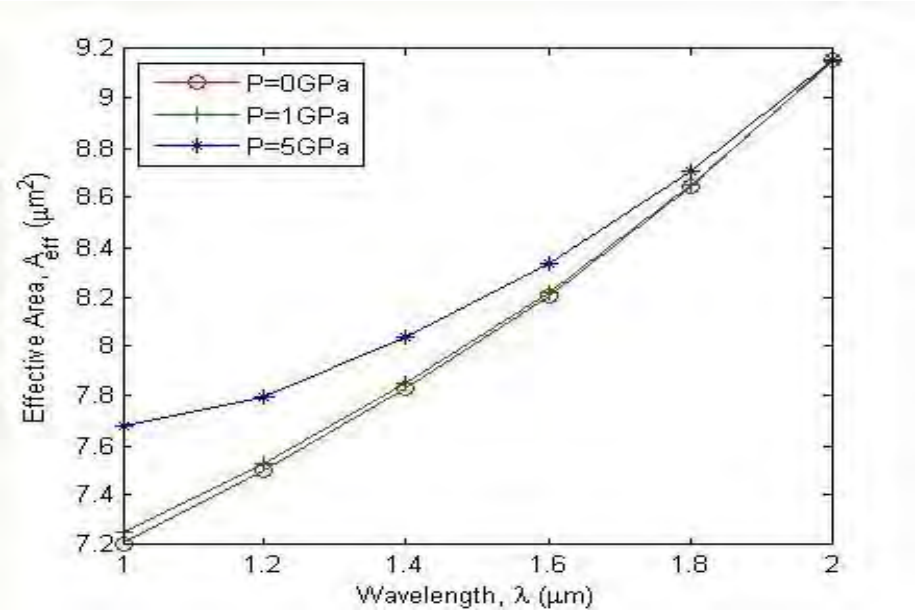

Fig.5.26 Effective area as a function of wavelength and external stress for hexagonal PCF, where d=1.4μm, Λ=2.5μm and Nr=4.

5.2.5 Dispersion

Fig.5.27 shows dispersion as a function of wavelength and number of air hole rings, where d=1.4μm and Λ=2.5μm. It shows that dispersion increases with the increase of number of air hole rings.

Hexagonal PCF with Nr=1 exhibits negative dispersion but hexagonal PCFs with Nr=2 and 3 exhibits positive dispersion. Again it also shows that external stress induces higher dispersion. This is more clear from Fig.5.28 that shows dispersion as a function of wavelength and external stress, where d=1.4μm, Λ=2.5μm and Nr=4. That depicts the effect of external stress on dispersion properties with external stress P=0, 1 and 5GPa. From the figure it is clear that higher external stress causes greater dispersion.

It is also found that hexagonal PCF with higher air hole diameter shows higher dispersion and this increases with the increase of external stress. Fig.5.29 shows dispersion as a function of wavelength and air hole diameter with external stress P=0GPa and 5GPa, where Λ=2.5μm and Nr=4. It depicts that hexagonal PCFs with larger air hole diameter induce higher dispersion than smaller air hole diameter. Hexagonal PCFs with d=08μm shows negative dispersion but hexagonal PCFs with d=1.4μm and 1.6μm exhibits positive dispersion.

We know that area of air in PCF cross section can be varied by varying air hole diameter and number of air hole rings. With the increase of number air hole ring and air hole diameter amount of air in fiber cross section increases. From the results it is clear that hexagonal PCFs shows negative dispersion with less amount of air in fiber cross section but it shows positive dispersion with greater amount of air in fiber cross section.

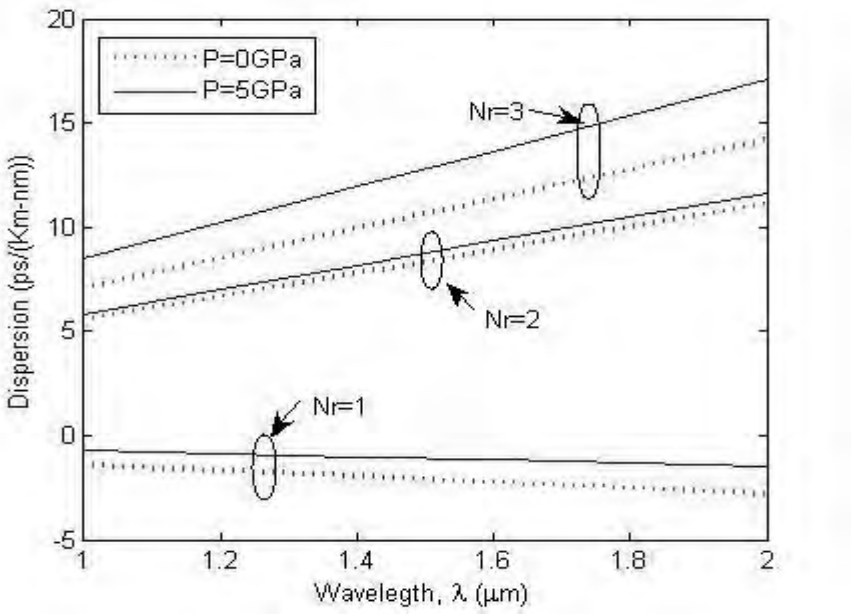

Fig.5.27 Dispersion as a function of wavelength and number of air hole rings for hexagonal PCFs, where d=1.4μm and Λ=2.5μm.

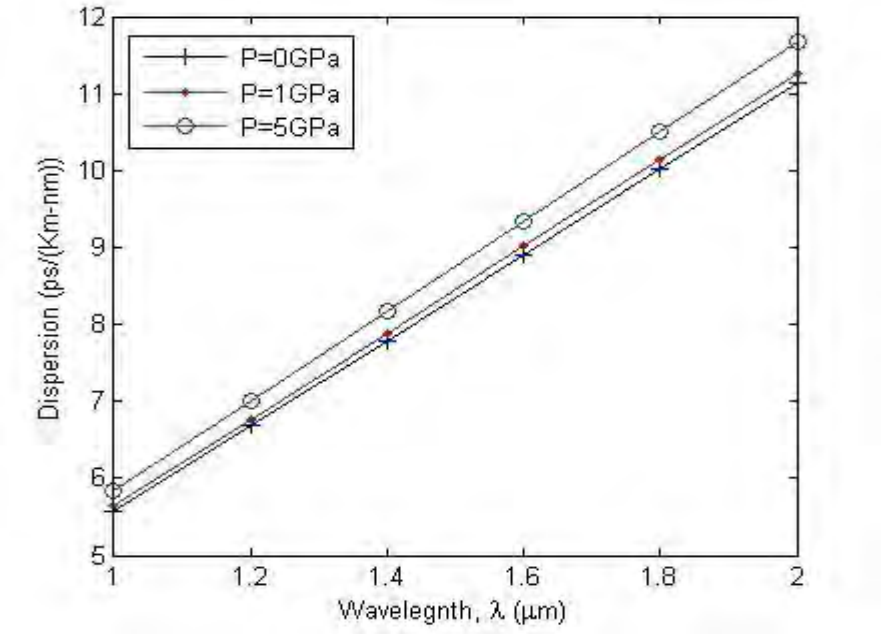

Fig5.28 Dispersion as a function of wavelength and external stress for hexagonal PCF, where d=1.4μm, Λ=2.5μm and Nr=4.

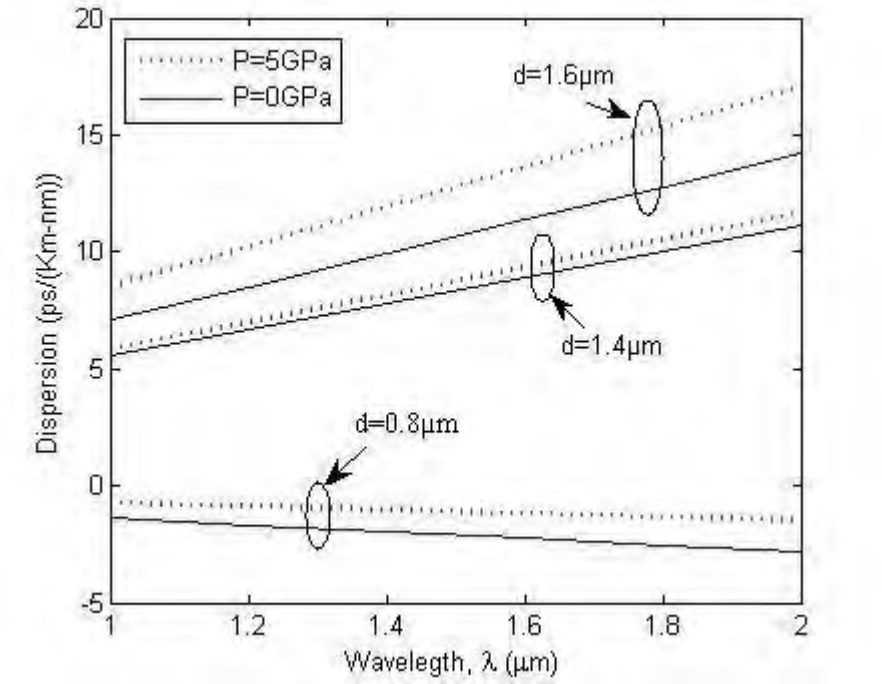

Fig.5.29 Dispersion as a function of wavelength and air hole diameter for hexagonal PCFs, where Λ=2.5μm and Nr=4.

5.3 OCTAGONAL PCFs

In this section we have observed the propagation properties of octagonal PCFs, where the fibers have been designed by octagonal air hole arrangement [11]. At first the results have been found for unstressed PCFs then external stress have been applied on fiber boundary to identify the effect on PCFs propagation properties. With the change of air hole diameter, total amount of air in fiber cross section also changes. To observe the effect of this change on octagonal PCFs propagation properties, we have designed the fiber structures by varying only air hole diameter, where other design parameters have been considered same. From the simulation result we have got the modal solution of all octagonal PCFs. Then we have used these results to calculate effective index, birefringence, confinement loss, effective area and dispersion for all octagonal PCFs. Again we repeated the experiment for stressed PCFs and we found the changes of propagation properties of octagonal PCFs due to external stress. Fig.5.30 shows the arrow displacement under external stress for octagonal air hole arrangement PCF with external stress 5GPa, where d=1.2µm, Λ=2.5 µm and Nr=4. Here the arrows show that uniform stress have been applied on fiber boundary from all direction. Fig.5.31 shows surface total displacement under external stress for octagonal air hole arrangement PCF with external stress 5GPa, where d=1.2µm, Λ=2.5µm and Nr=4. The color bur indicates amount of displacement in fiber cross section due to external stress. Fig.5.32 presents surface power flow, time average z component under external stress for octagonal air hole arrangement with external stress 5GPa, where d=1.4µm, Λ=2.5µm and Nr=4. It shows the single mode power flow through the core and the effective index of eigenvalule solution.

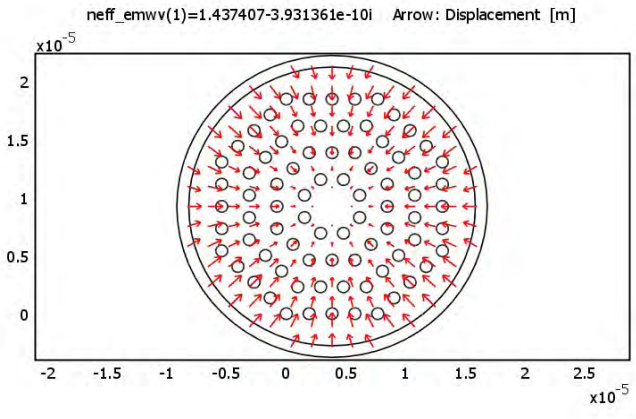

Fig.5.30 Arrow displacement under external stress for octagonal PCF with external stress 5GPa, where d=1.2µm, Λ=2.5 µm and Nr=4.

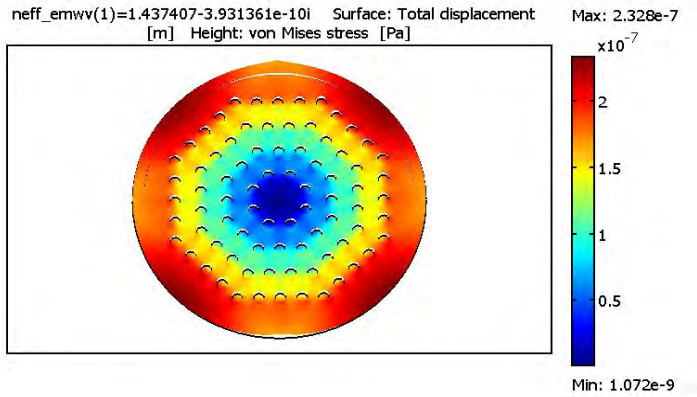

Fig.5.31 Surface total displacement under external stress for octagonal PCF with external stress 5GPa, where d=1.2μm, Λ=2.5μm and Nr=4.

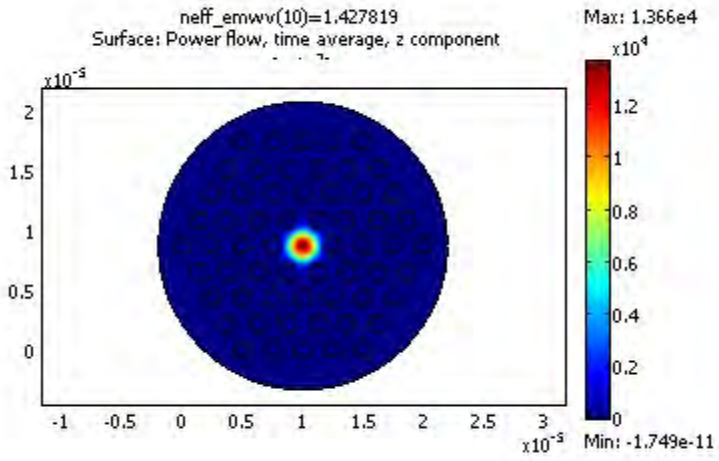

Fig. 5.32 Surface power flow, time average z component under external stress for octagonal PCF with external stress 5GPa, where d=1.4μm, Λ=2.5μm and Nr=4.

5.3.1 Effective Index

At first to compare the results we considered here two octagonal PCF structures with different air hole diameter (d=0.8μm and 1.6μm), where both PCFs are considered under both stressed (P=5GPa) and unstressed (P=0GPa) condition. The experimental results show that effective index decreases with the increase of wavelength for octagonal PCF that is given in Fig.5.33, where Λ=2.5μm and Nr=4. Again Fig.5.34 shows effective index as a function of external stress and air hole diameter for

octagonal PCF, where λ=1.55μm, Λ=2.5μm and Nr=4. In this figure we have considered different octagonal PCF structures by varying air hole diameter (d=0.8 μm, 1.0 μm, 1.2 μm, 1.4 μm and 1.6 μm). We have observed the variation of effective index with the change of external stress (P=0GPa, 1GPa, 2GPa, 3GPa, 4GPa and 5GPa). Both figures depicts that effective index is higher for smaller air diameter than larger. It is also clear that higher external stress causes higher effective index and this change is more for longer wavelength.

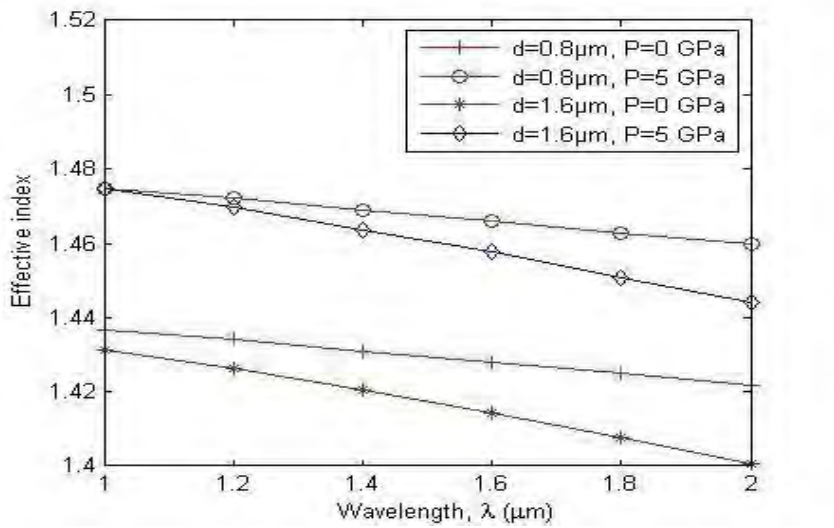

Fig. 5.33 Effective index as a function of wavelength, air hole diameter and external stress for octagonal PCF, where Λ=2.5μm and Nr=4.

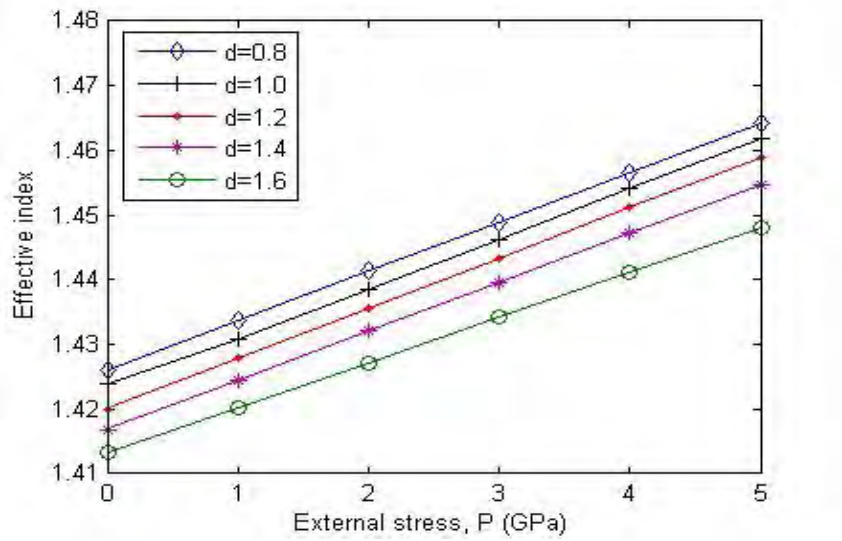

Fig.5.34 Effective index as a function of external stress and air hole diameter for octagonal PCF, where λ=1.55μm, Λ=2.5μm and Nr=4.

5.3.2 Birefringence

Birefringence is the difference between modal effective index of x and y axis. Fig.5.35 shows birefringence as a function of wavelength for octagonal PCF, where d=1.4μm, Λ=2.5μm and Nr=4. It shows that birefringence increases with the increase of wavelength. But it is very small (order of 10^{-6}) for all operating wavelengths (λ=1.0μm to 2.0μm). Again Fig.5.36 shows the effect of external stress and variation of air hole diameter on birefringence properties of octagonal PCFs. Fig.5.36 (a) shows birefringence as a function of air hole diameter, where λ=1.55μm, Λ=2.5μm and Nr=4. In this figure we have considered octagonal PCFs have been designed by varying air hole diameter from d=0.8μm to d=1.6μm and external stress have been applied periodically from 0GPa to 5GPa on the fiber boundary. The figure depicts that birefringence is peak for the octagonal PCF with d=1.4μm. We can also see that birefringence increases with the increase of external stress for octagonal PCFs with all air hole diameters. Furthermore birefringence for stressed and unstressed octagonal PCFs with different air hole diameter not greater than order of 10^{-6}. Now Fig.5.36 (b) specially shows birefringence as a function of external stress for octagonal PCF with d=1.4 μm, where λ=1.55μm, Λ=2.5μm and Nr=4. From this figure it is clear that birefringence increases almost linearly with the increase of external stress for octagonal PCF with d=1.4 μm.

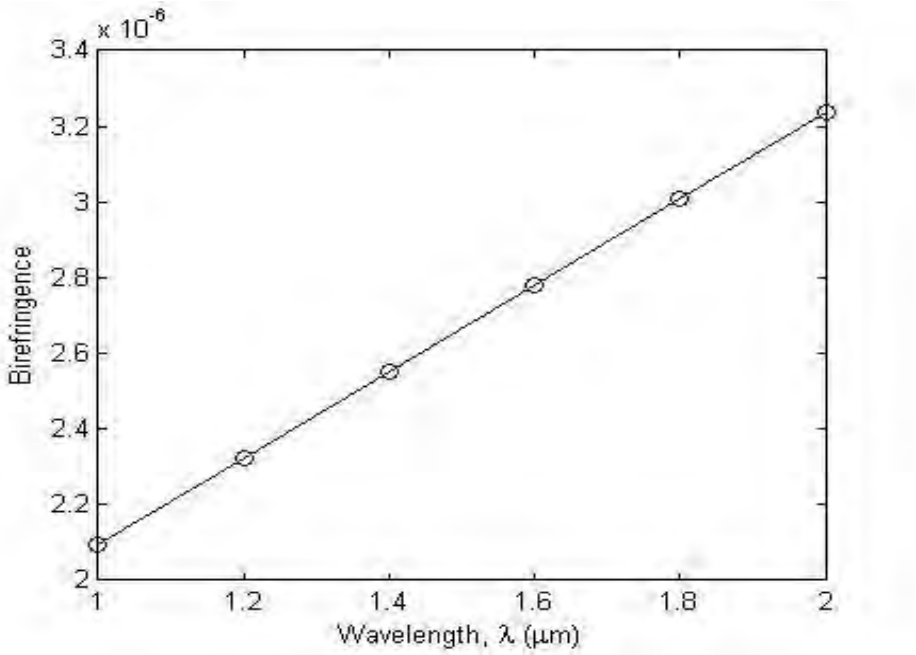

Fig.5.35 Birefringence as a function of wavelength for octagonal PCF, where d=1.4μm, Λ=2.5μm and Nr=4.

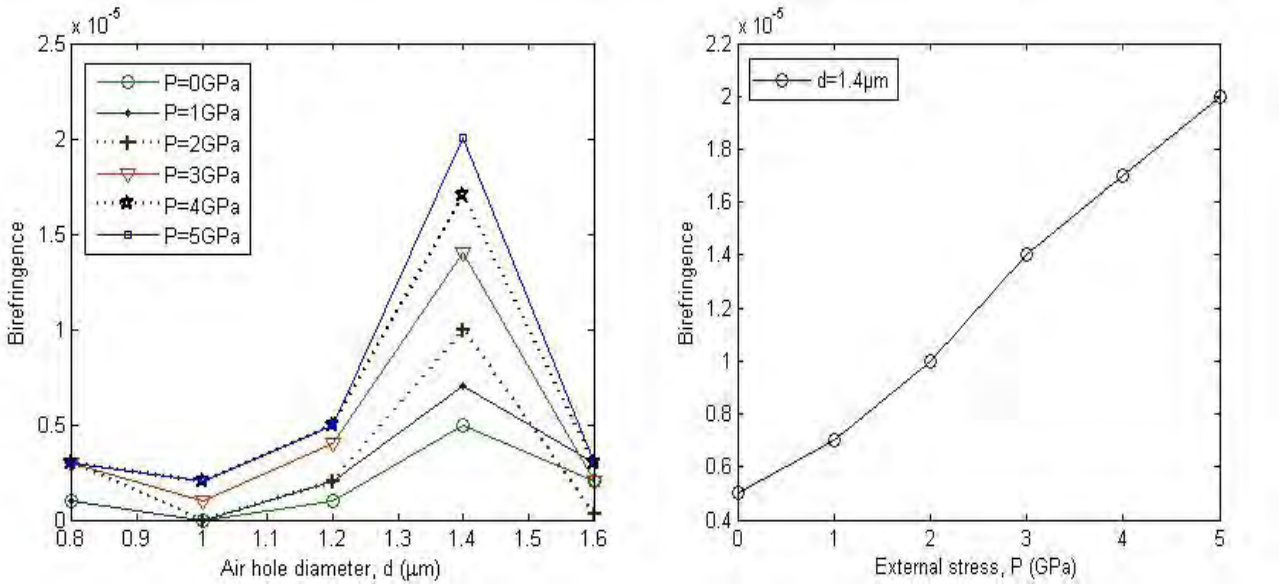

(a) (b)

Fig.5.36 (a) Birefringence as a function of air hole diameter, (b) birefringence as a function of external stress for octagonal PCFs, where λ=1.55μm, Λ=2.5μm and Nr=4.

5.3.3 Confinement Loss

With the change of air hole diameter total amount of air also changes in fiber cross section. Confinement loss is very much dependent on total amount of air in PCF cross section. This change is very large for octagonal PCFs. Confinement is very high for octagonal PCFs with smaller air hole diameter and it increases with the increase of external stress. Here we have presented the results separately for different PCFs by varying air hole diameter, which is shown in Fig.5.37 (a) d=0.8μm, (b) d=1.0μm, (c) d=1.2μm, (d) d=1.4μm and 1.6μm, where λ=1.55μm, Λ=2.5μm and Nr=4. From the figures we can find with the application of P=0GPa to 3GPa external stress confinement increases with the increase of external stress but it remains almost unchanged with higher stress. Octagonal PCFs with d=0.8μm causes confinement loss of order of 10^{-3}, d=1.0μm causes confinement loss of order of 10^{-5}, d=1.2μm causes confinement loss of order of 10^{-8}, d=1.4μm d=1.6μm both causes confinement loss of order of 10^{-13}. From the experimental data we can see that with larger air hole diameter (d>1.4μm) octagonal PCFs show very low confinement loss and they remains almost flattened with the increase of external stress. Fig.5.38. shows confinement loss as a function of wavelength for octagonal PCF, where d=1.4μm, Λ=2.5μm and Nr=4. From the figures

we can see that confinement loss for unstressed (P=0GPa) octagonal PCF increases with the increase of wavelength and this change is more sharp when λ>1.4μm. But it remains almost unchanged over the operating wavelength with higher external stress (P=5GPa).

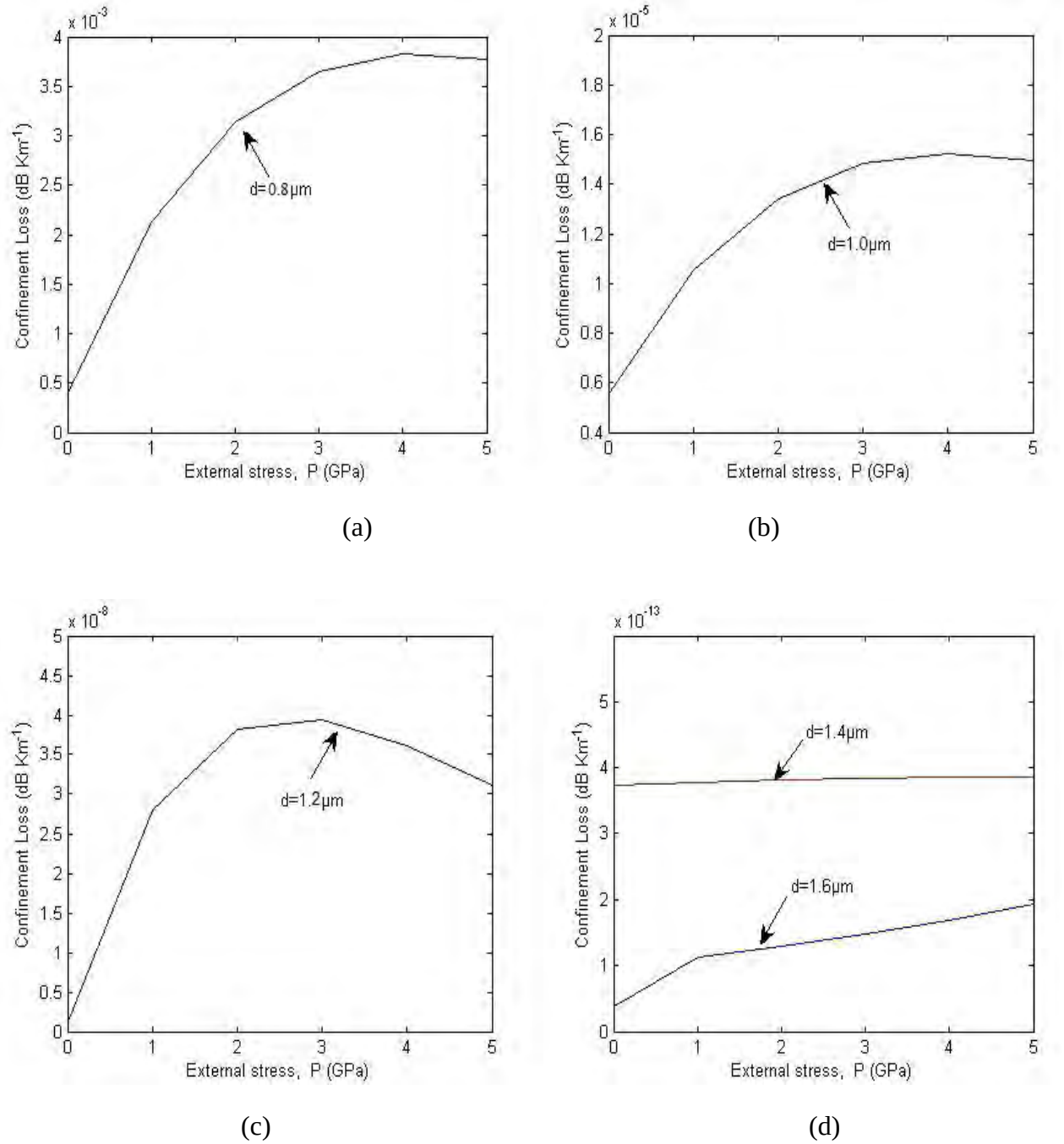

Fig.5.37 Confinement loss as a function of external stress and air hole diameter for octagonal PCFs (a) d=0.8μm, (b) d=1.0μm, (c) d=1.2μm, (d) d=1.4μm and 1.6μm, where λ=1.55μm, Λ=2.5μm and Nr=4.

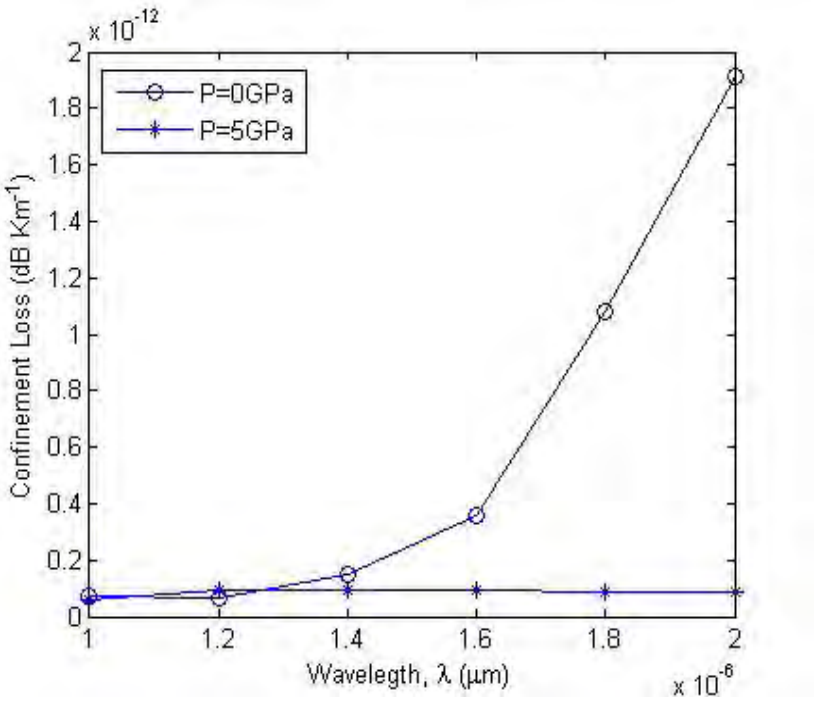

Fig.5.38 Confinement loss as a function of wavelength for octagonal PCF, where d=1.4μm, Λ=2.5μm and Nr=4.

5.3.4 Effective Area

Fig.5.39 shows that effective area as a function of wavelength for octagonal PCF, where d=1.4μm, Λ=2.5μm and Nr=4. Here the figure shows that effective area increases with the increase of wavelength, which matches with the result found in [8]. The results are shown for both unstressed (P=0GPa) and stressed (P=5GPa) octagonal PCFs. With the application of external stress effective area of octagonal PCF increases for smaller wavelength, it remains almost unchanged for λ=1.6μm and decreases with larger wavelength. External stress induce change of effective area of octagonal PCF is very small.

Fig.5.40 shows that effective area as function of external stress for octagonal PCF, where d=1.4μm, Λ=2.5μm and Nr=4. From the figure we can see that effective area increases with the increase of external stress and this change is very small. From the experimental data we can see that effective area of octagonal PCF with external stress P=0GPa is 9.4224μm^2 and P=5GPa is 9.4734 μm^2, where λ=1.6μm, d=1.0μm, Λ=2.5μm and Nr=4.

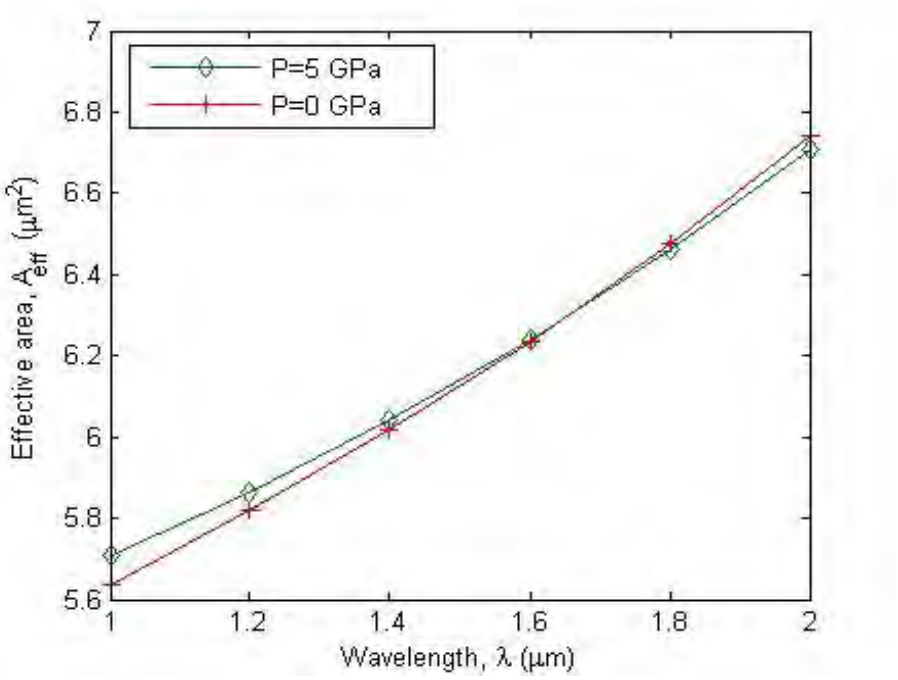

Fig.5.39 Effective area as function of wavelength for octagonal PCF, where d=1.4μm, Λ=2.5μm and Nr=4.

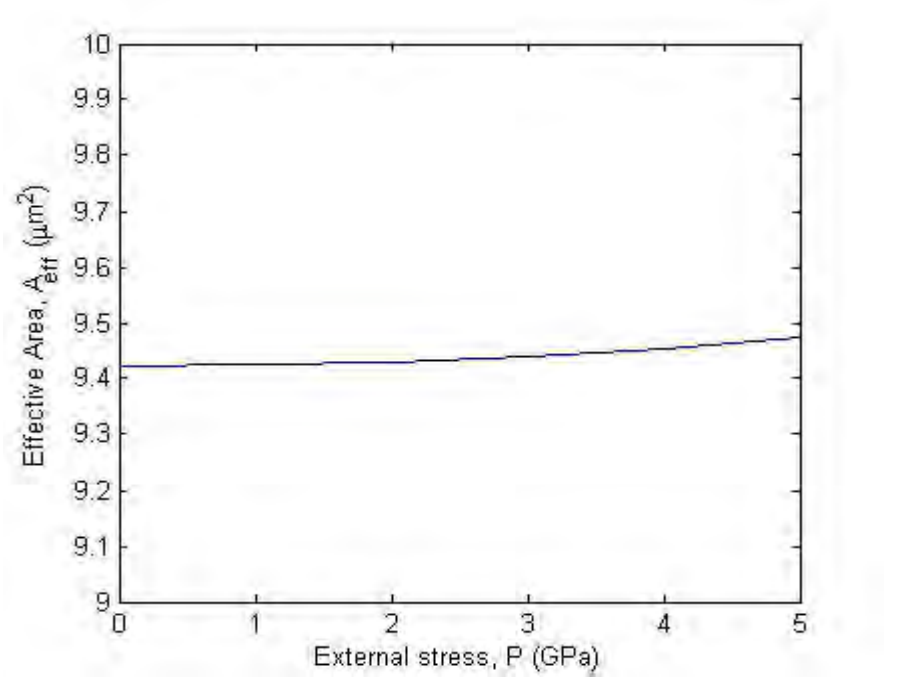

Fig.5.40 Effective area as function of external stress for octagonal PCF, where λ=1.55μm, d=1.4μm, Λ=2.5μm and Nr=4.

5.3.5 Dispersion

Fig.5.41 shows dispersion as a function of wavelength for octagonal PCF, where Λ=2.5μm and Nr=4. The figure shows dispersion for octagonal PCFs with d=1.4μm and d=1.6μm. Dispersion increases linearly with the increase of wavelength for both types of octagonal PCFs. Again we can see that dispersion for octagonal PCF with d=1.6μm is higher than d=1.4μm. Furthermore external stress causes increase of dispersion. From the figure it is clear that external stress induced dispersion of octagonal PCF with d=1.4μm increases comparatively more than d=1.6μm. Furthermore stress induced change of dispersion for octagonal PCF with d=1.6μm is very small.

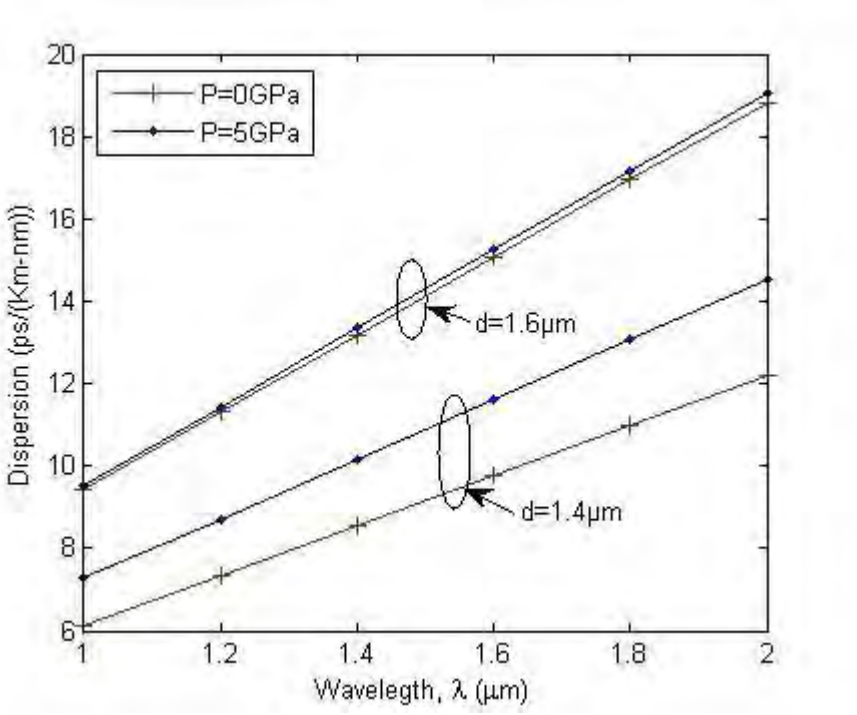

Fig.5.41 Dispersion as a function of wavelength for octagonal PCFs, where Λ=2.5μm and Nr=4.

5.4 COMPARISON BETWEEN SQUARE, HEXAGONAL AND OCTAGONAL PCFs

In section 5.1, 5.2 and 5.3 we have discussed about external stress effect on square, hexagonal and octagonal PCFs propagation properties respectively. Now in this section a comparison of stress effect on square, hexagonal and octagonal PCFs is going to be made with same design and operating parameters.

5.4.1 Effective Index

Here we have made the comparison of external stress effect on effective index for square, hexagonal and octagonal PCFs with different number of air hole rings and air hole diameter. Fig.5.42 shows effective index as a function of wavelength, number of air hole ring and external stress for square and hexagonal PCFs, where d=1.4μm, Λ=2.5μm and Nr=4. From the figure we can see that effective index decreases with the decreases of wavelength. Again effective index of square PCFs is always higher than hexagonal and PCFs with higher number of air hole rings show higher effective index. With the application of 5GPa external stress effective index increases and this change is comparatively greater for square than hexagonal.

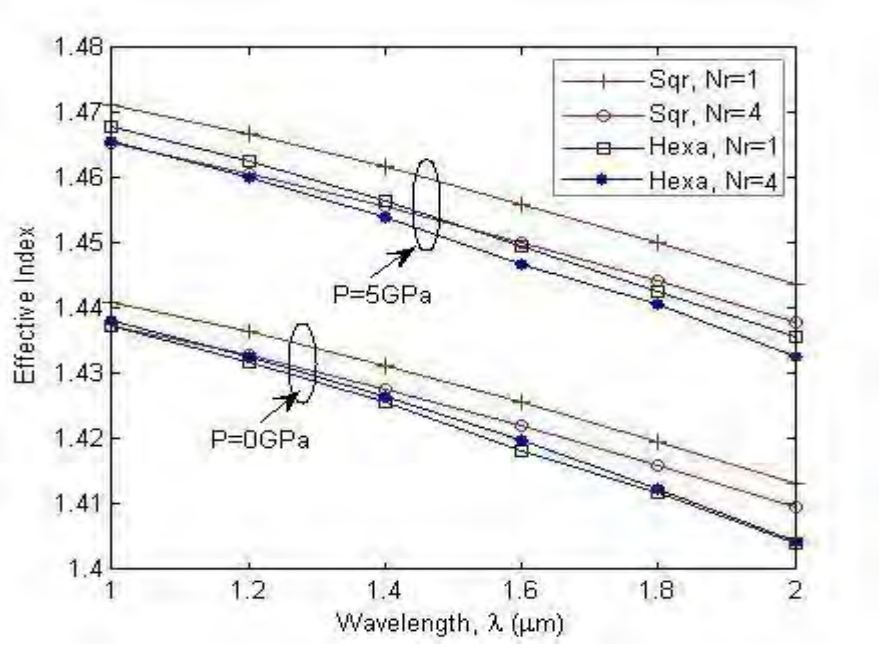

Fig.5.42 Effective index as a function of wavelength, number of air hole ring and external stress for square and hexagonal PCFs, where d=1.4μm, Λ=2.5μm and Nr=4.

Now Fig.5.43 shows effective index as a function of air hole diameter and external stress for hexagonal and octagonal PCFs, where λ=1.55μm, Λ=2.5μm and Nr=4. We can see from this figure that effective index decreases with the increase of air hole diameter for hexagonal and octagonal PCFs. Effective index of hexagonal PCF is always higher than octagonal. It also shows that higher external stress induces higher effective index and this effect is comparatively larger for the PCFs with larger air hole diameter.

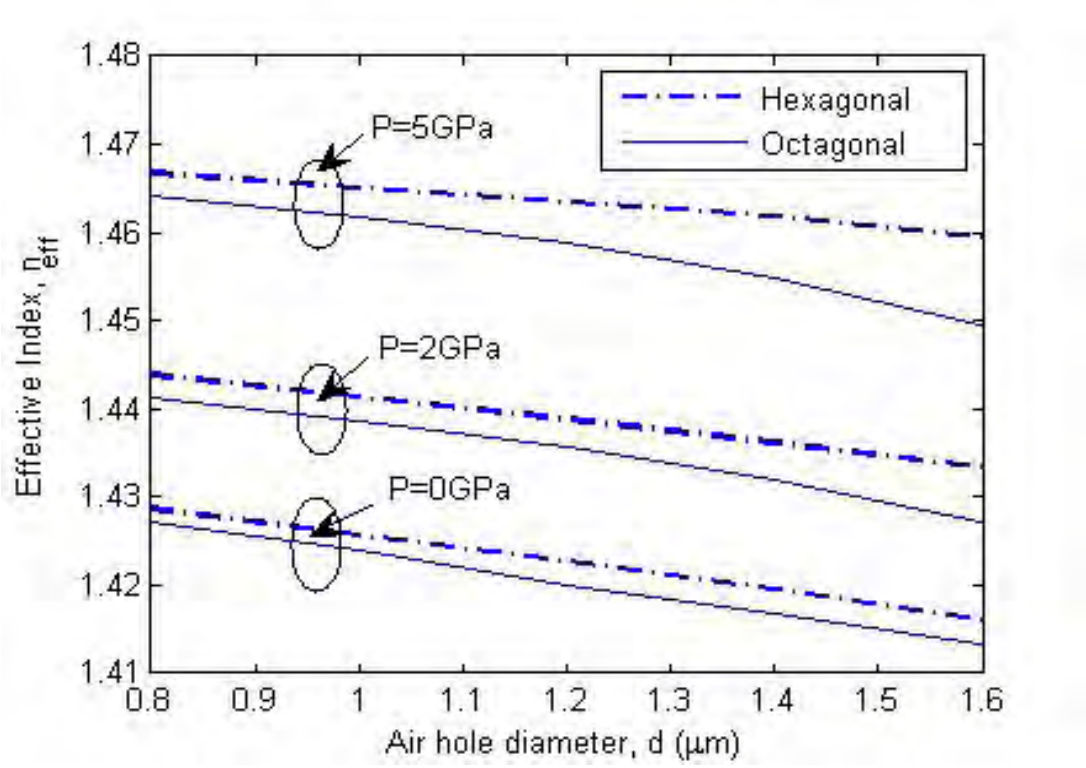

Fig.5.43 Effective index as a function of air hole diameter and external stress for hexagonal and octagonal PCFs, where λ=1.55μm, Λ=2.5μm and Nr=4.

Fig.5.44 shows the combined result of effective index as a function of wavelength for square, hexagonal and octagonal PCFs, where d=1.4μm, Λ=2.5μm and Nr=4. The figure depicts that for all PCFs (square, hexagonal and octagonal) effective index decreases with the decrease of wavelength. It also shows that effective index of octagonal PCFs is less than both square and hexagonal. With the increase of external stress effective index increases for all types of PCFs but this change is comparatively more for square and hexagonal PCFs than octagonal.

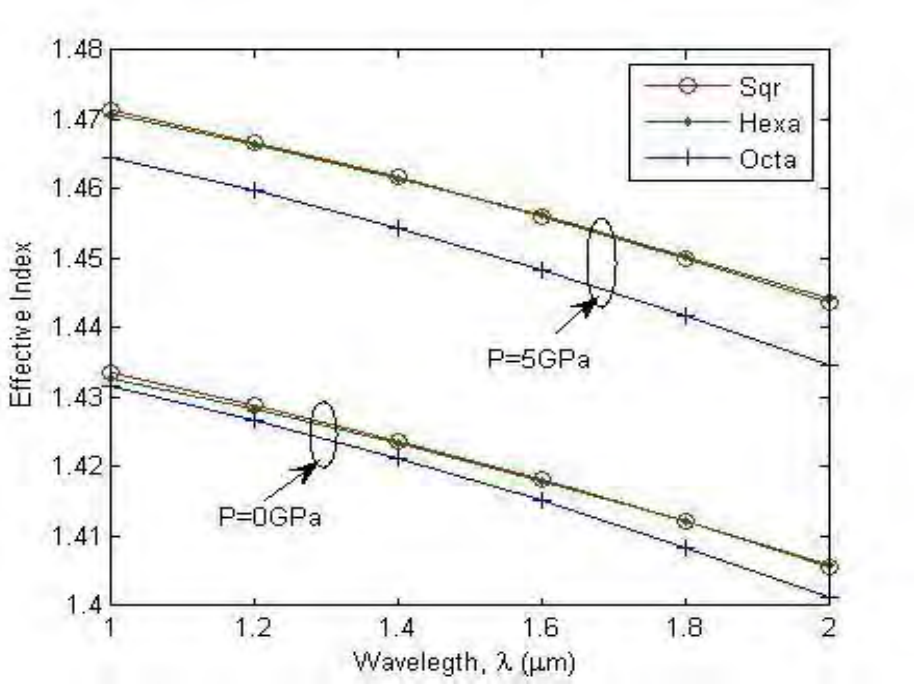

5.44 Effective index as a function of wavelength for square, hexagonal and octagonal PCFs, where d=1.4μm, Λ=2.5μm and Nr=4.

5.4.2 Birefringence

Birefringence increases with the increase of wavelength for square, hexagonal and octagonal PCFs. Fig.5.45 shows birefringence as a function of wavelength for (a) square, hexagonal and octagonal PCFs (b) square and octagonal PCFs, where d=1.4μm, Λ=2.5μm and Nr=4. From Fig.5.45 (a) depicts that without considering external stress birefringence is almost same (order of 10^{-6}) for square and hexagonal PCFs. With 5GPa external stress birefringence increases very sharply (order of 10^{-4}) for hexagonal PCF but this change is very low for square and octagonal PCF. Again Fig.5.45 (b) shows that for unstressed octagonal PCFs birefringence is lower than square. But birefringence for octagonal PCF with 5GPa external stress is comparatively higher than square.

Again Fig.5.46 shows birefringence as a function of external stress for (a) square, hexagonal and octagonal PCFs, (b) square and octagonal PCFs, where λ=1.55μm, d=1.4μm, Λ=2.5μm and Nr=4. From Fig.5.46 (a) we can see that with the increase of external stress birefringence increases almost linearly for hexagonal PCFs and it is always higher than square and octagonal PCFs. Furthermore Fig.5.46 (b) presents that change of birefringence properties due to external stress effect is more for octagonal PCFs than square.

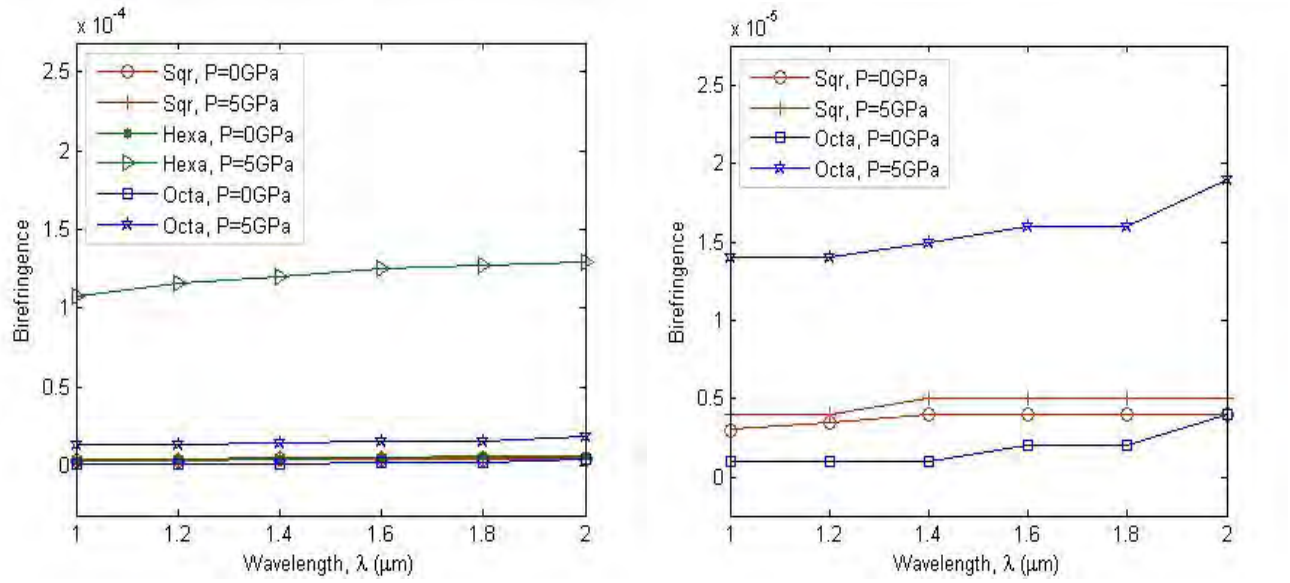

(a) (b)

Fig.5.45 Birefringence as a function of wavelength and external stress for (a) square, hexagonal and octagonal PCFs (b) square and octagonal PCFs, where d=1.4μm, Λ=2.5μm and Nr=4.

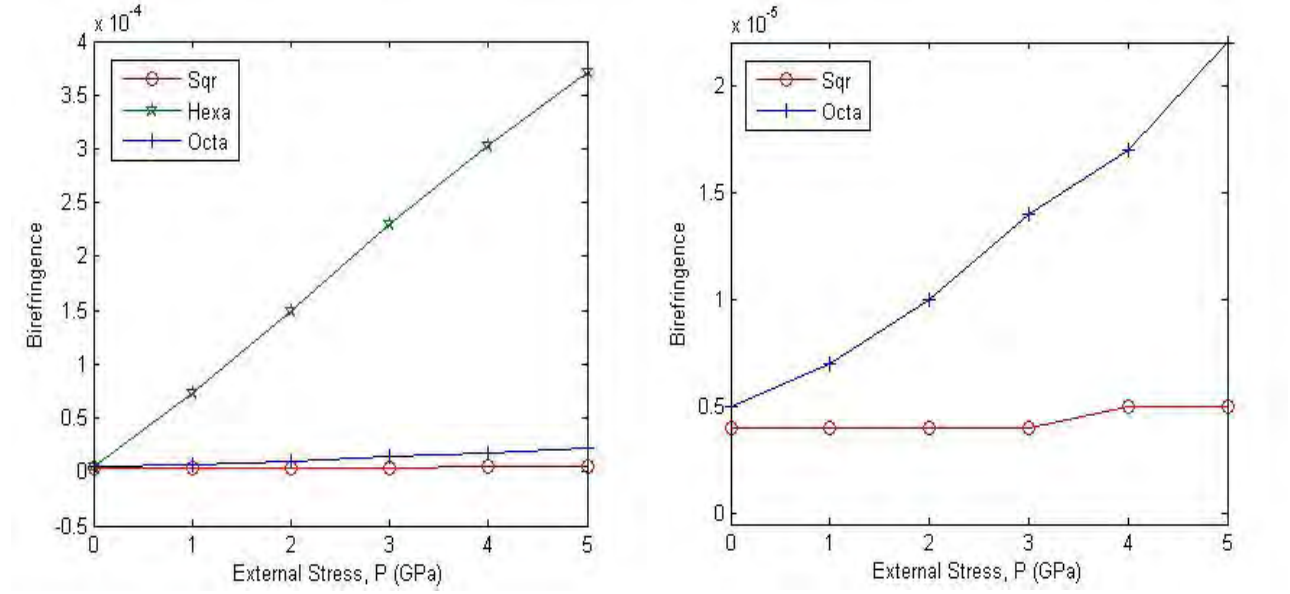

(a) (b)

Fig.5.46 Birefringence as a function of external stress for (a) square, hexagonal and octagonal PCFs, (b) square and octagonal PCFs, where λ=1.55μm, d=1.4μm, Λ=2.5μm and Nr=4.

5.4.3 Confinement Loss

The following figures Fig.5.47 (a) and (b) show confinement loss as a function of wavelength for square and hexagonal PCFs, where d=1.4µm and Λ=2.5µm. Fig.5.47 (a) shows the results for the PCFs with Nr=1 and Fig.5.47 (b) shows the result for the PCFs with Nr=4. Both figures depict that confinement loss increase with the increase of wavelength and it is always higher for hexagonal PCFs than square. They also show that higher external stress induces higher confinement loss. It is noticeable that external stress induced confinement loss is very high for both square and hexagonal PCFs with Nr=1 and it increases sharply for all operating wavelengths (λ=1.0µm to 2.0µm). Furthermore square and hexagonal PCFs with Nr=4 shows low confinement loss (order of 10^{-4}) and it increases very slowly against external stress for smaller wavelengths (λ smaller than 1.4µm) but with longer wavelengths (λ greater than 1.4µm) it increases very sharply.

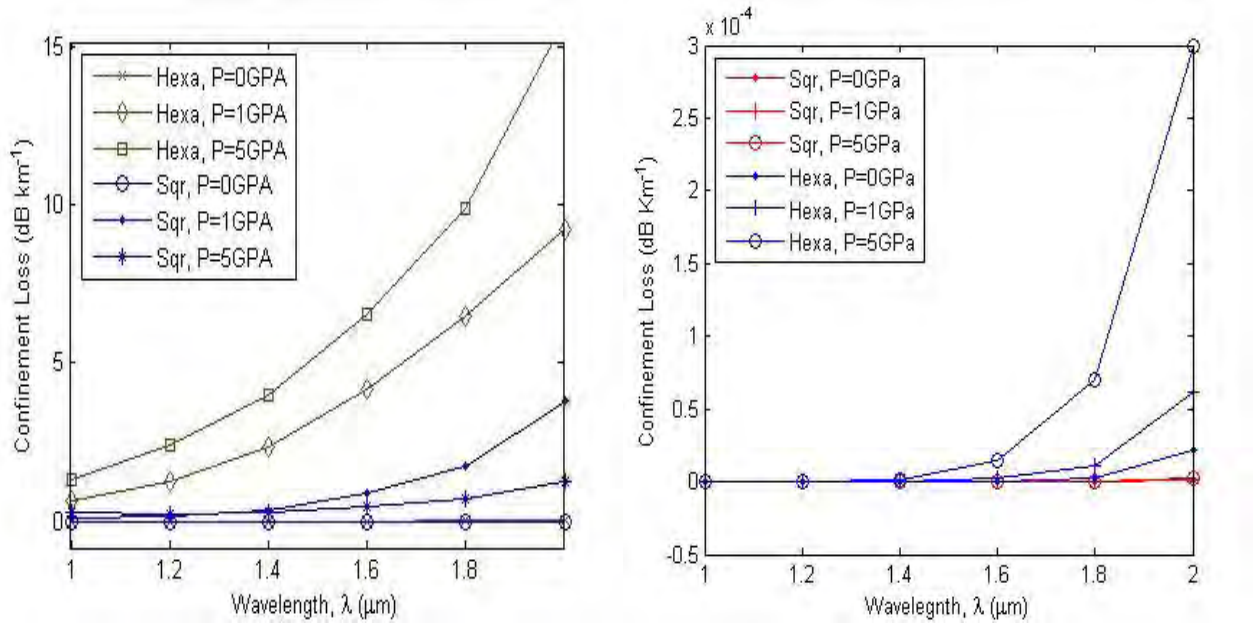

(a) (b)

Fig.5.47 Confinement loss as a function of wavelength for square and hexagonal PCFs with (a) Nr=1 and (b) Nr=4, where d=1.4µm and Λ=2.5µm.

We have presented here the combined results for different hexagonal and octagonal PCFs to observe the variation of external stress induced confinement loss as a function of air hole diameter. Fig.5.48

(a) and (b) show confinement loss as a function of external stress and air hole diameter for hexagonal and octagonal PCFs, where λ=1.55μm, Λ=2.5μm, Nr=4 and (a) d=0.8μm to 1.0μm and (b) d=1.2μm to 1.6μm. The figures show that confinement loss is always higher for hexagonal PCFs than octagonal and it increases with the increase of stress. It also shows that both PCFs with larger air hole diameter show low confinement loss than smaller.

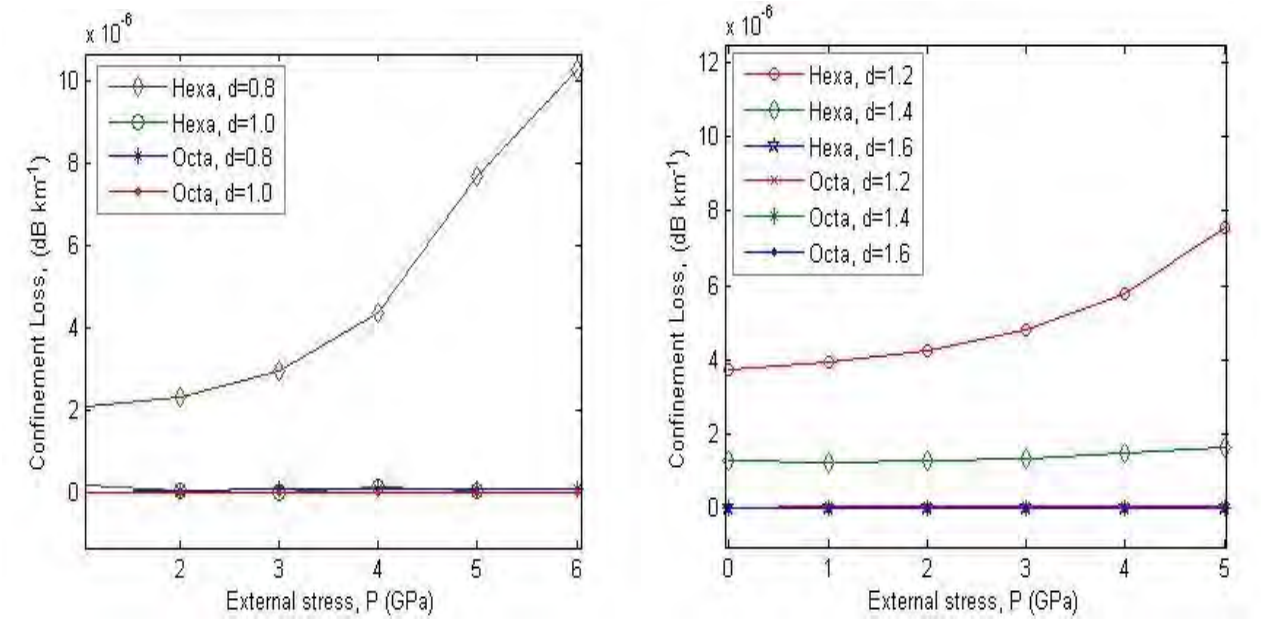

(a) (b)

Fig.5.48 Confinement loss as a function of external stress and air hole diameter for hexagonal and octagonal PCFs, where λ=1.55μm, Λ=2.5μm and Nr=4.

Now Fig.5.49 (a) presents confinement loss as a function of wavelength and external stress and (b) presents confinement loss as a function of external stress for square, hexagonal and octagonal PCFs. These figures show the combined results for square, hexagonal and octagonal PCFs. To compare the results we considered same design and operating parameters (where λ=1.55μm, d=1.4μm, Λ=2.5μm and Nr=4) for them. They depicts that confinement for hexagonal PCFs is higher than square and octagonal. Again confinement loss of square PCFs is higher than octagonal. External stress causes increase of confinement loss for all types of PCFs and this change is more for hexagonal PCFs than others.

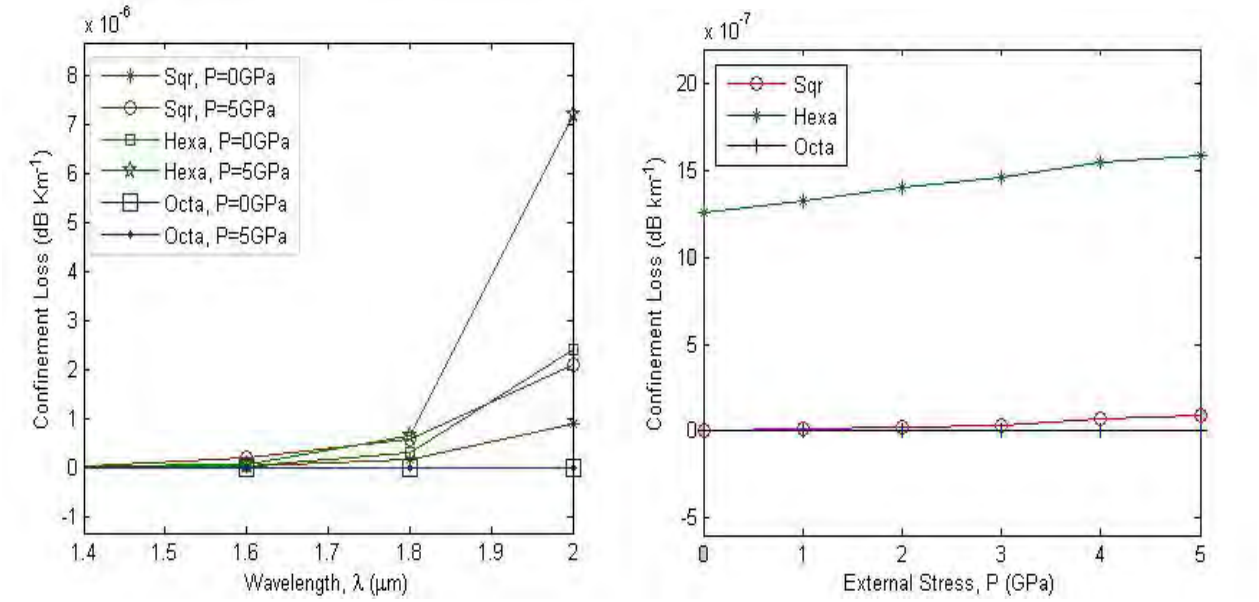

(a) (b)

Fig.5.49 (a) confinement loss as a function of wavelength and external stress for square, hexagonal and octagonal and (b) confinement loss as a function of external stress for square, hexagonal and octagonal PCFs, where λ=1.55μm, d=1.4μm, Λ=2.5μm and Nr=4.

5.4.4 Effective Area

Fig.5.50 shows that effective area as a function of wavelength and number of air hole rings for square and hexagonal PCFs, where d=1.4μm and Λ=2.5μm. It depicts that effective area increases with the increase of wavelength for both square and hexagonal PCFs and it is always higher for square PCFs. Furthermore it shows that with the increase of Nr it decreases for both types of PCFs that matches with the result found in [21].

Fig.5.51 shows effective area as a function of wavelength and external stress for hexagonal and octagonal PCFs, where d=1.4μm, Λ=2.5μm and Nr=4. This figure shows that effective area increases with the increases of wavelength and it is always higher for hexagonal PCFs than octagonal. It also shows 5GPa external stress induces higher effective area with shorter wavelength than longer. But external stress induced change of effective area is very small for all types of PCFs. That is shown in Fig.5.52, which presents the combined results of effective area as a function of external stress for square, hexagonal and octagonal PCFs. To compare the results here we have

considered same parameters λ=1.55µm, d=1.4µm, Λ=2.5µm and Nr=4 for all PCFs. From this figure we can find also that effective area of hexagonal and square PCFs are higher than octagonal.

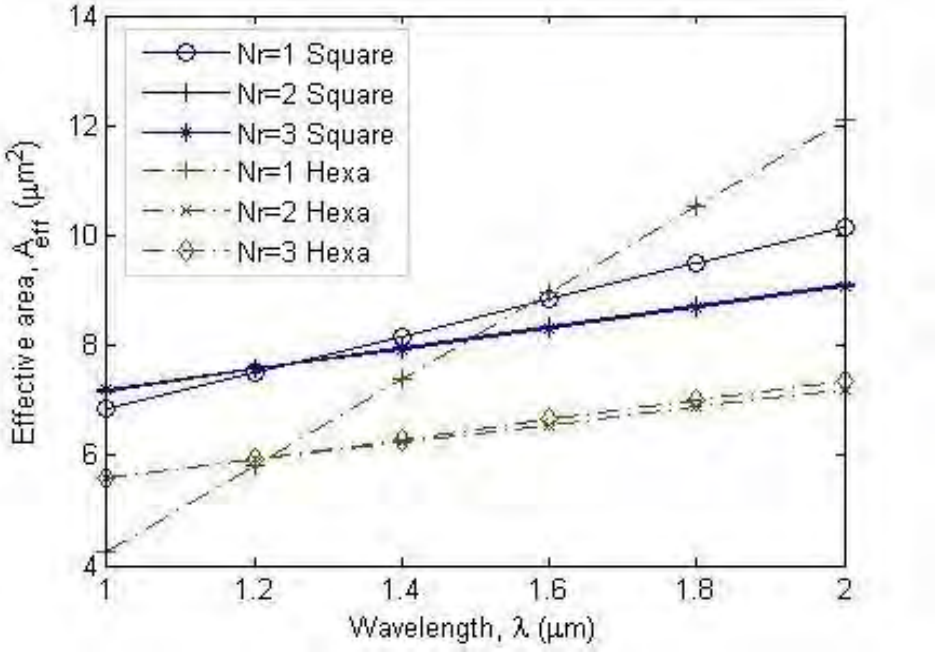

Fig.5.50 Effective area as a function of wavelength and number of air hole rings for square and hexagonal PCFs, where d=1.4µm and Λ=2.5µm.

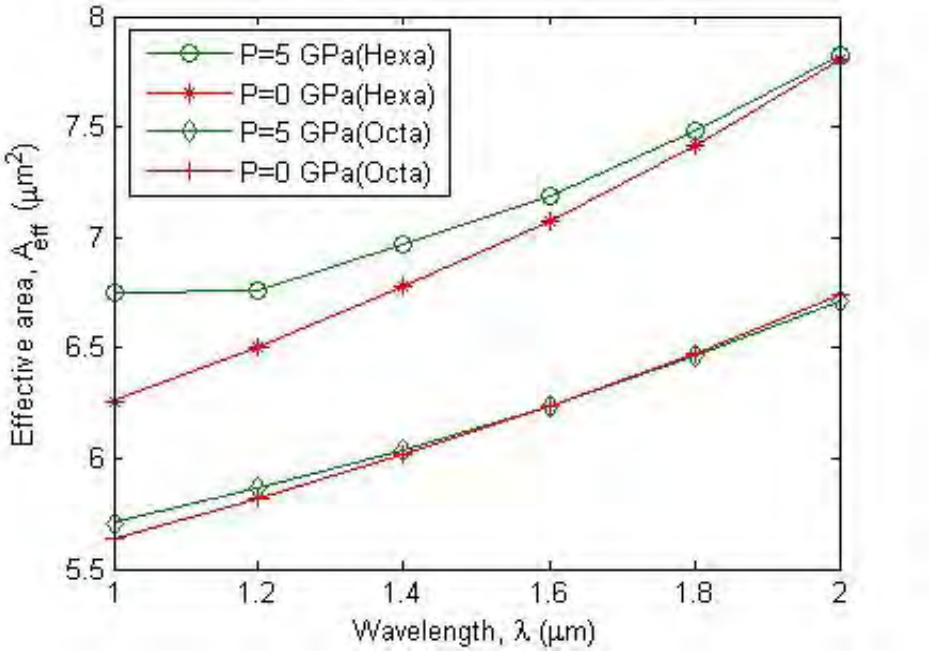

Fig.5.51 Effective area as a function of wavelength and external stress for hexagonal and octagonal PCFs, where d=1.4µm, Λ=2.5µm and Nr=4.

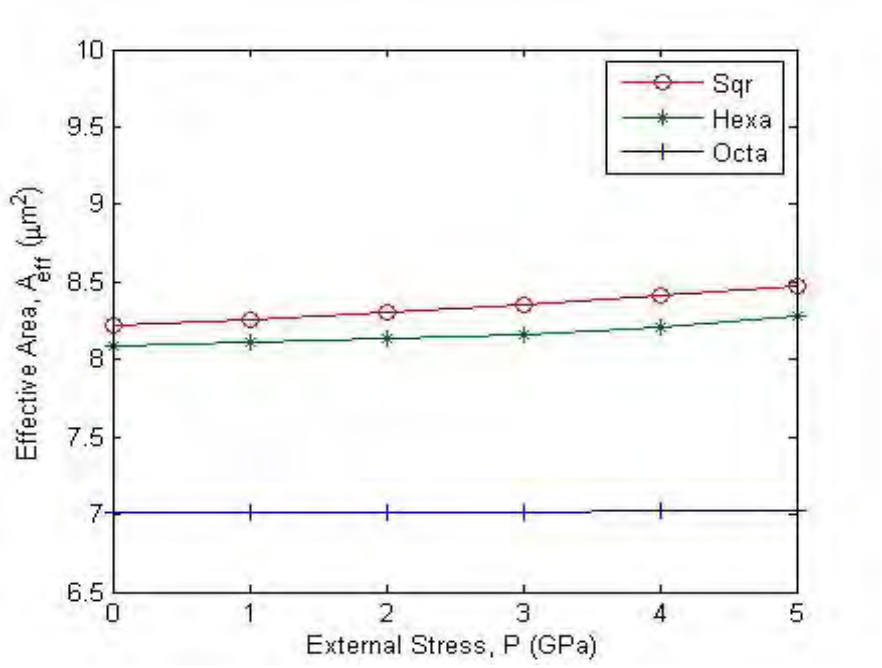

Fig.5.52 Effective area as a function of external stress for square, hexagonal and octagonal PCFs, where λ=1.55μm, d=1.4μm, Λ=2.5μm and Nr=4.

5.4.5 Dispersion

Dispersion for all types of PCFs (square, hexagonal and octagonal) increases linearly with the increase of wavelength that is shown in Fig.5.53 and Fig.5.54. Dispersion as a function of wavelength and number of air hole rings for unstressed square and hexagonal PCFs has been shown in Fig.5.53, where d=1.4μm, Λ=2.5μm and P=0GPa. This figure depicts the change of dispersion properties for square and hexagonal PCFs with different air hole diameter. With the increase of number of air hole diameter dispersion also increases for both types of PCFs but hexagonal PCF with Nr=1 shows comparatively very low dispersion than Nr=2 and 3. Square and hexagonal PCFs with Nr=2 and 3 generates almost same dispersion.

Fig.5.54 shows dispersion as a function of wavelength and external stress for square, hexagonal and octagonal PCFs, where all design and operating parameters are same (d=1.4μm, Λ=2.5μm and Nr=4). To compare the stress effect on the PCFs we considered here P=0GPa (unstressed) and 5GPa. From the figure we can find that dispersion for octagonal PCF is higher than hexagonal and square. Again hexagonal PCF shows higher dispersion than square. With 5GPa external stress all types of PCFs show higher dispersion than 0GPa and this change is greater for octagonal PCFs.

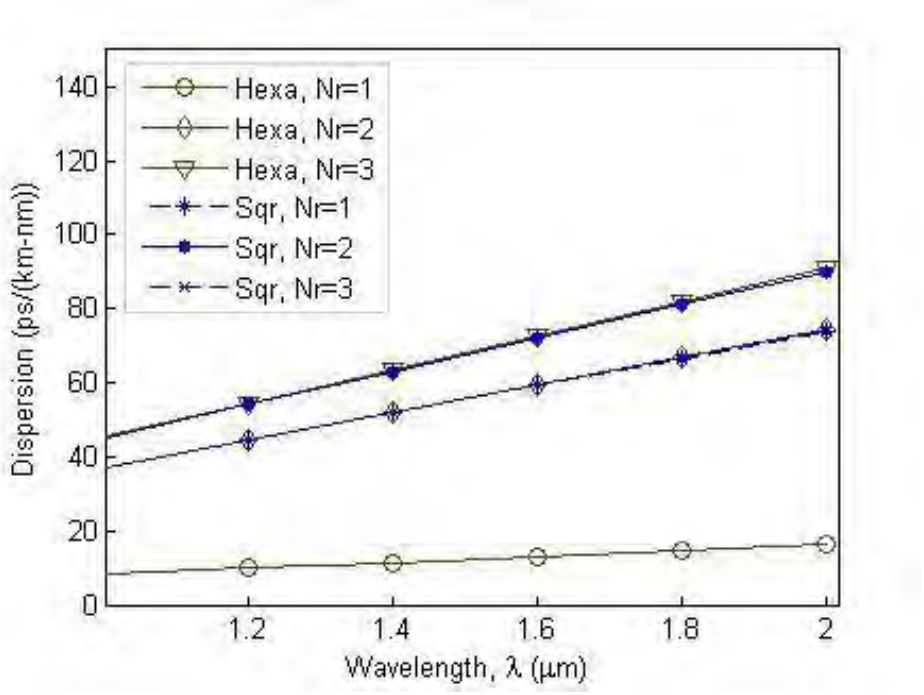

Fig.5.53 Dispersion as a function of wavelength and number of air hole rings for square and hexagonal PCFs, where d=1.4μm, Λ=2.5μm and P=0GPa.

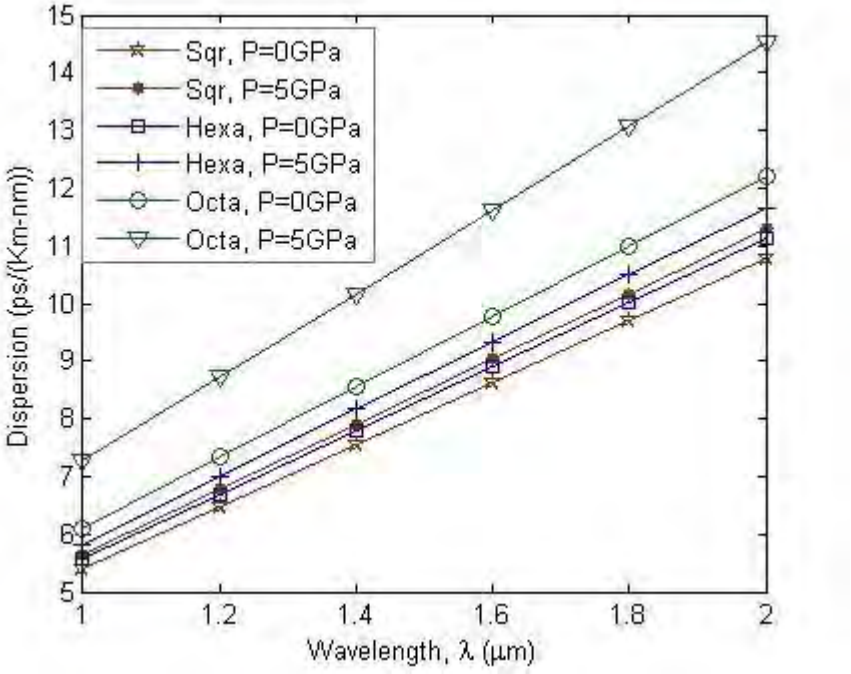

Fig.5.54 Dispersion as a function of wavelength and external stress for square, hexagonal and octagonal PCFs, where d=1.4μm, Λ=2.5μm and Nr=4.

5.5 RESULTS IN BRIEF

The experimental results in brief have been shown here in table 5.1. From the table we can find find that without external stress square and octagonal PCFs show comparatively low confinement loss where as square PCF shows high birefringence and high confinement loss. Again octagonal PCFs show comparatively higher dispersion than others.

Table 5.1 Experimental results in brief.

Properties	**Square PCF**	**Hexagonal PCF**	**Octagonal PCF**
Without external stress	-Low birefringence -low confinement loss -low dispersion.	-High birefringence (order of 10-4) -high confinement loss -low dispersion.	-Very low birefringence -very low confinement loss (order of 10-12) -Comparatively high dispersion.
Considering external stress	Less stress sensitive for -birefringence -dispersion and -confinement loss.	-Stress induced birefringence is high -high sensitivity for confinement loss	-Very low stress sensitivity for birefringence, and confinement loss properties.

Table 5.2 Applications of Different Designed PCFs.

Type of PCF	**Propagation properties**	**Suggested Applications**
Square	Low birefringence, low confinement loss and low dispersion	Good for the uses as waveguide in communication system
Hexagonal	High birefringence	Good as polarization maintaining fiber
Octagonal	Low birefringence, low confinement loss and high dispersion	Good as dispersion compensator fiber

5.6 VERIFICATION OF OUR EXPERIMENTAL RESULT WITH PUBLISHED WORK

In the following Fig. 5.55 and Fig. 5.56 we have verified our experimental results with the published work in [32]. Fig. 5.55 shows effective index as function of wavelength, where (a) presents the results for [32] and (b) presents our experimental results. From this figure we can see that our experimental results match with the published results. Again Fig. 5.56 presents birefringence against wavelength, where (a) presents the results for [32] and (b) presents our experimental results. This figure also shows that our calculated results agree with the results from [32]. Now it is clear that our experimental process is correct.

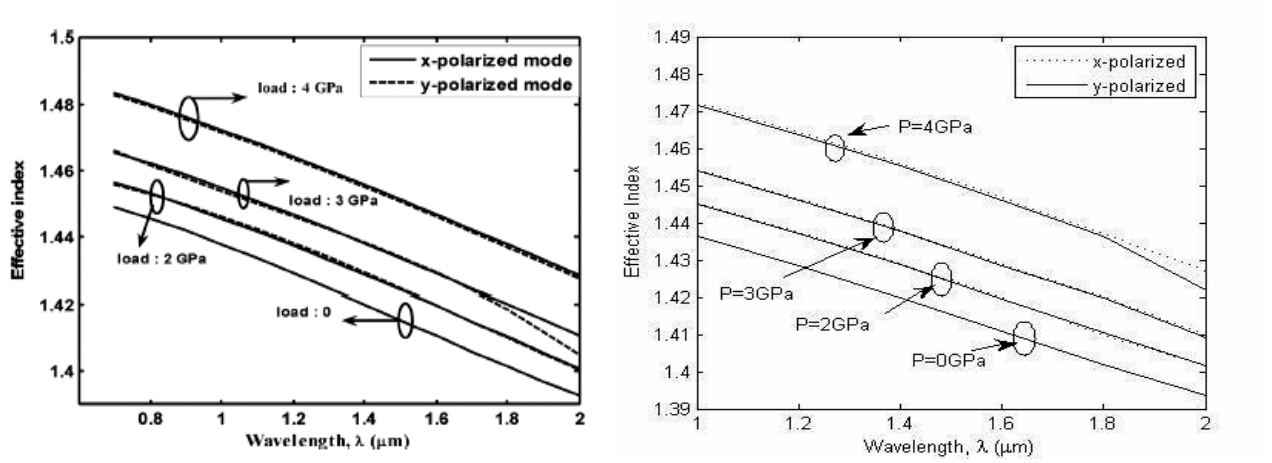

(a) (b)

Fig. 5.55 Effect of external stress on effective index and birefringence (4-ring PCF with d=1.4μm, Λ=2.3μm) (a) Hossain et. al. (2010) and (b) Our experimental result.

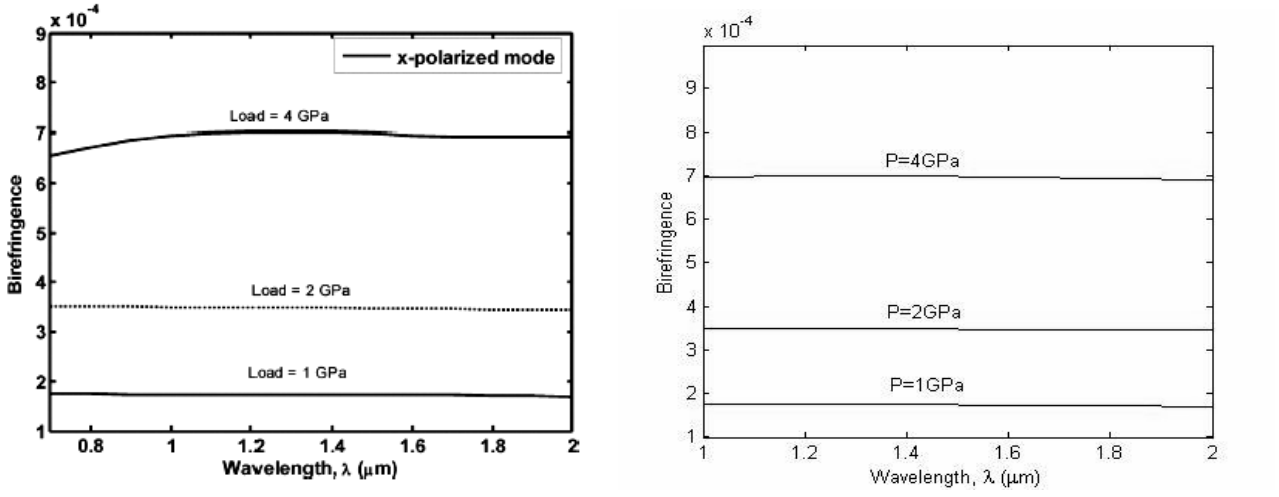

(a) (b)

Fig. 5.56 Phase birefringence versus wavelength (four-ring PCF with d=1.4 μm, A=2.3 μm) at different external pressure conditions (a) Hossain et. al. (2010) and (b) Our experimental result.

5.7 COMPARISON WITH OTHER RELATED PUBLISHED WORKS

Many experiments and investigation has been carried out using different analysis techniques and tools to understand the propagation properties of various PCFs. Propagation properties of PCFs have been investigated widely using different analysis techniques and tools. But few works has been done to understand the external stress effects on PCFs. These research works mainly carried out on effective index, birefringence, polarization mode dispersion and confinement loss properties only for hexagonal air-holes arranged PCFs with few design parameters. Here we have made a comparison of our research work with other published works. Table 5.1 shows the relative comparison among different research works.

Table 5.3 Comparison among different related research works.

Propertie	Ref. of research works	Shape of PCF	Performance of propagation properties under external stress	Numerical data
Birefringence	Zhu et al. (2003) [27]	Hexagonal PCFs by varying air hole diameter.	Birefringence increases with the increase of stress and decreases with the increase of air hole diameter.	At 2GPa external stress it shows order of 10^{-4} birefringence.
	Alam et al. (2004) [29]	Hexagonal PCFs with both symmetric and asymmetric air holes are considered.	Birefringence increases more when the air hole diameter is larger. The x-polarized fundamental mode gets higher effective refractive index at high external stress.	At 2GPa when d = 5μm, the birefringence is about 16 times larger than that of d = 3μm and the value is order of 10^{-5}.
	Tian et al. (2008) [31]	Hexagonal PCFs with fixed pitch and the air hole diameter.	Birefringence increases with the increase of stress. The dependence of wavelength on phase modal birefringence is significantly decreased when stress optical effect is considered.	At 2GPa external stress induced birefringence reaches to order of 10^{-3}.

Birefringence	In this research work	Square, hexagonal and octagonal PCFs with different number of air hole rings and air hole diameter.	With the increase of external stress birefringence increases almost linearly for all types of PCFs and it is always higher for hexagonal than square and octagonal. Again change of birefringence properties due to external stress effect is more for octagonal PCFs than square.	At external stress 2GPa, hexagonal, octagonal and square PCFs show birefringence of order of 10^{-4}, 10^{-5} and 10^{-6} respectively.
Confinement loss	Tian et al. (2008) [31]	Hexagonal PCFs with fixed pitch and the air hole diameter, where $d/\Lambda = 0.5$.	The results of simulation show us strong stress dependence of confinement loss. Where confinement loss increases with the increase of external stress.	Fig.4 shows that at 1.6 μm wavelength force 2GPa causes confinement loss around order of 10^{-3} (dB/Km).
	In this research work	Square, hexagonal and octagonal PCFs with different number of air hole rings and air hole diameter.	Confinement loss increases with the increase of stress and this change is very sharp for longer wavelength. It is always higher for hexagonal PCFs than square and octagonal. PCFs with larger air hole diameter and higher number of air hole rings show lower confinement loss.	With pitch 2.5 μm air hole diameter 1.4μm and number of air hole rings 4, square, hexagonal and octagonal PCFs with external stress 2GPa show confinement loss of order of 10-7, 10-5 and 10-12 respectively.

As far we know external effects on effective area and material dispersion has not been explore for PCFs. In our research work we have also observed these two properties for stressed and unstressed PCFs.

Table 5.4 Comparison in Brief.

Ref.	**Design of PCF**	**Properties**	**Numerical Data**
Zhu et al. (2003) [27]	Hexagonal PCFs by varying air hole diameter.	Birefringence Increases with the increase of stress	At 2GPa external stress it shows order of **10-4** birefringence.
Alam et al. (2004) [29]	Hexagonal PCFs with both symmetric and asymmetric air holes.	Birefringence Increases with the increase of stress	At 2GPa when d = 5µm, the birefringence is about 16 times larger than that of d = 3µm and the value is order of **10-5**.
Tian et al. (2008) [31]	Hexagonal PCFs with fixed pitch and the air hole diameter.	Birefringence Increases with the increase of stress	At 2GPa external stress induced birefringence reaches to order of **10-3**.
In our research work	Square Hexagonal, Octagonal, Nr=1, 2, 3 and 4, d=0.8 t0 2.0µm	Variation of birefringence with different design parameters. Change of birefringence with the application of stress.	At external stress 2GPa, hexagonal, octagonal and square PCFs show birefringence of order of 10-4, 10-5 and 10-6 respectively.

5.8 FABRICATION CHALLENGES OF PCFS

The main fabrication problems are presence of deformed air holes, emergence of additional holes, and perturbations of the structure's symmetry. Only small amounts of dust on the glass surface can result in a significant increase in fiber attenuation as well as lead to fiber breaks during fabrication or subsequent rewinding. PCFs therefore need to be fabricated under strict clean room conditions.

Chapter 6

CONCLUSION

6.1 CONCLUSION OF THIS WORK

In this research work, analysis has been carried out to observe the effect of uniform thermal and external stress on propagation properties of square, hexagonal and octagonal air hole arranged PCFs. We have considered here both stressed and unstressed PCFs to understand the effect of stress on the propagation properties like– effective index, birefringence, confinement loss, effective area and dispersion. The COMSOL Multiphysics FEMLAB modeling has been used as simulation tool, where a combination of structural mechanics module and electromagnetic module has been used to carry out the stress analysis and optical mode analysis of the PCFs respectively. At first uniform external stress has been applied on fiber boundary from all direction and stress analysis has been carried out to find out the stress induced changes of fiber materials properties due to stress-optical effect. Then mode analysis with FEM has been made on the cross-section of a fiber in the x-y plane to find out the effect of external stress on propagation properties of PCFs.

From analysis and experiment we have found that AFF of square PCF smaller than AFF of hexagonal PCF smaller than AFF of octagonal PCF. Again total amount of air in fiber cross section is 33% greater for octagonal PCF than square and hexagonal PCFs, where all design parameters are considered same. Fiber propagation properties can vary with the change of AFF and total amount of air in the fiber cross section. Again with the application of external stress fiber deformation takes place and amount of deformation is not same for all PCFs. It varies depending on AFF, total amount of air and circular symmetry in fiber cross section. Fiber deformation and stress distribution in fiber cross section both causes change in fiber propagation properties.

It is further observed that effective index of octagonal PCFs is less than both square and hexagonal PCFs with higher number of air hole rings show lower effective index. Effective index decreases with the increase of air hole diameter. With the increase of external stress effective index increases for all types of PCFs but this change is comparatively more for square and hexagonal PCFs than octagonal and stress induced change is higher for the PCFs with larger air hole diameter.

With the increase of external stress birefringence increases almost linearly for hexagonal PCFs and it is always higher than square and octagonal PCFs. Again the change of birefringence properties due to external stress effect is more for octagonal PCFs than square.

Confinement loss for hexagonal PCFs is higher than square and octagonal PCFs and it increases with the increase of stress. PCFs with lower number of air hole rings, show very high confinement loss. For this case stress induced changes also higher. It is also found that PCFs with larger air hole diameter show low confinement loss than smaller.

Effective area increases with the increases of wavelength but this change is very small. Again it is always higher for hexagonal PCFs than square and octagonal. As well as 5GPa external stress induces comparatively higher effective area with shorter wavelength than longer for all types of PCFs.

We also found that dispersion for octagonal PCF is higher than hexagonal and square. Furthermore hexagonal PCF shows higher dispersion than square. With 5GPa external stress all types of PCFs show higher dispersion than 0GPa and this change is greater for octagonal than other PCFs.

There are many applications of PCFs. Depending on the type of application specific properties of PCFs get importance. Such as for PMF and sensor high birefringence fibers are suitable. Again a fiber with very low birefringence, confinement loss and dispersion is applicable for under water and under communication system. PCFs with large effective area are used as optical amplifier and so on. Large design flexibility of PCF allows controlling its novel properties. In this research work we have explored external stress effect on these properties. Our finding will help to find the appropriate designing of PCF for some of particular application.

6.2 RECOMMENDATION FOR FUTURE WORKS

In this research work we have carried out our research to find out the effect of uniform stress and thermal effects on different PCFs. Further external stress effect on other novel PCFs should be observed to identify their properties for both stressed and unstressed conditions. So future research work related to our work can be done as in the following direction.

1. External stress effect on other standard PCFs (with other designs) should be done to understand their performance under external stress and thermal effect.

2. It is also important to observe the effect of non uniform stress on PCFs propagation properties under ground and communication system.

3. External stress induced changes are not same in both x and y coordinates. That causes different polarized propagation properties, which play significant role to characterize the PCFs. New research can be done to find out the effects for different coordinates.

4. Amount of deformation as well as stability of PCFs structure and related changes of propagation properties under external stress can be find out though further research work.

5. It is also important to know the permanence and durability of stress induced fiber deformation (strain) after removal of stress.

6. Theoretical analysis and formulation can be done to establish the relationship between external stress, fiber deformation and change of propagation properties.

In summary, effect of stress may have positive or negative effect on PCFs performance depending on its application in practical field. So, further research works should be carried out to find out the roles of stress on PCFs by using different design and analysis methods.

REFERENCES

[1] Mynbaev D. K. and Scheiner L. L., “Fiber-optic communications technology”, Low Price Edition, Prentice Hall, 2000.

[2] Photonic crystal fiber - www.rp-photonics.com/encyclopedia.html

[3] Senior J. M., “Optical fiber communications – principles and practices”, 2nd edition, Prentice – Hall of India Private Limited, 2005.

[4] Russell P. S. J., “Photonic-crystal fibers”, Journal of Lightwave Technology, vol. 24, no. 12, pp. 4729–4749, 2006.

[5] Poli F., Cucinotta A. and Selleri S., “Photonic crystal fibers”, Springer series in material science 102.

[6] Photonic crystal fiber – http://en.wikipedia.org/wiki/photonic-crystal_fiber

[7] Russell P., “Photonic Crystal Fibers: A Historical Account”, IEEE Lasers and Electro-Optics Society Newsletter, vol. 11, pp. 11-15, 2007.

[8] Knight J. C., Birks T. A., Russell P. S. J., and Atkin D. M., “All-silica single-mode fiber with photonic crystal cladding,” Opt. Letters, vol. 21, pp. 1547–1549, 1996.

[9] Poli F., Foroni M., Bottacini M., Fuochi M., Burani N., Rosa L., Cucinotta A., and Selleri S., “Single-mode regime of square-lattice photonic crystal fibers”, Journal of Optical Society of America A, vol. 22, no.8, pp. 1655–1661, 2005.

[10] Saitoh K. and Koshiba M., “Numerical modeling of photonic crystal fibers”, Journal of Lightwave Technology, vol. 23, no. 11, pp. 3580 – 3590, 2005.

[11] Chiang J. S. and Wu T. L., “Analysis of propagation characteristics for an octagonal photonic crystal fiber (O-PCF)”, Optics Communications Journal, vol. 258, no. 2, pp. 170–176, 2006.

[12] Vincetti L., Maini M., Poli F., Cucinotta A., and Selleri S., “Numerical analysis of hollow core photonic band gap fibers with modified honeycomb lattice”, Optical and Quantum Electronics, vol. 38, no. 9-11, pp. 903-912, 2006.

[13] Selleri S., Cucinotta A., “Analysis and design of photonic crystal fibers: Solid and hollow core fibers through the finite element method”, International Journal for Computation and Mathematics in Electrical and Electronic Engineering, vol. 27, no. 6, pp. 1227 – 1235, 2008.

[14] Obayya S. S. A., Rahman B. M. A. and Grattan K. T. V., "Accurate finite element modal solution of photonic crystal fibers," lEEE Proceedings, Optoelectronics, vol. 152, no. 5, pp. 241-246, 2005.

[15] Bouk A. H., Cucinotta A., Poli F., and Selleri S., “Dispersion properties of square-lattice photonic crystal fibers”, Optics Express, vol. 12, no. 5, pp. 941–946, 2004.

[16] Saitoh K., Koshiba M., Hasegawa T., and Sasaoka E., “Chromatic dispersion control in photonic crystal fibers: application to ultra flattened dispersion”, Optics Express, vol. 11, no. 8, pp. 843–852, 2003.

[17] Kuhlmey B., Renversez G., and Maystre D., “Chromatic dispersion and losses of microstructured optical fibers”, Applied Optics, vol. 42, no. 4, pp. 634–639, 2003.

[18] Liu Y. C. and Lai Y., “Optical birefringence and polarization dependent loss of square- and rectangular-lattice holey fibers with elliptical air holes: numerical analysis”, Optics Express, vol. 13, no. 1, pp. 225–235, 2005.

[19] Zhao-Lun L., Lan-Tian L. and Wei W., “Tailoring nonlinearity and dispersion of photonic crystal fibers using hybrid cladding”, Brazilian Journal of Physics, vol. 39, no. 1, pp. 50-54, 2009.

[20] Ortigosa-Blanch A., Knight J. C., Wadsworth W. J., Arriaga J., Mangan B. J., Birks T. A., and Russell P. S. J., “Highly birefringent photonic crystal fibers”, Optical Letter, vol. 25, no. 18, pp. 1325–1327, 2000.

[21] Mortensen N. A., “Effective area of photonic crystal fibers”, Optic Express, vol. 10, no. 7, pp. 314-348, 2002.

[22] White T. P., McPhedran R. C., Sterke C. M., Botten L. C., and Steel M. J., “Confinement losses in microstructured optical fibers”, Optics Letters, vol. 26, no. 21, pp. 1660–1662, 2001.

[23] Vincetti L., “Confinement losses in honeycomb fibers”, IEEE Photonics Technology Letters, vol. 16, no. 9, pp. 2048–2050, 2004.

[24] Uddin M. J. and Alam M. S., “Dispersion and Confinement Loss of Photonic Crystal Fiber”, Asian Journal of Information Technology, vol. 7, pp. 344-349, 2008.

[25] Vincetti L., Poli F., and Selleri S., “Confinement loss and nonlinearity analysis of air-guiding modified honeycomb photonic bandgap fibers”, IEEE Photonics Technology Letters, vol. 18, no. 3, pp. 508–510, 2006.

[26] Okamoto K., Hosaka T. and Edahiro T., “Stress analysis of optical fibers by a finite element method”, IEEE Journal. Quantum Electronics, vol. 17, pp. 2123-2129, 1981.

[27] Zhu Z. and Brown T. G., “Stress-induced birefringence in micro structured optical fibers”, Optical Letters, vol. 28, no. 23, pp. 495 – 503, 2003.

[28] Szpulak M., Martynkien T. and Urbanczyk W., “Effects of hydrostatic pressure on phase and group modal birefringence in micro-structured holey fibers”, Applied Optics Journal, vol. 43, no. 24, pp. 4739-4744, 2004.

[29] Alam M. S., Somasiri N., Rahman B. M. A. and Grattan K. T. V., “Effects of High External Pressure on Photonic Crystal Fiber,” Proceedings of the Third International Conference on Electrical and Computer Engineering, ICECE, pp. 245-248, 2004.

[30] Bock W. J., Chen J., Eftimov T., and Urbanczyk W., “A photonic crystal fiber sensor for pressure measurements”, IEEE Proceedings, Transactions on Instrumentation and Measurement, vol. 55, no. 4, pp. 1119–1123, 2006.

[31] Tian H., Yu Z., Han L. and Liu Y., “Birefringence and confinement loss properties in photonic crystal fibers under lateral stress”, IEEE Photonic Technology. Letter, vol. 20, no. 22, pp.1830-1831, 2008.

[32] Hossain M. A. and Alam M. S., “Polarization properties of photonic crystal fibers considering thermal and external stress effects”, Proceedings of International Conference on Advanced Communication Technology, ISSN. 1738-9445, pp. 879 – 883, 2010.

[33] Sellmeier_equation -http://en.wikipedia.org/wiki/Sellmeier_equation

[34] COMSOL Multiphysics, version 3.2a, 2005.

OUTCOMES OF THIS RESEARCH WORK

1. **M. R. Khatun** and M. S. Islam, "Effect of External Stress on Propagation Properties of Hexagonal and Octagonal PCF", Proceedings of 6th International Conference on Industrial and Information Systems (ICIIS 2011), pp-434-438, held on 16th – 19th August 2011, Kandy, Sri Lanka.

2. **M. R. Khatun** and M. S. Islam, "Analysis of Confinement Loss and Birefringence in Hexagonal and Octagonal PCF due to External Stress", Proceedings of 1st International Conference on Mechanical Engineering and Renewable Energy (ICMERE 2011), held on 22nd – 24th December 2011, Chittagong, Bangladesh.

3. **M. R. Khatun** and M. S. Islam, "Birefringence properties of Hexagonal and Octagonal air hole arranged PCFs under External Stress", Proceedings of 4th International Conference on Mechanical Engineering (ICME 2011), held on 18th – 20th December 2011, Dhaka, Bangladesh.

4. **M. R. Khatun** and M. S. Islam, "Propagation Properties and Stress Sensitivity of Square and Hexagonal Photonic Crystal Fiber", Proceedings of 14th International Conference on Information and Communication Technology (ICCIT 2011), held on 22nd – 24th December 2011, Dhaka, Bangladesh.